

# 1 Global maps of soil temperature

2 *Running head: Global maps of soil temperature*

3

4 Jonas J. Lembrechts<sup>1,\*</sup>, Johan van den Hoogen<sup>2,\*</sup>, Juha Aalto<sup>3,4</sup>, Michael B. Ashcroft<sup>5,6</sup>, Pieter De Frenne<sup>7</sup>, Julia  
5 Kempainen<sup>8</sup>, Martin Kopecký<sup>9,10</sup>, Miska Luoto<sup>4</sup>, Ilya M. D. Maclean<sup>11</sup>, Thomas W. Crowther<sup>2</sup>, Joseph J. Bailey<sup>12</sup>,  
6 Stef Haesen<sup>13</sup>, David H. Klings<sup>14,15</sup>, Pekka Niittynen<sup>4</sup>, Brett R. Scheffers<sup>16</sup>, Koenraad Van Meerbeek<sup>13</sup>, Peter  
7 Aartsma<sup>17</sup>, Otar Abdalaze<sup>18</sup>, Mehdi Abedi<sup>19</sup>, Rien Aerts<sup>20</sup>, Negar Ahmadian<sup>19</sup>, Antje Ahrends<sup>21</sup>, Juha M. Alatalo<sup>22</sup>,  
8 Jake M. Alexander<sup>23</sup>, Camille Nina Allonsius<sup>24</sup>, Jan Altman<sup>9</sup>, Christof Ammann<sup>25</sup>, Christian Andres<sup>26</sup>, Christopher  
9 Andrews<sup>27</sup>, Jonas Ardö<sup>28</sup>, Nicola Arriga<sup>29</sup>, Alberto Arzac<sup>30</sup>, Valeria Aschero<sup>31,32</sup>, Rafael L. Assis<sup>33</sup>, Jakob Johann  
10 Assmann<sup>34,35</sup>, Maaïke Y. Bader<sup>36</sup>, Khadijeh Bahalkeh<sup>19</sup>, Peter Barančok<sup>37</sup>, Isabel C. Barrio<sup>38</sup>, Agustina Barros<sup>39</sup>,  
11 Matti Barthel<sup>26</sup>, Edmund W. Basham<sup>14</sup>, Marijn Bauters<sup>40</sup>, Manuele Bazzichetto<sup>41</sup>, Luca Belelli Marchesini<sup>42</sup>,  
12 Michael C. Bell<sup>43</sup>, Juan C. Benavides<sup>44</sup>, José Luis Benito Alonso<sup>45</sup>, Bernd J. Berauer<sup>46,47</sup>, Jarle W. Bjerke<sup>48</sup>, Robert  
13 G. Björk<sup>49,50</sup>, Mats P. Björkman<sup>49,50</sup>, Katrin Björnsdóttir<sup>51</sup>, Benjamin Blonder<sup>52</sup>, Pascal Boeckx<sup>40</sup>, Julia Boike<sup>53,54</sup>,  
14 Stef Bokhorst<sup>20</sup>, Bárbara N. S. Brum<sup>55</sup>, Josef Brůna<sup>9</sup>, Nina Buchmann<sup>26</sup>, Pauline Buysse<sup>56</sup>, José Luís Camargo<sup>57</sup>,  
15 Otávio C. Campoe<sup>58</sup>, Onur Candan<sup>59</sup>, Rafaella Canessa<sup>60,61</sup>, Nicoletta Cannone<sup>62</sup>, Michele Carbognani<sup>63</sup>, Jofre  
16 Carnicer<sup>64,65</sup>, Angélica Casanova-Katny<sup>66</sup>, Simone Cesarz<sup>67,68</sup>, Bogdan Chojnicki<sup>69,69</sup>, Philippe Choler<sup>70,71</sup>, Steven L.  
17 Chown<sup>72</sup>, Edgar F. Cifuentes<sup>73</sup>, Marek Čiliak<sup>74</sup>, Tamara Contador<sup>75,76</sup>, Peter Convey<sup>77</sup>, Elisabeth J. Cooper<sup>78</sup>,  
18 Edoardo Cremonese<sup>79</sup>, Salvatore R. Curasi<sup>80</sup>, Robin Curtis<sup>11</sup>, Maurizio Cutini<sup>81</sup>, C. Johan Dahlberg<sup>82,83</sup>, Gergana N.  
19 Daskalova<sup>84</sup>, Miguel Angel de Pablo<sup>85</sup>, Stefano Della Chiesa<sup>86</sup>, Jürgen Dengler<sup>87,88,67</sup>, Bart Deronde<sup>89</sup>, Patrice  
20 Descombes<sup>90</sup>, Valter Di Cecco<sup>91</sup>, Michele Di Musciano<sup>92</sup>, Jan Dick<sup>27</sup>, Romina D. Dimarco<sup>93,94</sup>, Jiri Dolezal<sup>9,95</sup>, Ellen  
21 Dorrepaal<sup>96</sup>, Jiří Dušek<sup>97</sup>, Nico Eisenhauer<sup>67,68</sup>, Lars Eklundh<sup>28</sup>, Brian Enquist<sup>98</sup>, Todd E. Erickson<sup>99,100</sup>, Brigitta  
22 Erschbamer<sup>101</sup>, Werner Eugster<sup>26</sup>, Robert M. Ewers<sup>102</sup>, Dan A. Exton<sup>103</sup>, Nicolas Fanin<sup>104</sup>, Fatih Fazlioglu<sup>59</sup>, Iris  
23 Feigenwinter<sup>26</sup>, Giuseppe Fenu<sup>105</sup>, Olga Ferlian<sup>67,68</sup>, M. Rosa Fernández Calzado<sup>106</sup>, Eduardo Fernández-  
24 Pascual<sup>107</sup>, Manfred Finckh<sup>108</sup>, Rebecca Finger Higgins<sup>109</sup>, T'ai G. W. Forte<sup>63</sup>, Erika C. Freeman<sup>110</sup>, Esther R.  
25 Frei<sup>111,112</sup>, Eduardo Fuentes-Lillo<sup>113,1,114</sup>, Rafael A. García<sup>113,115</sup>, María B. García<sup>116</sup>, Charly Géron<sup>117</sup>, Mana  
26 Gharun<sup>26</sup>, Dany Ghosh<sup>118</sup>, Khatuna Gigauri<sup>119</sup>, Anne Gobin<sup>120,121</sup>, Ignacio Goded<sup>29</sup>, Mathias Goeckede<sup>122</sup>, Felix  
27 Gottschall<sup>67,68</sup>, Keith Goulding<sup>123</sup>, Sanne Govaert<sup>7</sup>, Bente Jessen Graae<sup>124</sup>, Sarah Greenwood<sup>125</sup>, Caroline  
28 Greiser<sup>82</sup>, Achim Grelle<sup>126</sup>, Benoit Guénard<sup>127</sup>, Mauro Guglielmin<sup>128</sup>, Joannès Guillemot<sup>129,130</sup>, Peter Haase<sup>131,132</sup>,  
29 Sylvia Haider<sup>133,67</sup>, Aud H. Halbritter<sup>134</sup>, Maroof Hamid<sup>135</sup>, Albin Hammerle<sup>136</sup>, Arndt Hampe<sup>137</sup>, Siri V.  
30 Haugum<sup>134,138</sup>, Lucia Hederová<sup>9</sup>, Bernard Heinesch<sup>139</sup>, Carole Helfter<sup>140</sup>, Daniel Hepenstrick<sup>87</sup>, Maximiliane  
31 Herberich<sup>141</sup>, Mathias Herbst<sup>142</sup>, Luise Hermanutz<sup>143</sup>, David S. Hik<sup>144</sup>, Raúl Hoffrén<sup>145</sup>, Jürgen Homeier<sup>146</sup>, Lukas  
32 Hörtnagl<sup>26</sup>, Toke T. Høye<sup>147</sup>, Filip Hrbacek<sup>148</sup>, Kristoffer Hylander<sup>82</sup>, Hiroki Iwata<sup>149</sup>, Marcin Antoni Jackowicz-  
33 Karczyski<sup>150,28</sup>, Hervé Jactel<sup>151</sup>, Järvi Järveoja<sup>152</sup>, Janusz Olejnik<sup>153</sup>, Szymon Jastrzębowski<sup>154</sup>, Anke Jentsch<sup>47,155</sup>,  
34 Juan J. Jiménez<sup>156</sup>, Ingibjörg S. Jónsdóttir<sup>157</sup>, José João L. L. Souza<sup>158</sup>, Tommaso Jucker<sup>159</sup>, Alistair S. Jump<sup>160</sup>,  
35 Radosław Juszczak<sup>69</sup>, Róbert Kanka<sup>37</sup>, Vít Kašpar<sup>9,161</sup>, George Kazakis<sup>118</sup>, Julia Kelly<sup>162</sup>, Anzar A. Khuroo<sup>135</sup>, Leif  
36 Klemetsson<sup>49</sup>, Marcin Klisz<sup>154</sup>, Natascha Kljun<sup>162</sup>, Alexander Knohl<sup>163</sup>, Johannes Kobler<sup>164</sup>, Jozef Kollár<sup>37</sup>, Olaf  
37 Kolle<sup>165</sup>, Martyna M. Kotowska<sup>146</sup>, Bence Kovács<sup>166</sup>, Juergen Kreyling<sup>167</sup>, Andrea Lamprecht<sup>168</sup>, Simone I. Lang<sup>169</sup>,  
38 Christian Larson<sup>170</sup>, Keith Larson<sup>171</sup>, Kamil Laska<sup>148,172</sup>, Gueric le Maire<sup>129,130</sup>, Rachel I. Leihy<sup>173</sup>, Luc Lens<sup>174</sup>, Bengt  
39 Liljebldh<sup>49</sup>, Annalea Lohila<sup>175,176</sup>, Juan Lorite<sup>106,177</sup>, Benjamin Loubet<sup>56</sup>, Joshua Lynn<sup>134</sup>, Martin Macek<sup>9</sup>, Roy  
40 Mackenzie<sup>75</sup>, Enzo Magliulo<sup>178</sup>, Regine Maier<sup>26</sup>, Francesco Malfasi<sup>62</sup>, František Máliš<sup>179</sup>, Matěj Man<sup>9</sup>, Giovanni  
41 Manca<sup>29</sup>, Antonio Manco<sup>180</sup>, Tanguy Manise<sup>139</sup>, Paraskevi Manolaki<sup>181,182,183</sup>, Felipe Marciniak<sup>55</sup>, Marianna  
42 Nardino<sup>184</sup>, Radim Matula<sup>10,185</sup>, Ana Clara Mazzolari<sup>32</sup>, Sergiy Medinets<sup>186,187,188</sup>, Volodymyr Medinets<sup>186</sup>, Camille  
43 Meeussen<sup>7</sup>, Sonia Merinero<sup>82</sup>, Rita de Cássia Guimarães Mesquita<sup>189</sup>, Katrin Meusburger<sup>190</sup>, Filip J. R.  
44 Meysman<sup>191</sup>, Sean T. Michaletz<sup>192</sup>, Ann Milbau<sup>193</sup>, Dmitry Moiseev<sup>194</sup>, Pavel Moiseev<sup>194</sup>, Andrea Mondoni<sup>195</sup>, Ruth  
45 Monfries<sup>21</sup>, Leonardo Montagnani<sup>196</sup>, Mikel Moriana-Armendariz<sup>78</sup>, Umberto Morra di Cella<sup>197</sup>, Martin  
46 Mörsdorf<sup>198</sup>, Jonathan R. Mosedale<sup>199</sup>, Lena Muffler<sup>146</sup>, Miriam Muñoz-Rojas<sup>200,99</sup>, Jonathan A. Myers<sup>201</sup>, Isla H.

47 Myers-Smith<sup>84</sup>, Laszlo Nagy<sup>202</sup>, Ilona Naujokaitis-Lewis<sup>203</sup>, Emily Newling<sup>204</sup>, Lena Nicklas<sup>101</sup>, Georg Niedrist<sup>205</sup>,  
48 Armin Niessner<sup>206</sup>, Mats B. Nilsson<sup>152</sup>, Signe Normand<sup>34,35</sup>, Marcelo D. Nosetto<sup>207,208</sup>, Yann Nouvellon<sup>129,130</sup>,  
49 Martin A. Nuñez<sup>209,94</sup>, Romà Ogaya<sup>210,211</sup>, Jérôme Ogée<sup>104</sup>, Joseph Okello<sup>40,212,213</sup>, Jørgen Eivind Olesen<sup>214</sup>, Øystein  
50 Opedal<sup>215</sup>, Simone Orsenigo<sup>216</sup>, Andrej Palaj<sup>37</sup>, Timo Pampuch<sup>217</sup>, Alexey V. Panov<sup>218</sup>, Meelis Pärtel<sup>219</sup>, Ada  
51 Pastor<sup>220,182</sup>, Anibal Pauchard<sup>113,115</sup>, Harald Pauli<sup>168</sup>, Marian Pavelka<sup>97</sup>, William D. Pearse<sup>221,222</sup>, Matthias Peichl<sup>152</sup>,  
52 Loïc Pellissier<sup>223,224</sup>, Rachel M. Penczykowski<sup>225</sup>, Josep Penuelas<sup>210,211</sup>, Matteo Petit Bon<sup>169,78,9</sup>, Alessandro  
53 Petraglia<sup>63</sup>, Shyam S. Phartyal<sup>226</sup>, Gareth K. Phoenix<sup>227</sup>, Casimiro Pio<sup>228</sup>, Andrea Pitacco<sup>229</sup>, Camille Pitteloud<sup>223,224</sup>,  
54 Roman Plichta<sup>185</sup>, Francesco Porro<sup>195</sup>, Miguel Portillo-Estrada<sup>1</sup>, Jérôme Poulénard<sup>230</sup>, Rafael Poyatos<sup>65,231</sup>,  
55 Anatoly S. Prokushkin<sup>218,30</sup>, Radoslaw Puchalka<sup>232,233</sup>, Mihai Puşcaş<sup>234,235,236</sup>, Dajana Radujković<sup>1</sup>, Krystal  
56 Randall<sup>237</sup>, Amanda Ratier Backes<sup>133,67</sup>, Sabine Remmele<sup>206</sup>, Wolfram Remmers<sup>238</sup>, David Renault<sup>41,239</sup>, Anita C.  
57 Risch<sup>240</sup>, Christian Rixen<sup>111</sup>, Sharon A. Robinson<sup>241</sup>, Bjorn J.M. Robroek<sup>242</sup>, Adrian V. Rocha<sup>243</sup>, Christian  
58 Rossi<sup>244,245</sup>, Graziano Rossi<sup>195</sup>, Olivier Roupsard<sup>246,247,248</sup>, Alexey V. Rubtsov<sup>30</sup>, Patrick Saccone<sup>168</sup>, Clotilde Sagot<sup>249</sup>,  
59 Jhonatan Sallo Bravo<sup>250,251</sup>, Cinthya C. Santos<sup>252</sup>, Judith M. Sarneel<sup>253</sup>, Tobias Scharnweber<sup>217</sup>, Jonas  
60 Schmeddes<sup>167</sup>, Marius Schmidt<sup>254</sup>, Thomas Scholten<sup>255</sup>, Max Schuchardt<sup>47</sup>, Naomi Schwartz<sup>256</sup>, Tony Scott<sup>123</sup>, Julia  
61 Seeber<sup>205,257</sup>, Ana Cristina Segalin de Andrade<sup>252</sup>, Tim Seipel<sup>170</sup>, Philipp Semenchuk<sup>258</sup>, Rebecca A. Senior<sup>259</sup>, Josep  
62 M. Serra-Diaz<sup>260</sup>, Piotr Sewerniak<sup>261</sup>, Ankit Shekhar<sup>26</sup>, Nikita V. Sidenko<sup>218</sup>, Lukas Siebicke<sup>163</sup>, Laura Siegwart  
63 Collier<sup>143,262</sup>, Elizabeth Simpson<sup>221</sup>, David P. Siqueira<sup>263</sup>, Zuzana Sitková<sup>264</sup>, Johan Six<sup>26</sup>, Marko Smiljanic<sup>217</sup>, Stuart  
64 W. Smith<sup>124,265</sup>, Sarah Smith-Tripp<sup>266</sup>, Ben Somers<sup>267</sup>, Mia Vedel Sørensen<sup>124</sup>, Bartolomeu Israel Souza<sup>268</sup>, Arildo  
65 Souza Dias<sup>269,252</sup>, Marko J. Spasojevic<sup>270</sup>, James D. M. Speed<sup>271</sup>, Fabien Spicher<sup>272</sup>, Angela Stanisci<sup>273</sup>, Klaus  
66 Steinbauer<sup>168</sup>, Rainer Steinbrecher<sup>274</sup>, Michael Steinwandter<sup>205</sup>, Michael Stemkovski<sup>221</sup>, Jörg G. Stephan<sup>275</sup>,  
67 Christian Stiegler<sup>163</sup>, Stefan Stoll<sup>238,276</sup>, Martin Svátek<sup>185</sup>, Miroslav Svoboda<sup>10</sup>, Torbern Tagesson<sup>28,277</sup>, Andrew J.  
68 Tanentzap<sup>110</sup>, Franziska Tanneberger<sup>278</sup>, Jean-Paul Theurillat<sup>279,280</sup>, Haydn J. D. Thomas<sup>84</sup>, Andrew D. Thomas<sup>281</sup>,  
69 Katja Tielbörger<sup>61</sup>, Marcello Tomaselli<sup>63</sup>, Urs Albert Treier<sup>34,35</sup>, Mario Trouillier<sup>217</sup>, Pavel Dan Turtureanu<sup>234,282,236</sup>,  
70 Rosamond Tutton<sup>283</sup>, Vilna A. Tyystjärvi<sup>4,3</sup>, Masahito Ueyama<sup>284</sup>, Karol Ujházy<sup>179</sup>, Mariana Ujházyová<sup>74</sup>, Domas  
71 Uogintas<sup>285</sup>, Anastasiya Vladimirovna Urban<sup>218,185</sup>, Josef Urban<sup>185,30</sup>, Marek Urbaniak<sup>153</sup>, Tudor-Mihai Ursu<sup>286</sup>,  
72 Francesco Primo Vaccari<sup>287</sup>, Stijn Van de Vonder<sup>288</sup>, Liesbeth van den Brink<sup>61</sup>, Maarten Van Geel<sup>289</sup>, Vigdis  
73 Vandvik<sup>134</sup>, Pieter Vangansbeke<sup>7</sup>, Andrej Varlagin<sup>290</sup>, G.F. (Ciska) Veen<sup>291</sup>, Elmar Veenendaal<sup>292</sup>, Susanna E.  
74 Venn<sup>293</sup>, Hans Verbeek<sup>294</sup>, Erik Verbruggen<sup>1</sup>, Frank G.A. Verheijen<sup>295</sup>, Luis Villar<sup>296</sup>, Luca Vitale<sup>297</sup>, Pascal  
75 Vittoz<sup>298</sup>, Maria Vives-Ingla<sup>65</sup>, Jonathan von Oppen<sup>34,35</sup>, Josefine Walz<sup>96</sup>, Runxi Wang<sup>127</sup>, Yifeng Wang<sup>283</sup>, Robert  
76 G. Way<sup>283</sup>, Ronja E. M. Wedegärtner<sup>124</sup>, Robert Weigel<sup>146</sup>, Jan Wild<sup>9,161</sup>, Matthew Wilkinson<sup>43</sup>, Martin  
77 Wilmking<sup>217</sup>, Lisa Wingate<sup>104</sup>, Manuela Winkler<sup>168</sup>, Sonja Wipf<sup>244</sup>, Georg Wohlfahrt<sup>136</sup>, Georgios Xenakis<sup>299</sup>, Yan  
78 Yang<sup>300</sup>, Zicheng Yu<sup>301,302</sup>, Kailiang Yu<sup>303</sup>, Florian Zellweger<sup>112</sup>, Jian Zhang<sup>304,305</sup>, Zhaochen Zhang<sup>304</sup>, Peng Zhao<sup>152</sup>,  
79 Klaudia Ziemblińska<sup>153</sup>, Reiner Zimmermann<sup>206,306</sup>, Shengwei Zong<sup>307</sup>, Viacheslav I. Zyryanov<sup>218</sup>, Ivan Nijs<sup>1</sup>,  
80 Jonathan Lenoir<sup>272 ,+,x</sup>

81 \* These authors contributed equally to this work

82 x Corresponding authors

83 + These authors contributed equally to this work

84 \*\* See end of manuscript for affiliations

85

## 86 Corresponding authors

87 Jonas Lembrechts ([Jonas.lembrechts@uantwerpen.be](mailto:Jonas.lembrechts@uantwerpen.be), <https://orcid.org/0000-0002-1933-0750>).

88 Jonathan Lenoir ([jonathan.lenoir@u-picardie.fr](mailto:jonathan.lenoir@u-picardie.fr), <https://orcid.org/0000-0003-0638-9582>).

89

90 **Abstract**

91 Research in global change ecology relies heavily on global climatic grids derived from  
92 estimates of air temperature in open areas at around 2 m above the ground. These climatic  
93 grids thus fail to reflect conditions below vegetation canopies and near the ground surface,  
94 where critical ecosystem functions are controlled and most terrestrial species reside. Here we  
95 provide global maps of soil temperature and bioclimatic variables at a 1-km<sup>2</sup> resolution for 0–  
96 5 and 5–15 cm depth. These maps were created by calculating the difference (i.e., offset)  
97 between *in-situ* soil temperature measurements, based on time series from over 1200 1-km<sup>2</sup>  
98 pixels (summarized from 8500 unique temperature sensors) across all of the world’s major  
99 terrestrial biomes, and coarse-grained air temperature estimates from ERA5-Land (an  
100 atmospheric reanalysis by the European Centre for Medium-Range Weather Forecasts). We  
101 show that mean annual soil temperature differs markedly from the corresponding 2 m  
102 gridded air temperature, by up to 10°C (mean =  $3.0 \pm 2.1^\circ\text{C}$ ), with substantial variation across  
103 biomes and seasons. Over the year, soils in cold and/or dry biomes are substantially warmer  
104 ( $3.6 \pm 2.3^\circ\text{C}$  warmer than gridded air temperature), whereas soils in warm and humid  
105 environments are on average slightly cooler ( $0.7 \pm 2.3^\circ\text{C}$  cooler). The observed substantial and  
106 biome-specific offsets underpin that the projected impacts of climate and climate change on  
107 biodiversity and ecosystem functioning are inaccurately assessed when air rather than soil  
108 temperature is used, especially in cold environments. The global soil-related bioclimatic  
109 variables provided here are an important step forward for any application in ecology and  
110 related disciplines. Nevertheless, we highlight the need to fill remaining global gaps by  
111 collecting more *in-situ* measurements of microclimate conditions to further enhance the  
112 spatiotemporal resolution of global soil temperature products for ecological applications.

113

114 **Keywords:** microclimate, bioclimatic variables, soil temperature, global maps, temperature offset,  
115 soil-dwelling organisms, near-surface temperatures

## 116 Introduction

117 With the rapidly increasing availability of big data on species distributions, functional traits  
118 and ecosystem functioning (Bond-Lamberty & Thomson, 2018, Bruelheide *et al.*, 2018,  
119 Kissling *et al.*, 2018, Kattge *et al.*, 2019, Lenoir *et al.*, 2020), we can now study biodiversity  
120 and ecosystem responses to global changes in unprecedented detail (Senior *et al.*, 2019,  
121 Steidinger *et al.*, 2019, Van Den Hoogen *et al.*, 2019, Antão *et al.*, 2020). However, despite  
122 this increasing availability of ecological data, most spatially-explicit studies of ecological,  
123 biophysical and biogeochemical processes still make use of the same global gridded  
124 temperature data (Soudzilovskaia *et al.*, 2015, Van Den Hoogen *et al.*, 2019, Du *et al.*, 2020).  
125 Most of these gridded air temperature datasets are based on long-term climatologies of  
126 rather coarse spatiotemporal resolutions: monthly and annual means, or bioclimatic  
127 derivatives, based on 30-yr time series averaged within 1 km to 50 km grid cells. Additionally,  
128 these coarse temperature grids are constructed based on measurements from standard  
129 meteorological stations that record free-air temperature inside well-ventilated protective  
130 shields placed up to 2 m above-ground in open, shade-free habitats, where abiotic conditions  
131 may differ substantially from those actually experienced by most organisms (World  
132 Meteorological Organization, 2008, Lembrechts *et al.*, 2020).

133 Ecological patterns and processes often relate more directly to below-canopy soil  
134 temperature rather than to well-ventilated air temperature inside a weather station. Near-  
135 surface, rather than air, temperature better predicts ecosystem functions like biogeochemical  
136 cycling (e.g., organic matter decomposition, soil respiration and other aspects of the global  
137 carbon balance) (Schimel *et al.*, 2004, Pleim & Gilliam, 2009, Portillo-Estrada *et al.*, 2016,  
138 Hursh *et al.*, 2017, Gottschall *et al.*, 2019, Davis *et al.*, 2020, Perera-Castro *et al.*, 2020).  
139 Similarly, the use of soil temperature in correlative analyses or predictive models may  
140 improve predictions of climate impacts on organismal physiology and behaviour, as well as  
141 on population and community dynamics and species distributions (Körner & Paulsen, 2004,  
142 Schimel *et al.*, 2004, Ashcroft *et al.*, 2008, Kearney *et al.*, 2009, Scherrer *et al.*, 2011, Opedal  
143 *et al.*, 2015, Berner *et al.*, 2020, Zellweger *et al.*, 2020). Given the key role of soil-related  
144 processes for both aboveground and belowground parts of the ecosystem and their  
145 feedbacks to the atmosphere (Crowther *et al.*, 2016), adequate soil temperature data are  
146 critical for a broad range of fields of study, such as ecology, biogeography, biogeochemistry,

147 agronomy, soil science and climate system dynamics. Nevertheless, existing global soil  
148 temperature products such as those from ERA5-Land (Copernicus Climate Change Service  
149 (C3S), 2019), with a resolution of  $0.08 \times 0.08$  degrees ( $\approx 9 \times 9$  km at the equator), remain too  
150 coarse for most ecological applications.

151 The direction and magnitude of the – often multi-degree – difference or *offset* between *in-*  
152 *situ* soil temperature and coarse-gridded air temperature products result from a combination  
153 of two factors: (i) the (vertical) microclimatic difference between air and soil temperature,  
154 and (ii) the (horizontal) mesoclimatic difference between air temperature in flat, cleared  
155 areas (i.e., where meteorological stations are located) and air temperature within different  
156 vegetation types (e.g., below a dense canopy of trees) or topographies (e.g., within a ravine  
157 or on a ridge) (Lembrechts *et al.*, 2020, De Frenne *et al.*, 2021). In essence, the offset is thus  
158 the combination of both the vertical and horizontal differences that result from factors  
159 affecting the energy budget at the Earth’s surface, principally radiative energy: the ground  
160 absorbs radiative energy, which is transferred to the air by convective heat exchange,  
161 evaporation and spatial variation in net radiation, and lower convective conductance near the  
162 Earth’s surface results in horizontal and vertical variation in temperature (Richardson, 1922,  
163 Geiger, 1950). Both these vertical and horizontal differences in temperature vary significantly  
164 across the globe and in time as a result of environmental conditions affecting the radiation  
165 budget (e.g., as a result of topographic orientation, canopy cover or surface albedo),  
166 convective heat exchange and evaporation (e.g., foliage density, variation in the degree of  
167 wind shear caused by surface friction) and the capacity for the soil to store and conduct heat  
168 (e.g., water content and soil structure and texture) (Geiger, 1950, Zhang *et al.*, 2008, Way &  
169 Lewkowicz, 2018, De Frenne *et al.*, 2019).

170 While the physics of soil temperatures have long been well-understood (Richardson, 1922,  
171 Geiger, 1950), the creation of high-resolution global gridded soil temperature products has  
172 not been feasible before, amongst others due to the absence of detailed global *in-situ* soil  
173 temperature measurements (Lembrechts & Lenoir, 2019, Lembrechts *et al.*, 2020). Recently,  
174 however, the call for microclimate temperature data with spatiotemporal resolutions  
175 relevant to the studied organism and, most importantly, values representative of *in-situ*  
176 conditions (i.e., microhabitat) as experienced by these organisms has become more urgent  
177 (Bramer *et al.*, 2018), while global data availability has rapidly increased (Lembrechts *et al.*,

178 2020). In this paper, we mainly address the point on the representativeness of *in-situ*  
179 conditions by generating global gridded maps of below-canopy and near-surface soil  
180 temperature at 1-km<sup>2</sup> resolution (in line with most existing global air temperature products).  
181 These maps are representative of the habitat conditions experienced by organisms living  
182 under vegetation canopies, in the topsoil or near the soil surface. They were created using  
183 the abovementioned offset between gridded air temperature data and *in-situ* soil  
184 temperature measurements. We expect these soil temperature maps to be substantially  
185 more representative of actual microclimatic conditions than existing products – even though  
186 still at a relatively coarse spatial resolution of 1-km<sup>2</sup> and summarizing multi-decadal averages  
187 – as they capture relevant near- and below-ground abiotic conditions where ecosystem  
188 functions and processes operate (Daly, 2006, Bramer *et al.*, 2018, Körner & Hiltbrunner,  
189 2018). Indeed, the offset between free-air (macroclimate) and soil (microclimate)  
190 temperature, and between cleared areas and other habitats, can easily reach up to ±10°C  
191 annually, even at the coarse 1-km<sup>2</sup> spatial resolution used here (Zhang *et al.*, 2018,  
192 Lembrechts *et al.*, 2019, Wild *et al.*, 2019).

193 To create the global gridded soil temperature maps introduced above, we used over 8500  
194 time series of soil temperature measured *in-situ* across the world's major terrestrial biomes,  
195 compiled and stored in the SoilTemp database (Lembrechts *et al.*, 2020) (Fig. 1a,  
196 Supplementary Material Fig. S1) and averaged into 1200 (or 1000 for the second soil layer)  
197 unique 1-km<sup>2</sup> pixels. First, to illustrate the magnitude of the studied effect, we visualized the  
198 global and biome-specific patterns in the mean annual offset between *in-situ* soil temperature  
199 (topsoil: 0–5 cm and second layer: 5–15 cm depth) and coarse-scale interpolated air  
200 temperature from ERA5-Land (soil temperature minus air temperature, hereafter called the  
201 *temperature offset*, sensu (De Frenne *et al.*, 2021); elsewhere called the *surface offset* (Smith  
202 & Riseborough, 1996, Smith & Riseborough, 2002)) using the average within 1 × 1 km grid  
203 cells. Next, we used a machine learning approach with 31 environmental explanatory  
204 variables (including macroclimate, soil, topography, reflectance, vegetation and  
205 anthropogenic variables) to model the spatial variation in monthly temperature offsets at a 1  
206 × 1 km resolution for all continents except Antarctica (as absent in many of the used predictor  
207 variable layers). Using these offsets, we then calculated relevant soil-related bioclimatic  
208 variables (SBIO), mirroring the existing global bioclimatic variables for air temperature.

209 Finally, we compare our new global soil temperature product with a similar one calculated  
210 using coarser-resolution soil temperature data from ERA5-Land (Copernicus Climate Change  
211 Service (C3S), 2019).

## 212 **Methods**

### 213 ***Data acquisition***

214 Analyses are based on SoilTemp, a global database of microclimate time series (Lembrechts  
215 *et al.*, 2020). We compiled soil temperature measurements from 9362 unique sensors (mean  
216 duration 2.9 years, median duration 1.0 year, ranging from 1 month to 41 years) from 60  
217 countries, using both published and unpublished data sources (Fig. 1, Supplementary Material  
218 Fig. S1). Each sensor corresponds to one independent time series.

219 We used time series spanning a minimum of one month, with a temporal resolution of four  
220 hours or less. Sensors of any type were included (Supplementary Material Table S1), as long  
221 as they measured *in situ*. Sensors in experimentally manipulated plots, i.e., plots in which  
222 microclimate has been manipulated, were excluded. Most data (> 90%) came from low-cost  
223 rugged microclimate loggers such as iButtons (Maxim Integrated, USA) or TMS4-sensors (Wild  
224 *et al.*, 2019), with measurement errors of around 0.5–1°C (note that we are using °C over K  
225 throughout, for ease of understanding), while in a minority of cases sensors with higher  
226 meteorological specifications such as industrial or scientific grade thermocouples and  
227 thermistors (measurement errors of less than 0.5°C) were used. Contributing datasets mostly  
228 consisted of short-term regional networks of microclimate measurements, yet also included  
229 a set (< 5%) of soil temperature sensors from long-term research networks equipped with  
230 weather stations (e.g., Pastorello *et al.*, 2017). By combining these two types of data, a much  
231 higher spatial density of sensors and broader distribution of microhabitats could be obtained  
232 than by using weather station data only.

233 About 68% of sensors measured in time intervals located between 2010 and 2020 and 93%  
234 between 2000 and 2020; we thus focus on the latter period in our analyses. Additionally, given  
235 the relatively short time frame covered by most individual sensors, we were not able to test  
236 for systematic differences in the temperature offset between old and recent data sets, and  
237 thus we did not correct for this in our models. We strongly urge future studies to assess such

238 temporal dynamics in the offset, once long-term microclimate data have become sufficient  
239 and more available.

240 For each of the individual 9362 time series, we calculated monthly mean, minimum (5%  
241 percentile of all monthly values) and maximum (95% percentile) temperature, after checking  
242 all time series for plausibility and erroneous data. These monthly values, while perhaps not  
243 fully intercomparable between the northern and southern hemisphere, are those that have  
244 traditionally been used to calculate bioclimatic variables (Fick & Hijmans, 2017). Months with  
245 more than one day of missing data, either at the beginning or end of the measurement period,  
246 or due to logger malfunctioning during measurement, were excluded, resulting in a final  
247 subset of 380 676 months of soil temperature time series that were used for further analyses.  
248 For each sensor with more than twelve months of data, we calculated moving averages of  
249 annual mean temperature, using each consecutive month as a starting month and calculating  
250 the mean temperature including the next eleven months. We used these moving averages to  
251 make maximal use of the full temporal extent covered by each sensor, because each time  
252 series spanned a different time period, often including parts of calendar years only. Next,  
253 these moving averages were further summarized to one mean annual average per 1-km<sup>2</sup> pixel  
254 (see below, under '*Global and biome-level analyses*').

255 The selected dataset contained sensors installed strictly belowground, measuring  
256 temperature at depths between 0 and 200 cm below the ground surface. Sensors recording  
257 several measurements at the same site but located at different (vertical) depths were  
258 included separately (the 9362 unique sensors thus came from 7251 unique loggers).

259 Sensors were grouped in different soil depth categories (0–5, 5–15, 15–30, 30–60, 60–100,  
260 100–200 cm, Supplementary Material Table S2) to incorporate the effects of soil temperature  
261 dampening. We limited our analyses to the topsoil (0–5 cm) and the second soil layer (5–15  
262 cm), as we currently lack sufficient global coverage to make trustworthy models at deeper  
263 soil depths (8519 time series, about 91%, came from the two upper depth layers). Due to  
264 uncertainty in identification of these soil depths between studies (e.g., due to litter layers),  
265 no finer categorisation is used.



266 We tested for potential bias in temporal resolution (i.e., measurement interval) by calculating  
267 mean, minimum and maximum temperature for a selection of 2000 months for data  
268 measured every 15 minutes, and the same data aggregated to 30, 60, 90, 120 and 240  
269 minutes. Monthly mean, minimum and maximum temperature calculated with any of the  
270 aggregated datasets differed on average less than 0.2°C from the ones with the highest  
271 temporal resolution. We were thus confident that pooling data with different temporal  
272 resolutions of 4 hours or finer would not significantly affect our results.

### 273 ***Temperature offset calculation***

274 For each monthly value at each sensor location (see Supplementary Material Table S3 for  
275 number of data points per month), we extracted the corresponding monthly means of the 2  
276 m air temperature from the European Centre for Medium-Range Weather (ECMWF)  
277 Forecast's 5<sup>th</sup> reanalysis (ERA5) (from 1979–1981) and ERA5-Land from 1981–2020  
278 (Copernicus Climate Change Service (C3S), 2019), hereafter called ERA5L. The latter dataset  
279 models the global climate with a spatial resolution of 0.08 × 0.08 degrees ( $\approx 9 \times 9$  km at the  
280 equator) with an hourly resolution, converted into monthly means using daily means for the  
281 whole month. Similarly, monthly minima and maxima were obtained from TerraClimate  
282 (Abatzoglou *et al.*, 2018) for the period 2000 to 2020 at a 0.04 × 0.04 degrees ( $\approx 4 \times 4$  km at  
283 the equator) resolution. Monthly means for TerraClimate were not available, we therefore  
284 estimated them by averaging the monthly minima and maxima. Finally, we also obtained  
285 monthly mean temperatures from CHELSA (Karger *et al.*, 2017a, Karger *et al.*, 2017b) for the  
286 period 2000 to 2013 at a 30 × 30 arc second ( $\approx 1 \times 1$  km at the equator) resolution. In our  
287 modelling exercises (see section '*Integrative modelling*' below), we opted to use the mean  
288 temperature offsets as calculated based on ERA5L rather than on CHELSA. While CHELSA's  
289 higher spatial resolution is definitely an advantage, its time period (stopping in 2013)  
290 insufficiently overlapped with the time period covered by our *in-situ* measurements (2000 to  
291 2020), so temperature offsets based on the CHELSA dataset were only used for comparative  
292 purposes. We used TerraClimate to model offsets in monthly minimum and maximum  
293 temperature.

294 We calculated moving annual averages of the gridded air temperature data similar to those  
295 we computed for soil temperature. These were used to create annual temperature offset  
296 values following the same approach as above.

297 The offset between the *in situ* measured soil temperature in the SoilTemp database and the  
298 2 m free-air temperature obtained from the air-temperature grids (ERA5L, TerraClim and  
299 CHELSA, hereafter called 'gridded air temperature') was calculated by subtracting the  
300 monthly or annual mean air temperature from the monthly or annual mean soil temperature.  
301 Positive offset values indicate a measured soil temperature higher than gridded air  
302 temperature, while negative offset values represent cooler soils. Similarly, monthly minimum  
303 and maximum air temperature were subtracted from minimum and maximum soil  
304 temperature, respectively. Monthly minima and maxima of the soil temperature were  
305 calculated as, respectively, the 5% lowest and highest instantaneous measurement in that  
306 month, to correct for outliers, which can be especially pronounced at the soil surface (Speak  
307 *et al.*, 2020). As a result, patterns in minima and maxima are more conservative estimates  
308 than if we had used the absolute lowest and highest values.

309 Importantly, the temperature offset calculated here is a result of three key groups of drivers:  
310 (1) height effects (2 m versus 0–15 cm below the soil surface); (2) environmental or habitat  
311 effects (e.g., spatial variability in vegetation, snow or topography); and (3) spatial scale effects  
312 (resolution of gridded air temperature) (Lembrechts *et al.*, 2020). We investigated the  
313 potential role of scale effects by comparing gridded air temperature data sources with  
314 different resolutions (ERA5L, TerraClimate and CHELSA, see below). Height effects and  
315 environmental effects are however not disentangled here, as the offset we propose  
316 incorporates both the difference between air and soil temperature (vertically), as well as the  
317 difference between free-air macroclimate and *in situ* microclimate (horizontally) in one  
318 measure (Lembrechts *et al.*, 2020). While it can be argued that it would be better to treat  
319 both vertical and horizontal effects separately, this would require a similar database of  
320 coupled *in-situ* air and soil temperature measurements, which is not yet available. Using *in*  
321 *situ* measured air temperature could also solve spatial mismatches (i.e., spatially averaged air  
322 temperature represents the whole 1 to 81 km<sup>2</sup> pixel, depending on pixel size, not only the  
323 exact location of the sensor). However, coupled air and soil temperature measurements are  
324 not only rare, but the air temperature measurements also have large measurement errors,

325 especially in open habitats. These errors can be up to several degrees in open habitats when  
326 using non-standardized sensors, loggers and shielding (Maclean *et al.*, 2021). Hence, using *in*  
327 *situ* measured air temperature without correcting for these measurement errors would be  
328 misleading.

### 329 ***Global and biome-level analyses***

330 For the purpose of visualization, annual offsets were first averaged in hexagons with a  
331 resolution of approximately 70 000 km<sup>2</sup>, using the dggridR-package in R (Barnes *et al.*, 2017)  
332 (Fig. 1). Next, we plotted mean, minimum and maximum annual soil temperature as a  
333 function of corresponding gridded air temperature from ERA5, TerraClimate and CHELSA and  
334 used generalized additive models (GAMs, package mgcv; Wood, 2012) to visualise deviations  
335 from the 1:1-line (i.e., temperature offsets deviating from zero, Supplementary Figs. S4-5).

336 All annual and monthly values within each soil depth category and falling within the same 1-  
337 km<sup>2</sup> pixel were aggregated as a mean, resulting in a total of c. 1200 unique pixels at 0–5 cm,  
338 and c. 1000 unique pixels at 5–15 cm each month, across the globe (Supplementary Material  
339 Table S3). This averaging includes summarizing the data over space, i.e., multiple sensors  
340 within the same 1-km<sup>2</sup> pixel, and time, i.e., data from multi-year time series from a certain  
341 sensor, to reduce spatial and temporal autocorrelation and sampling bias. We assigned these  
342 1-km<sup>2</sup> averages to the corresponding Whittaker biome of their georeferenced location, using  
343 the package *plotbiomes* in R (Fig. 1 c, d, Supplementary Material Table S4-5 (Stefan & Levin,  
344 2018)). We ranked biomes based on their offset and compared this with the mean annual  
345 precipitation in each biome (Fig. 1b). This was done separately for each air temperature data  
346 source (ERA5L, TerraClimate and CHELSA), soil depth (0–5 cm, 5–15 cm) and timeframe  
347 (ERA5L 1979–2020, 2000–2020), as well as for the offset between monthly minimum and  
348 maximum soil temperature and the minimum and maximum gridded air temperature from  
349 TerraClimate. Our analyses showed that patterns were robust to variation in spatial  
350 resolution, sensor depth, climate interpolation method and temporal scale (Supplementary  
351 Material Figs. S2–5).

### 352 ***Acquisition of global predictor variables***

353 To create spatial predictive models of the offset between *in-situ* soil temperature and gridded  
354 air temperature, we first sampled a stack of global map layers at each of the logger locations  
355 within the dataset. These layers included long-term macroclimatic conditions, soil texture and  
356 physiochemical information, vegetation, radiation and topographic indices as well as  
357 anthropogenic variables. Details of all layers, including descriptions, units, and source  
358 information, are described in Supplementary Data S1. In short, information about soil texture,  
359 structure and physiochemical properties was obtained from SoilGrids (version 1 (Hengl *et al.*,  
360 2017)), limited to the upper soil layer (top 5 cm). Long-term averages of macroclimatic  
361 conditions (i.e., monthly mean, maximum and minimum temperature, monthly precipitation)  
362 was obtained from CHELSA (version 2017 (Karger *et al.*, 2017a)), which includes climate data  
363 averaged across 1979–2013, and from WorldClim (version 2 (Fick & Hijmans, 2017)). Monthly  
364 snow probability is based on a pixel-wise frequency of snow occurrence (snow cover >10%)  
365 in MODIS daily snow cover products (MOD10A1 & MYD10A1 (Hall *et al.*, 2002)) in 2001–2019.  
366 Spectral vegetation indices (i.e., averaged MODIS NDVI product MYD13Q1) and surface  
367 reflectance data (i.e., MODIS MCD43A4) were obtained from the Google Earth Engine Data  
368 Catalog ([developers.google.com/earth-engine/datasets](https://developers.google.com/earth-engine/datasets)) and averaged from 2015 to 2019.  
369 Landcover and topographic information were obtained from EarthEnv (Amatulli *et al.*, 2018).  
370 Aridity index (AI) and potential evapotranspiration (PET) layers were obtained from CGIAR  
371 (Zomer *et al.*, 2008). Anthropogenic information (population density) was obtained from the  
372 EU JRC ([ghsl.jrc.ec.europa.eu/ghs\\_pop2019.php](https://ghsl.jrc.ec.europa.eu/ghs_pop2019.php)). Aboveground biomass data were obtained  
373 from GlobBiomass (Santoro, 2018). Resolved ecoregion classifications were used to  
374 categorize sampling locations into biomes (Dinerstein *et al.*, 2017). With this set of predictor  
375 variables, we included information on all different categories of drivers of soil temperature.  
376 An important variable that had to be excluded was snow depth, due to the lack of a relevant  
377 1-km<sup>2</sup> resolution global product. The final set of predictor variables included 24 ‘static’  
378 variables and eight monthly layers (i.e., maximum, mean and minimum temperature,  
379 precipitation, cloud cover, solar radiation, water vapour pressure, and snow cover). As cloud  
380 cover estimates were not available for high-latitude regions in the Northern Hemisphere in  
381 January and December due to a lack of daylight, we excluded cloud cover as an explanatory  
382 variable for these months (i.e., ‘EarthEnvCloudCover\_MODCF\_monthlymean\_XX’, with XX  
383 representing the months in two-digit form Supplementary Data S1).

384 All variable map layers were reprojected and resampled to a unified pixel grid in EPSG:4326  
385 (WGS84) at 30 arc-sec resolution ( $\approx 1 \times 1$  km at the equator). Areas covered by permanent  
386 snow or ice (e.g., the Greenland ice cap or glaciated mountain ranges, identified using  
387 SoilGrids) were excluded from the analyses. Antarctic sampling points were excluded from  
388 the modelling data set owing to the limited coverage of several covariate layers in the region.

### 389 ***Integrative modelling***

390 To generate global maps of monthly temperature offsets (Fig. 2), we trained random forest  
391 (RF) models for each month, using the temperature offsets as the response variables and the  
392 global variable layers as predictors. We used a geospatial RF modelling pipeline as developed  
393 by van den Hoogen *et al.* (2021). RF models are particularly valuable here due to their capacity  
394 to uncover nonlinear relationships (e.g., due to increased decoupling of soil from air  
395 temperature in colder and thus snow-covered areas) and their ability to capture complex  
396 interactions among covariates (e.g., between snow and vegetation cover) (Olden *et al.*, 2008).

397 We performed a grid search procedure to tune the RF models across a range of 122  
398 hyperparameter settings (variables per split: 2–12, minimum leaf population: 2–12). During  
399 this procedure, we assessed each model's performance using k-fold cross-validation (k = 10;  
400 folds assigned randomly, stratified per biome), for each of the 122 models. The models' mean  
401 and standard deviation values were the basis for choosing the best of all evaluated models.  
402 This procedure was repeated for each month separately for the two soil depth layers (0–5 cm,  
403 5–15 cm), for offsets in mean, minimum and maximum temperature. The importance of  
404 explanatory variables was assessed using the variable importance and ordered by mean  
405 variable importance across all models. This variable importance adds up the decreases in the  
406 impurity criterion (i.e., the measure on which the local optimal condition is chosen) at each  
407 split of a node for each individual variable over all trees in the forest (van den Hoogen *et al.*,  
408 2021).

### 409 ***Soil bioclimatic variables***

410 The resulting global maps of the annual and monthly offsets between mean, minimum and  
411 maximum soil and air temperature were used to calculate relevant bioclimatic variables  
412 following the definition used in CHELSA, BIOCLIM, ANUCLIM and WorldClim (Xu & Hutchinson,

413 2011, Booth *et al.*, 2014, Fick & Hijmans, 2017, Karger *et al.*, 2017a) (Fig. 3–4). We calculated  
 414 11 soil bioclimatic layers (SBIO, Table 1). First, we calculated monthly soil mean, maximum  
 415 and minimum temperature by adding monthly temperature offsets to the respective CHELSA  
 416 monthly mean, maximum and minimum temperature (Karger *et al.*, 2017a). Next, we used  
 417 these soil temperature layers to compute the SBIO layers (O’Donnell & Ignizio, 2012). Wettest  
 418 and driest quarters were identified for each pixel based on CHELSA’s monthly values.

419 **Table 1:** Overview of soil bioclimatic variables as calculated in this study.

<b>Bioclimatic variable</b>	<b>Meaning</b>
SBIO1	annual mean temperature
SBIO2	mean diurnal range (mean of monthly (max temp - min temp))
SBIO3	isothermality (SBIO2/SBIO7) (×100)
SBIO4	temperature seasonality (standard deviation ×100)
SBIO5	max temperature of warmest month
SBIO6	min temperature of coldest month
SBIO7	temperature annual range (SBIO5-SBIO6)
SBIO8	mean temperature of wettest quarter
SBIO9	mean temperature of driest quarter
SBIO10	mean temperature of warmest quarter
SBIO11	mean temperature of coldest quarter

420

421 ***Model uncertainty***

422 To assess the uncertainty in the monthly models, we performed a stratified bootstrapping  
 423 procedure, with total size of the bootstrap samples equal to the original training data (van  
 424 den Hoogen *et al.*, 2021). Using biomes as a stratification category, we ensured the samples  
 425 included in each of the bootstrap training collections were proportionally representative of  
 426 each biome’s total area. Next, we trained RF models (with the same hyperparameters as  
 427 selected during the grid-search procedure) using each of 100 bootstrap iterations. Each of  
 428 these trained RF models was then used to classify the covariate layer stack, to generate per-  
 429 pixel 95% confidence intervals and standard deviation for the modelled monthly offsets (Fig.  
 430 5a, Supplementary Material Fig. S6a). The mean R<sup>2</sup> value of the RF models for the monthly  
 431 mean temperature offset was 0.70 (from 0.64 to 0.78) at 0–5 cm and 0.76 (0.63–0.85) at 5 to

432 15 cm across all twelve monthly models. Mean RMSE of the models was 2.20°C (1.94–2.51°C)  
433 at 0–5 cm, and 2.06°C (1.67–2.35°C) at 5–15 cm.

434 Importantly, model uncertainty as reported in Fig. 5a and Supplementary Material Fig. S6a  
435 comes on top of existing uncertainties in (1) *in-situ* soil temperature measurements and (2)  
436 the ERA5L macroclimate models as used in our models. However, both of those are usually  
437 under 1°C (Copernicus Climate Change Service (C3S), 2019, Wild *et al.*, 2019).

438 To assess the spatial extent of extrapolation, which is necessary due to the incomplete global  
439 coverage of the training data, we first performed a Principal Component Analysis (PCA) on the  
440 full environmental space covered by the monthly training data, including all explanatory  
441 variables as used in the models, and then transformed the composite image into the same PC  
442 spaces as of the sampled data (Van Den Hoogen *et al.*, 2019). Next, we created convex hulls  
443 for each of the bivariate combinations from the first 10 to 12 PCs, covering at least 90% of the  
444 sample space variation, with the number of PCs depending on the month. Using the  
445 coordinates of these convex hulls, we assessed whether each pixel fell within or outside each  
446 of these convex hulls, and calculated the percentage of bivariate combinations for which this  
447 was the case (Fig. 5b, Supplementary Material Fig. S6b). This process was repeated for each  
448 month, and for each of the two soil depths separately.

449 These uncertainty maps are important because one should be careful with extrapolation  
450 beyond the range of conditions covered by the environmental variables included in the  
451 original calibration dataset, especially in the case of non-linear patterns such as modelled  
452 here. The maps are provided as spatial masks to remove or reduce the weighting of the pixels  
453 for which predictions are beyond the range of values covered by the models during  
454 calibration. To assess this further, we used a spatial leave-one-out cross-validation analysis to  
455 test for spatial autocorrelation in the data set (Supplementary Material Fig. S7) (van den  
456 Hoogen *et al.*, 2021). This approach trains a model for each sample in the data set on all  
457 remaining samples, excluding data points that fall within an increasingly large buffer around  
458 that focal sample. Results show lowest confidence for May to September at 5–15 cm, likely  
459 driven by uneven global coverage of data points.

460 Finally, we compared the modelled mean annual temperature (SBIO1, topsoil layer) with a  
461 similar product based on monthly ERA5L topsoil (0–7 cm) temperature with a spatial  
462 resolution of  $0.1 \times 0.1$  degrees (Copernicus Climate Change Service (C3S), 2019). The  
463 corresponding SBIO1 based on ERA5L was calculated using the means of the monthly  
464 averages for each month over the period 1981 to 2016, and averaging these 12 monthly  
465 values into one annual product. We then visualized spatial differences between SBIO1 and  
466 ERA5, as well as differences across the macroclimatic gradient, to identify mismatches  
467 between both datasets.

468 All geospatial modelling was performed using the Python API in Google Earth Engine (Gorelick  
469 *et al.*, 2017). The R statistical software, version 4.0.2 (R Core Team, 2020), was used for data  
470 visualisations. All maps were plotted using the Mollweide projection (which preserves relative  
471 areas) to avoid large distortions at high latitudes.

#### 472 ***Sources of uncertainty***

473 There is a temporal mismatch between the period covered by CHELSA (1979–2013) and our  
474 *in-situ* measurements (2000–2020), which prevented us from directly using CHELSA climate to  
475 calculate the temperature offsets used in our models. This temporal mismatch might affect  
476 the offsets calculated here because the relationship between temperature offset and  
477 macroclimate will change through time as the climate warms. However, we are confident that  
478 our results are sufficiently robust to withstand this mismatch, given that we found high  
479 consistency in offset patterns between the different timeframes and air temperature datasets  
480 examined (Supplementary Material Figs. S2–5). Nevertheless, we strongly urge future  
481 research to disentangle these potential temporal dynamics, especially given the increasing  
482 rate at which the climate is warming (Xu *et al.*, 2018, GISTEMP Team, 2021).

483 Similarly, a potential bias could result from the mismatch in method and resolution between  
484 ERA5L – used to calculate the temperature offsets – and CHELSA, which was used to create  
485 the bioclimatic variables. However, even though temperature offsets have slightly larger  
486 variation when based on the coarser-grained ERA5L-data than on the finer-grained CHELSA-  
487 data, Supplementary Material Figs. S2–5 show that relationships between soil and air  
488 temperature are largely consistent in all biomes and across the whole global temperature



489 gradient. Therefore, the larger offsets created additional random scatter, yet no consistent  
490 bias.

491 Finally, we acknowledge that the 1-km<sup>2</sup> resolution gridded products might not be  
492 representative of conditions at the *in-situ* measurement locations within each pixel. This issue  
493 could be particularly significant for different vegetation types (here proxied at the pixel level  
494 using total aboveground biomass (unit: tons/ha i.e., Mg/ha, for the year 2010; Santoro, 2018)  
495 and NDVI (MODIS NDVI product MYD13Q1, averaged over 2015–2019)). To verify this, we  
496 compared a pixel's estimated aboveground biomass with the dominant *in-situ* habitat (forest  
497 versus open) surrounding the sensors in that pixel (Supplementary Table S6). Importantly, all  
498 sensors installed in forests fell indeed in pixels with more than 1 ton/ha aboveground  
499 biomass. Similarly, 75% or more of sensors in open terrain fell in pixels with biomass estimates  
500 of less than 1 ton/ha. Only in the temperate woodland biome was the match between *in-situ*  
501 habitat estimates and pixel-level aboveground biomass lower, with less than 95% of sensors  
502 in forested locations correctly placed in pixels with more than 1 ton/ha biomass, and less than  
503 50% of open terrain sensors in pixels with less than 1 ton/ha biomass. While our predictions  
504 will thus not be accurate for locations within a pixel that largely deviate from average  
505 conditions (e.g., open terrain in pixels identified as largely forested, or vice versa), they should  
506 be largely representative for those pixel-level averages.

## 507 **Results**

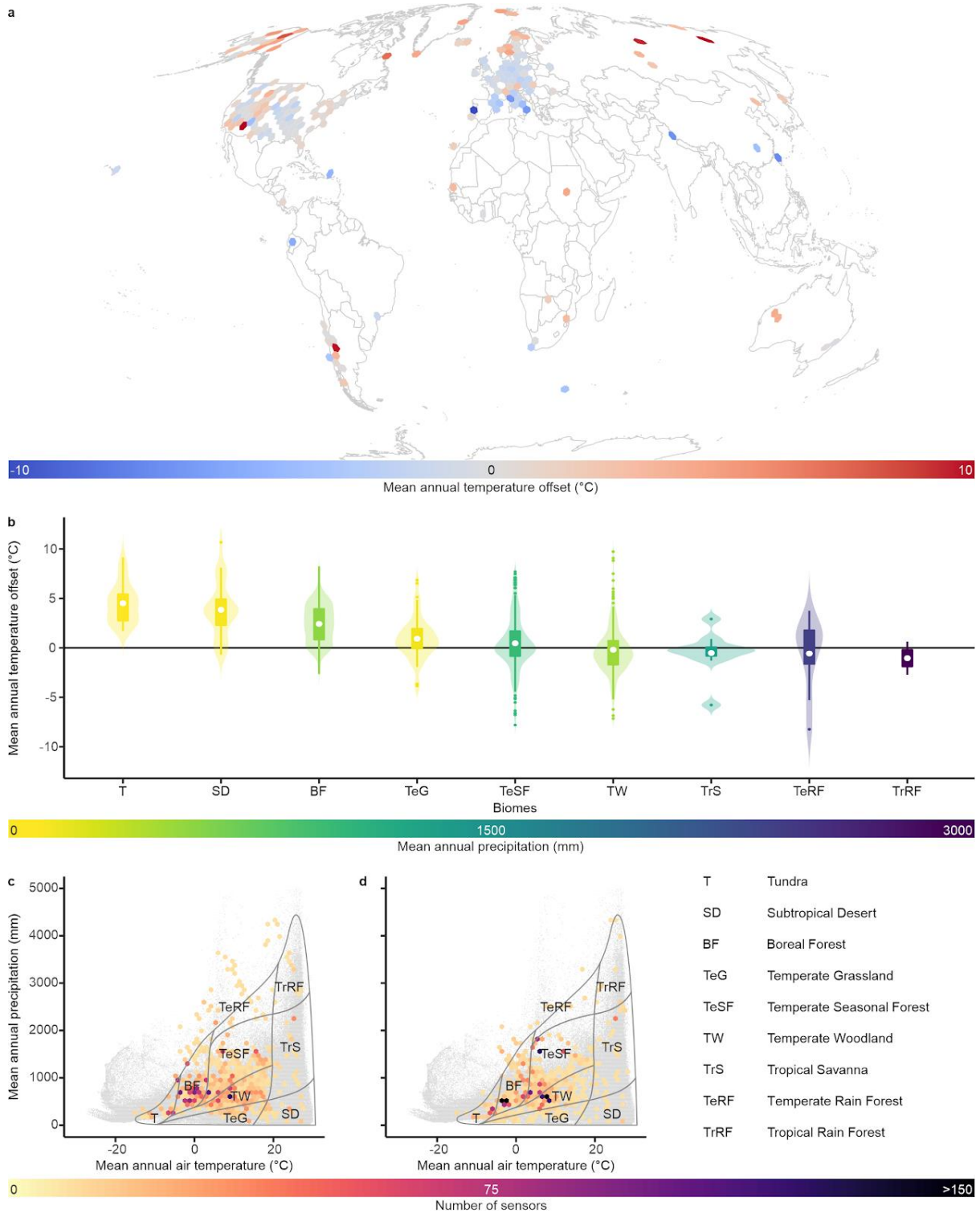
### 508 ***Biome-wide patterns in the temperature offset***

509 We found positive and negative temperature offsets of up to 10°C between *in situ* measured  
510 mean annual topsoil temperature and gridded air temperature (mean =  $3.0 \pm 2.1^\circ\text{C}$  standard  
511 deviation, Fig. 1, 0–5 cm depth; 5–15 cm is available in Supplementary Material Figs. S2, 5).  
512 The magnitude and direction of these temperature offsets varied considerably within and  
513 across biomes. Mean annual topsoil temperature was on average  $3.6 \pm 2.3^\circ\text{C}$  higher than  
514 gridded air temperature in cold and/or dry biomes, namely tundra, boreal forests, temperate  
515 grasslands and subtropical deserts. In contrast, offsets were slightly negative in warm and wet  
516 biomes (tropical savannas, temperate forests and tropical rainforests) where soils were, on  
517 average,  $0.7 \pm 2.7^\circ\text{C}$  cooler than gridded air temperature (Fig. 1b, Supplementary Material

518 Figs. S2 and 5; note, however, the lower spatial coverage in these biomes in Fig. 1a, c, d,  
519 Supplementary Material Table S4). Temperature offsets in annual minimum and maximum  
520 temperature amounted to c. 10°C maximum. While annual soil temperature minima were on  
521 average higher than corresponding gridded air temperature minima in all biomes,  
522 temperature offsets of annual maxima followed largely the same biome-related trends as  
523 seen for the annual means, albeit with the higher variability expected for temperature  
524 extremes (Supplementary Material Figs. S2g, h, S4g, h). Using different air temperature data  
525 sources did not alter the annual temperature offset and biome-related patterns (see Methods  
526 and Supplementary Material Figs. S2–5).

527 Soils in the temperate seasonal forest biome were on average 0.8°C ( $\pm$  2.2°C) cooler than air  
528 temperature within 1-km<sup>2</sup> grid cells of forested habitats, and 1.0°C ( $\pm$  4.0°C) warmer than the  
529 air within 1-km<sup>2</sup> grid cells of non-forested habitats, resulting in a biome-wide average of 0.5°C  
530 (Supplementary Material Table S7). Similar patterns were observed in other biomes.

531



532

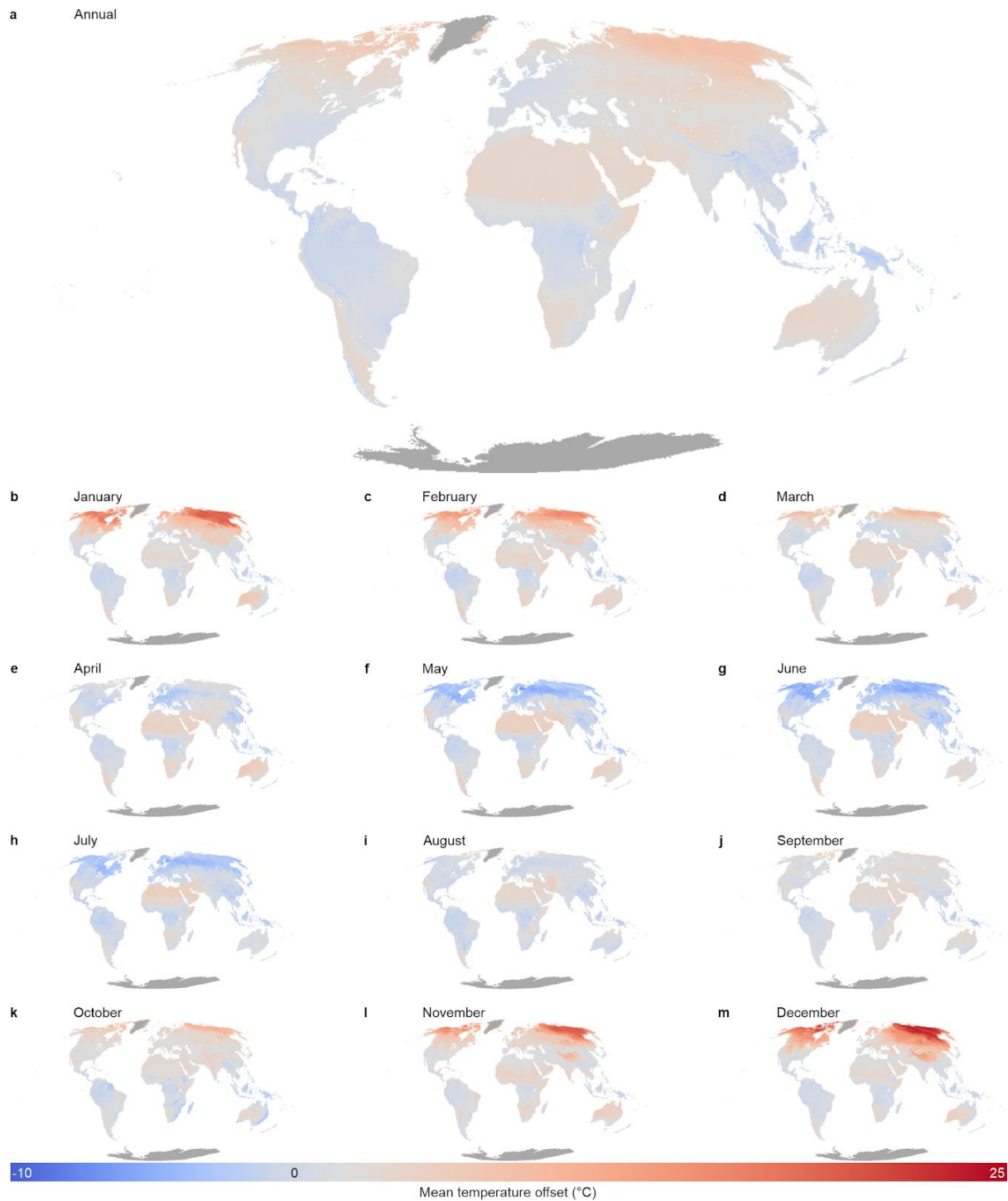
533 **Figure 1: Temperature offsets between soil and air temperature differed significantly among**  
 534 **biomes.** (a) Distribution of in-situ measurement locations across the globe, coloured by the mean  
 535 annual temperature offset (in °C) between in situ measured soil temperature (topsoil, 0–5 cm depth)  
 536 and gridded air temperature (ERA5L). Offsets were averaged per hexagon, each with a size of  
 537 approximately 70,000 km<sup>2</sup>. Mollweide projection. (b) Mean annual temperature offsets per Whittaker  
 538 biome (adapted from Whittaker 1970, based on geographic location of sensors averaged at 1 km<sup>2</sup>; 0–  
 539 5 cm depth), ordered by mean temperature offset and coloured by mean annual precipitation. (c–d)  
 540 Distribution of sensors in 2D climate space for the topsoil (c, 0–5 cm depth, N = 4530) and the second

541 *layer (d, 5–15 cm depth, N = 3989). Colours of hexagons indicate the number of sensors at each climatic*  
542 *location, with a 40 × 40 km resolution. Grey dots in the background represent the global variation in*  
543 *climatic space (obtained by sampling 1 000 000 random locations from the CHELSA world maps).*  
544 *Overlay with grey lines depicts a delineation of Whittaker biomes.*

#### 545 ***Temporal and spatial variation in temperature offsets***

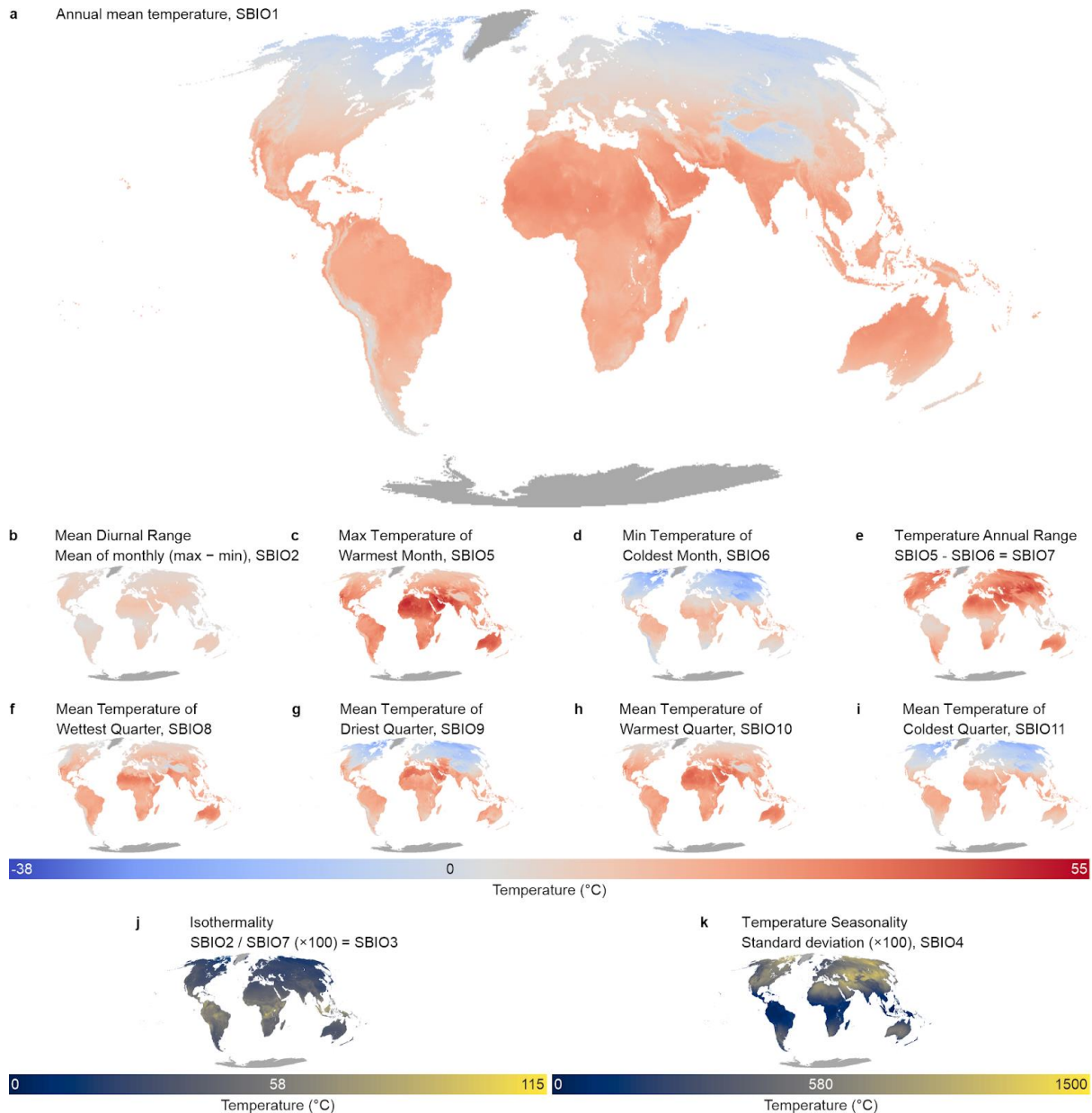
546 Our random forest modelling approach highlighted a strong seasonality in monthly  
547 temperature offsets, especially towards higher latitudes (Fig. 2). High-latitude soils were  
548 found to be several degrees warmer than the air (monthly offsets of up to 25°C) during their  
549 respective winter months, and cooler (up to 10°C) in summer months, both at 0–5 cm (Fig. 2)  
550 and 5–15 cm (Supplementary Material Fig. S8) soil depths. In the tropics and subtropics, soils  
551 in dry biomes (e.g., in the Sahara desert or southern Africa) were predicted to be warmer than  
552 air throughout most of the year, whilst soils in mesic biomes (e.g., tropical biomes in South  
553 America, central Africa and Southeast Asia) were modelled to be consistently cooler, at both  
554 soil depths. These global gridded products were then used to create temperature-based  
555 global bioclimatic variables for soils (SBIO, Fig. 3, Supplementary Material Fig. S9).

556



557

558 **Figure 2: Global modelled temperature offsets between soil and air temperature show strong**  
 559 **spatiotemporal variation across months.** Modelled annual (a) and monthly (b–m) temperature offset  
 560 (in °C) between in situ measured soil temperature (topsoil, 0–5 cm) and gridded air temperature.  
 561 Positive (red) values indicate soils that are warmer than the air. Dark grey represents regions outside  
 562 the modelling area.



564

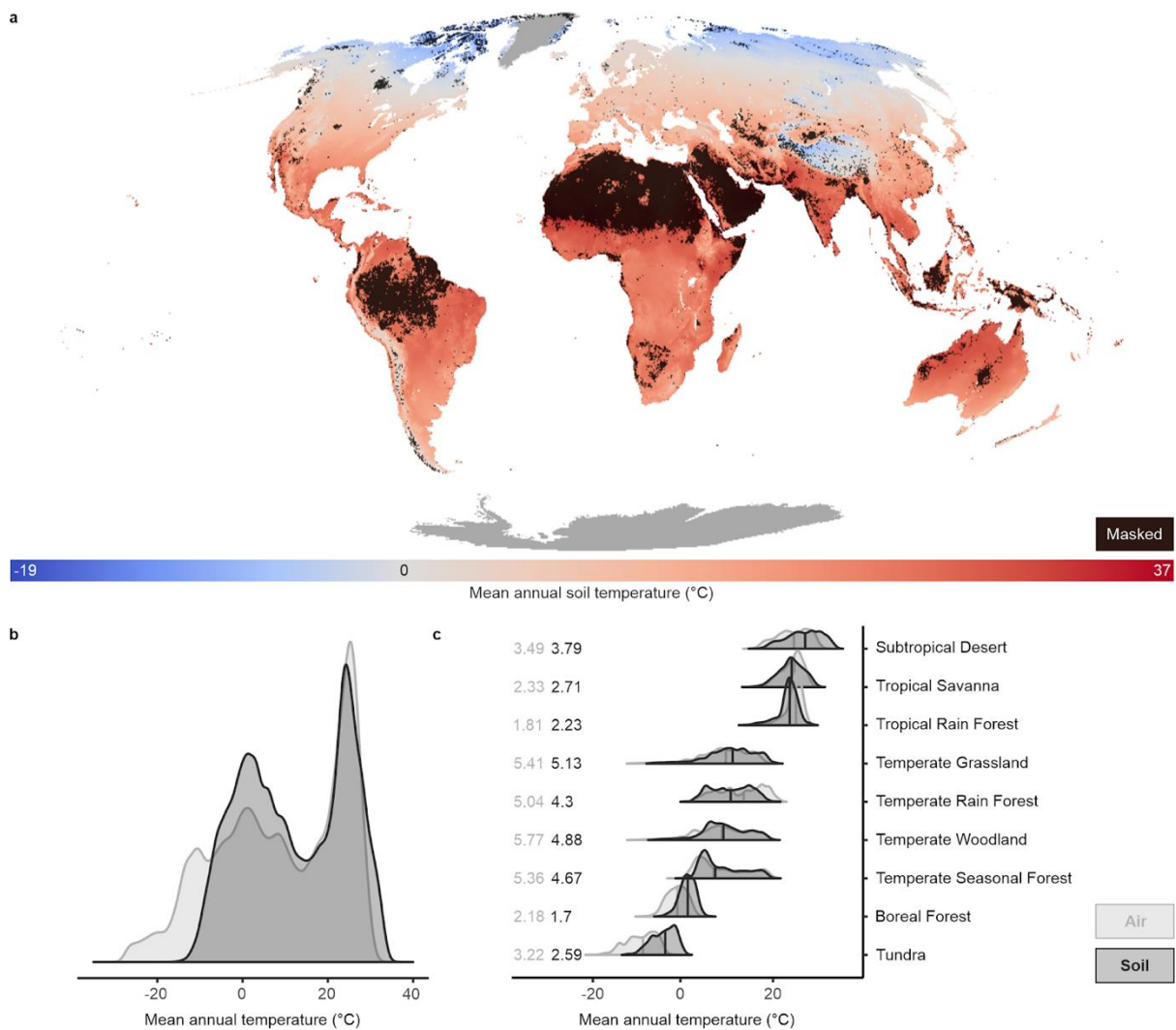
565 **Figure 3: Soil bioclimatic variables.** Global maps of bioclimatic variables for topsoil (0–5 cm depth)  
 566 climate, calculated using the maps of monthly soil climate (see Fig. 2), and the bioclimatic variables for  
 567 air temperature from CHELSA.

568

569 **Global variation in soil temperature**

570 We observed 17% less spatial variation in mean annual soil temperature globally (expressed  
 571 by the standard deviation) than in air temperature, largely driven by the positive offset  
 572 between soil and air temperature in cold environments (Fig. 4). Importantly, our machine  
 573 learning models slightly (up to 1°C, or around 10% of variation) underestimated temperature

574 offsets at both extremes of the temperature gradient at the 1-km<sup>2</sup> resolution (Supplementary  
 575 Material Fig. S10) and likely even more in comparison with finer-resolution products.  
 576 Estimates of the reduction in variation across space are thus conservative, especially in the  
 577 coldest biomes. The reduction in spatial temperature variation was observed in all cold and  
 578 cool biomes, with tundra and boreal forests having both a significant positive mean  
 579 temperature offset and a reduction of 20% and 22% in variation, respectively (Fig. 4c). In the  
 580 warmest biomes (e.g., tropical savanna and subtropical desert), however, we found an  
 581 increase in variation of, on average, 10%.



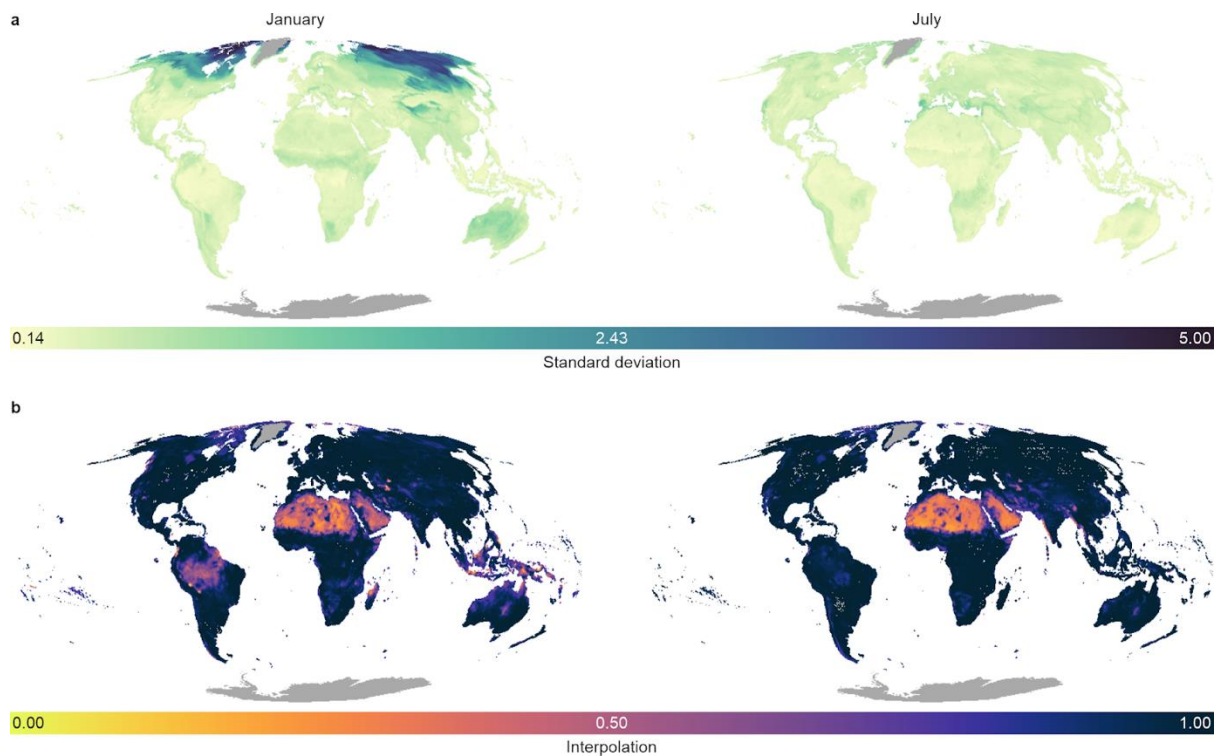
582

583 **Figure 4: Mean annual soil temperature shows significantly lower spatial variability than air**  
 584 **temperature.** (a) Global map of mean annual topsoil temperature (SBIO1, 0–5 cm depth, in °C), created  
 585 by adding the monthly offset between soil and air temperature for the period 2000–2020 (Fig. 2) to  
 586 the monthly air temperature from CHELSA. A black mask is used to exclude regions where our models  
 587 are extrapolating (i.e., interpolation values in Fig. 5 are < 0.9, 18% of pixels). Dark grey represents  
 588 regions outside the modelling area. (b–c) Density plots of mean annual soil temperature across the  
 589 globe (b) and for each Whittaker biome separately (c) for SBIO1 (dark grey, soil temperature),



590 compared with BIO1 from CHELSA (light grey, air temperature), created by extracting 1 000 000  
 591 random points from the 1-km<sup>2</sup> gridded bioclimatic products. The numbers in (c) represent the standard  
 592 deviations of air temperature (light grey) and soil temperature (dark grey). Biomes are ordered  
 593 according to the median annual soil temperature values from the highest temperature (subtropical  
 594 desert) to the lowest (tundra).

595 Our bootstrap approach to validate modelled monthly offsets indicated high consistency  
 596 among the outcomes of 100 bootstrapped models (Fig. 5, Supplementary Material Fig. S6a),  
 597 with standard deviations in most months and across most parts of the globe around or below  
 598  $\pm 1^\circ\text{C}$ . One exception to this was the temperature offset at high latitudes of the northern  
 599 hemisphere during winter months (standard deviation up to  $\pm 5^\circ\text{C}$  in the 0–5 cm layer).  
 600 Predictive performance was comparable across biomes, although with large variation in data  
 601 availability (Supplementary Material Fig. S11).



602

603 **Figure 5: Models of the temperature offset between soil and air temperature have low standard**  
 604 **deviations and good global coverage.** Analyses for the temperature offset between in situ measured  
 605 topsoil (0–5 cm depth) temperature and gridded air temperature. (a) Standard deviation (in  $^\circ\text{C}$ ) over  
 606 the predictions from a cross-validation analysis that iteratively varied the set of covariates  
 607 (explanatory data layers) and model hyperparameters across 100 models and evaluated model  
 608 strength using 10-fold cross-validation, for January (left) and July (right), as examples of the two most  
 609 contrasting months. (b) The fraction of axes in the multidimensional environmental space for which  
 610 the pixel lies inside the range of data covered by the sensors in the database. Low values indicate  
 611 increased extrapolation.

612

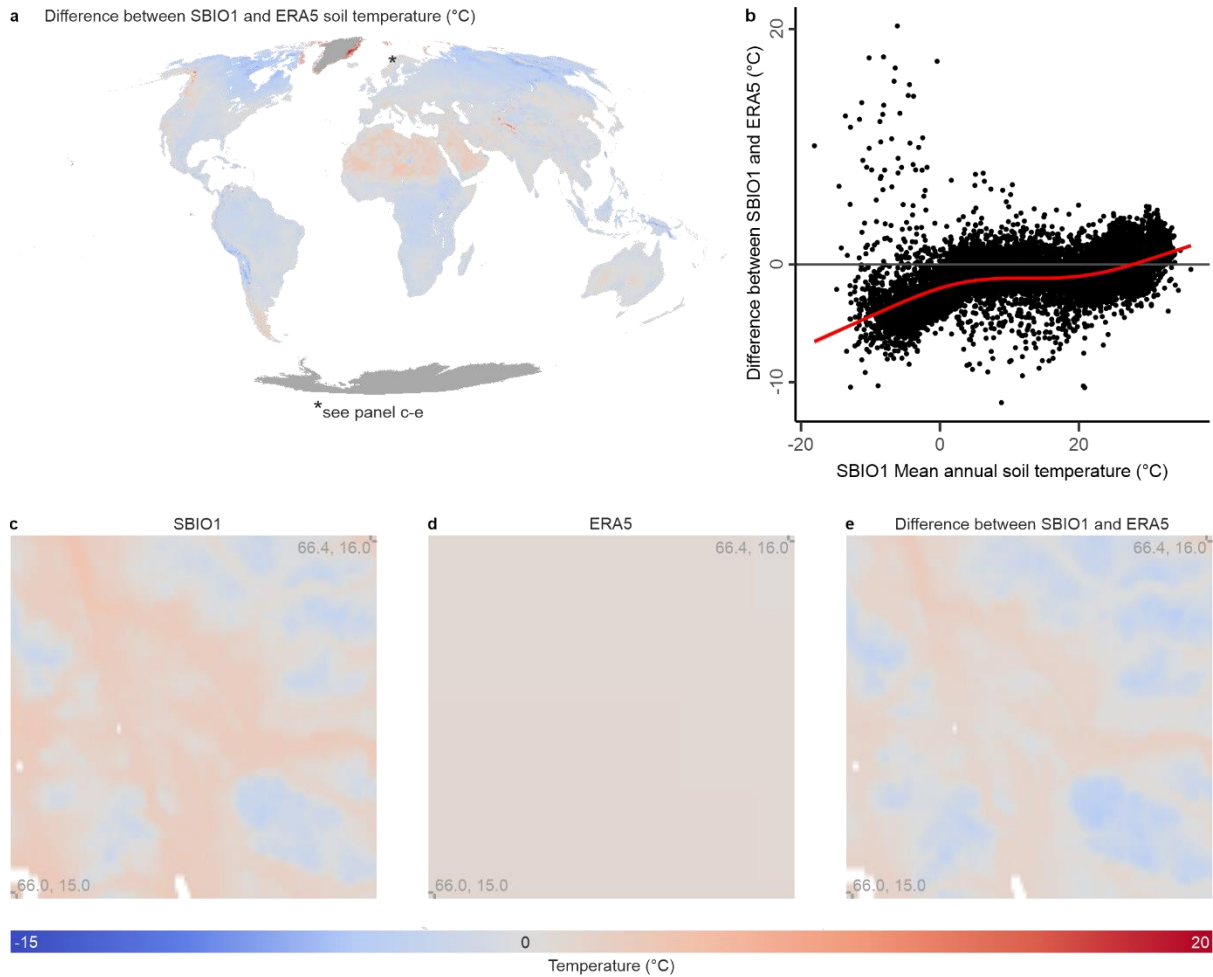
613



614 The importance of explanatory variables in the RF models was largely consistent across  
615 months. Macroclimatic variables such as incoming solar radiation as well as long-term  
616 averages in air temperature and precipitation were by far the most influential explanatory  
617 variables in the spatial models of the monthly temperature offset (Supplementary Material  
618 Figs. S12, 13).

619 We highlight that the current availability of *in-situ* soil temperature measurements is  
620 significantly lower in the tropics (Supplementary Material Table S5), where our model had to  
621 extrapolate temperatures beyond the range used to calibrate the model (Fig. 5b,  
622 Supplementary Material Fig. S6b).

623 Finally, our comparison with a mean annual soil temperature product derived from the  
624 coarse-resolution ERA5L topsoil temperature showed that spatial variability, e.g., driven by  
625 topographic heterogeneity, is much better captured here than in the coarser resolution of the  
626 ERA5L-based product (Fig. 6c-e). Nevertheless, our predictions at the coarse scale showed to  
627 be condensed within a 5°C range of values from the ERA5L-predictions, for more than 95% of  
628 pixels globally. Noteworthy, our predictions resulted in consistently cooler soil temperature  
629 predictions than topsoil conditions provided by ERA5L across large areas, such as the boreal  
630 and tropical forest biomes (Fig. 6a, b). Additionally, our models predicted lower values for  
631 SBIO1 than ERA5L in all regions with mean annual soil temperature below 0°C, except for a  
632 few locations around Greenland and Svalbard (Fig. 6a, b).



633

634 **Figure 6: The mean annual soil temperature (SBIO1, 1 x 1 km resolution) modelled here is**  
 635 **consistently cooler than ERA5L (9 x 9 km) soil temperature in forested areas.** (a) Spatial  
 636 representation of the difference between SBIO1 based on our model and based on ERA5L soil  
 637 temperature data. Negative values (blue colours) indicate areas where our model predicts cooler soil  
 638 temperature. Dark grey areas (Greenland and Antarctica) are excluded from our models. Asterisk in  
 639 Scandinavia indicates the highlighted area in panels d to f (see below). (b) Distribution of the difference  
 640 between SBIO1 and ERA5L along the macroclimatic gradient (represented by SBIO1 itself) based on a  
 641 random subsample of 50 000 points from the map in a). Red line from a Generalized Additive Model  
 642 (GAM) with  $k=4$ . (c-e) High-resolution zoomed panels of an area of high elevational contrast in Norway  
 643 (from 66.0-66.4° N, 15.0-16.0° E) visualizing SBIO1 (c), ERA5L (d) and their difference (e), to highlight  
 644 the higher spatial resolution as obtained with SBIO1.

645

## 646 **Discussion**

### 647 ***Global patterns in soil temperature***

648 We observed large spatiotemporal heterogeneity in the global offset between soil and air  
649 temperature, often in the order of several degrees annually and up to more than 20°C during  
650 winter months at high latitudes. These values are in line with empirical data from regional  
651 studies (Zhang *et al.*, 2018, Lembrechts *et al.*, 2019, Obu *et al.*, 2019). Both annual and  
652 monthly offsets showed clear discrepancies between cold and dry versus warm and wet  
653 biomes. The modelled monthly offsets covaried strongly negatively with both long-term  
654 averages in free-air temperature and solar radiation, linking to the well-known decoupling of  
655 soil from air temperature due to snow (for cold extremes in cold and cool biomes) (Grundstein  
656 *et al.*, 2005). However, the secondary importance of variables related to precipitation and soil  
657 structure hints to the additional distinction between wet and dry biomes at the warm end of  
658 the temperature gradient, where buffering due to shading, evapotranspiration and the  
659 specific heat of water (mostly against warm extremes in warm and wet biomes) results in  
660 cooler soil temperature (Geiger, 1950, Grundstein *et al.*, 2005, Hennon *et al.*, 2010, Wang &  
661 Dickinson, 2012, De Frenne *et al.*, 2013, Grünberg *et al.*, 2020), a less important process in  
662 warm and dry biomes (Wang & Dickinson, 2012, Greiser *et al.*, 2018, Zhou *et al.*, 2021). As  
663 such, these results highlight strong macroclimatic impacts on the soil microclimate across the  
664 globe (see also De Frenne *et al.*, 2019), yet with soil temperature importantly non-linearly  
665 related to air temperature at the global scale. This confirms that the latter is not sufficient as  
666 a proxy for temperature conditions near or in the soil. With our soil-specific global bioclimatic  
667 products, we have provided the means to correct for these important region-specific, non-  
668 linear differences between soil and air temperature at an unprecedented spatial resolution.

### 669 ***Drivers of the temperature offset***

670 Our empirical modelling approach enabled us to accurately map global patterns in soil  
671 temperature. In doing so we did not aim to disentangle the mechanisms governing the  
672 temperature offset: such an endeavour would require modelling the biophysics of energy  
673 exchange at the soil surface across biomes (Kearney *et al.*, 2019, Maclean *et al.*, 2019,  
674 Maclean & Klings, 2021). Importantly, many of the predictor variables used in our study (e.g.,  
675 long-term averages in macroclimatic conditions or solar radiation) are unlikely to represent

676 direct causal relationships underlying the temperature offset, but may rather indirectly relate  
677 to many ensuing factors that affect the functioning of ecosystems at fine spatial scales which,  
678 in turn, feedback on local temperature offsets, such as energy and water balances, snow  
679 cover, wind intensity and vegetation cover (De Frenne *et al.*, 2021). For example, while  
680 increased solar radiation itself would theoretically result in soils warming more than the air,  
681 high solar radiation at the global scale often coincides with high vegetation cover blocking  
682 radiation input to the soil, thus correlating with relatively cooler soils (De Frenne *et al.*, 2021).  
683 Our results highlight, however, that the complex relationship between microclimatic soil  
684 temperature and macroclimatic air temperature is predictable across large spatial extents  
685 thanks to broad scale patterns, even if this is governed by a multitude of local-scale factors  
686 involving fine spatiotemporal resolutions. Nevertheless, the predictive quality of our models  
687 was lower in high latitude regions, where high variation in the *in situ* measured offsets – likely  
688 driven by the interactions between snow, local topography and vegetation – reduced  
689 predictive power of the models at the 1-km<sup>2</sup> resolution (Greiser *et al.*, 2018, Way &  
690 Lewkowicz, 2018, Grünberg *et al.*, 2020, Myers-Smith *et al.*, 2020, Niittyinen *et al.*, 2020).

#### 691 **Implications for microclimate warming**

692 Our results highlight clear biome-specific differences in mean annual temperature between  
693 air and soil temperatures, as well as a significant reduction in the spatial variation in  
694 temperature in the soil or near the soil surface, especially in cold and cool biomes (Fig. 4).  
695 These patterns remain even despite the presence of often strongly opposing monthly offset  
696 trends (Fig. 2). The observed correlation between long-term averages in macroclimatic  
697 conditions and the annual temperature offset illustrates that soil temperature is unlikely to  
698 warm at the same rate as air temperature when macroclimate warms. Indeed, one degree of  
699 air temperature warming could result in either a bigger or smaller soil temperature change,  
700 depending on where along the macroclimatic gradient this is happening. These effects might  
701 be seen in cold biome soils most strongly, as they not only experience the largest (positive)  
702 temperature offsets and reductions in climate range compared to air temperature (Fig. 4b, c),  
703 but they are also expected to experience the strongest magnitude of macroclimate warming  
704 (Cooper, 2014, Overland *et al.*, 2014, Chen *et al.*, 2021, GISTEMP Team, 2021). As a result,  
705 mean annual temperatures in cold climate soils can be expected to warm slower than the  
706 corresponding macroclimate as offsets shrink with increasing macroclimate warming.

707 Contrastingly, predicted climate warming in hot and dry biomes could be amplified in the  
708 topsoil, where we show soils to become increasingly warmer than the air at higher  
709 temperatures. Similarly, changes in precipitation regimes – and thus soil moisture – can  
710 significantly alter the relationship between air and soil temperature, with critical implications  
711 for soil moisture-atmosphere feedbacks, especially in hot biomes (Zhou *et al.*, 2021). Indeed,  
712 as precipitation decreases, offsets could turn more positive and soil temperatures might  
713 warm even faster than the observed macroclimate warming. Therefore, future research  
714 should not only use soil temperature data as provided here to study belowground ecological  
715 processes (De Frenne *et al.*, 2013, Lembrechts *et al.*, 2020), it should also urgently investigate  
716 future scenarios of soil climate warming in light of changing air temperature and precipitation,  
717 at ecologically relevant spatial and temporal resolutions to incorporate the non-linear  
718 relationships exposed so far (Lembrechts & Nijs, 2020).

#### 719 **Within-pixel heterogeneity**

720 We chose to use a 1-km<sup>2</sup> resolution spatial grid to model mismatches between soil and air  
721 temperature, aggregating all values from different microhabitats within the same 1-km<sup>2</sup> grid  
722 cell (e.g., sensors in forested versus open patches) as well as all daily and diurnal variation  
723 within a month. We are aware that higher spatiotemporal resolutions would likely reveal the  
724 importance of locally heterogeneous variables. Finer-scale factors that affect the local  
725 radiation balance and wind (e.g., topography, snow and vegetation cover, urbanization) at  
726 the landscape to local scales and those that directly affect neighbouring locations (e.g.  
727 topographic shading and cold-air drainage, Whiteman, 1982, Ashcroft & Gollan, 2012,  
728 Lembrechts *et al.*, 2020) would probably have emerged as more important drivers at regional  
729 scales and with higher spatiotemporal resolutions than those used here (Supplementary  
730 Material Fig. S12). The latter is illustrated by the multi-degree Celsius difference in mean  
731 annual temperature between forested and non-forested locations within the same biome  
732 (Supplementary Material Table S7), as well as the lower accuracy obtained during winter  
733 months at high latitudes, where and when fine-scale spatial heterogeneity in snow cover and  
734 depth probably lowers models' predictability at the 1-km<sup>2</sup> resolution. *In-situ* measurements  
735 were largely from areas with a representative vegetation type, supporting the reliability of  
736 our predictions for the dominant habitat type within a pixel. However, improved accuracy at

737 high latitudes will depend on the future development of high-resolution snow depth and/or  
738 snow water equivalent estimates (Luojus *et al.*, 2010).

739 The SoilTemp database (Lembrechts *et al.*, 2020) will facilitate the necessary steps towards  
740 mapping soil temperature at higher spatiotemporal resolutions in the future, with its  
741 georeferenced time series of *in situ* measured soil and near-surface temperature and  
742 associated metadata. Nevertheless, when compared to existing soil temperature products  
743 such as those from ERA5L (Copernicus Climate Change Service (C3S), 2019), we emphasize  
744 that the increased resolution of our data products already provides a major technical  
745 advance, even though substantial finer within-pixel variation is still lost through  
746 spatiotemporal aggregation.

## 747 **Conclusions**

748 The spatial (biome-specific) and temporal (seasonally variable) offsets between air and soil  
749 temperature quantified here likely bias predictions of current and future climate impacts on  
750 species and ecosystems (Körner & Paulsen, 2004, Kearney *et al.*, 2009, Cooper, 2014, Opedal  
751 *et al.*, 2015, Graae *et al.*, 2018, Zellweger *et al.*, 2020, Bergstrom *et al.*, 2021). Temperature  
752 in the topsoil rather than in the air ultimately defines the distribution and performance of  
753 most terrestrial species, as well as many ecosystem functions at or below the soil surface  
754 (Pleim & Gilliam, 2009, Portillo-Estrada *et al.*, 2016, Hursh *et al.*, 2017, Gottschall *et al.*, 2019).  
755 As many ecosystem functions are highly correlated with temperature (yet often non-linear,  
756 Johnston *et al.*, 2021), soil temperature rather than air temperature should in those instances  
757 be the preferred predictor for estimating their rates and temperature thresholds (Rosenberg  
758 *et al.*, 1990, Coûteaux *et al.*, 1995, Schimel *et al.*, 1996). Correcting for the non-linear  
759 relationship between air and soil temperature identified here is thus vital for all fields  
760 investigating abiotic and biotic processes relating to terrestrial environments (White *et al.*,  
761 2020). Indeed, soil temperature, macroclimate and land-use change will interact to define the  
762 future climate as experienced by organisms, and high-resolution soil temperature data is  
763 needed to tackle current and future challenges.

764 By making our global soil temperature maps and the underlying monthly offset data openly  
765 available, we offer gridded soil temperature data for climate research, ecology, agronomy  
766 and other life and environmental sciences. Future research has the important task of further

767 improving the spatial and temporal resolution of global microclimate products as  
768 microclimate operates at much higher temporal resolutions, with temporal variation over  
769 hours, days, seasons and years (Potter *et al.*, 2013, Bütikofer *et al.*, 2020), as well as to confirm  
770 accuracy of predictions in undersampled regions in the underlying maps (Lembrechts *et al.*,  
771 2021). However, we are convinced that the maps presented here bring us one step closer to  
772 having accessible climate data exactly where it matters most for many terrestrial organisms  
773 (Ashcroft *et al.*, 2014, Niittyinen & Luoto, 2018, Lembrechts & Lenoir, 2019). We nevertheless  
774 highlight that there is still a long way to go towards global soil microclimate data with an  
775 optimal spatiotemporal resolution. We therefore urge all scientists to submit their  
776 microclimate time series to the SoilTemp database to fill data gaps and help to increase the  
777 spatial resolution until it matches with the scale at which ecological processes take place  
778 (Bütikofer *et al.*, 2020, Lembrechts *et al.*, 2020).

779

## 780 **Data availability**

781 All monthly data to train the models and reproduce the figures, sampled covariate data, and  
782 models are available at <https://doi.org/10.5281/zenodo.4558663>. Soil bioclim layers SBIO1-  
783 11 are also directly available in Google Earth Engine under  
784 projects/crowtherlab/soil\_bioclim/soil\_bioclim\_0\_5cm and  
785 projects/crowtherlab/soil\_bioclim/soil\_bioclim\_5\_15cm.

786

## 787 **Code availability**

788 All source code is available at <https://doi.org/10.5281/zenodo.4558663>.

789

## 790 **Acknowledgements**

791 JLL received funding from the Research Foundation Flanders (grant nr. 12P1819N) The project received funding from the Research  
792 Foundation Flanders (grants nrs, G018919N, W001919N). JA received funding from the University of Helsinki, Faculty of Science  
793 (MICROCLIM, grant nr. 7510145) and Academy of Finland Flagship (grant no. 337552). PDF, CM and PV received funding from the  
794 European Research Council (ERC) under the European Union's Horizon 2020 research and innovation programme (ERC Starting Grant  
795 FORMICA 757833). JK received funding from the Arctic Interactions at the University of Oulu and Academy of Finland (318930, Profi 4),  
796 Maa- ja vesitekniikan tuki ry., Tiina and Antti Herlin Foundation, Nordenskiöld Samfundet and Societas pro Fauna et Flora Fennica. MK  
797 received funding from the Czech Science Foundation (grant nr. 20-28119S) and the Czech Academy of Sciences (grant nr. RVO 67985939).  
798 TC received funding from DOB Ecology. National Geographic Society grant no. 9480-14 and WW-240R-17. MA received funding from CISSC  
799 (program ICRP (grant nr:2397) and INSF (grant nr: 96005914). The Royal Botanic Garden Edinburgh is supported by the Scottish  
800 Government's Rural and Environment Science and Analytical Services Division. JMA received funding from the Funding Org. Qatar

801 Petroleum (grant nr. QUEx-CAS-QP-RD-18/19). JMA received funding from the European Union's Horizon 2020 research and innovation  
802 program (grant no. 678841) and from the Swiss National Science Foundation (grant no. 31003A\_176044). JA was supported by research  
803 grants LTAUSA19137 (program INTER-EXCELLENCE, subprogram INTER-ACTION) provided by Czech Ministry of Education, Youth and Sports  
804 and 20-05840Y of the Czech Science Foundation. AA was supported by the Ministry of Science and Higher Education of the Russian  
805 Federation (grant FSRZ-2020-0014). SN, UAT, JJA, and JvO received funding from the Independent Research Fund Denmark (7027-00133B).  
806 LvdB, KT, MYB and RC acknowledge funding from the German Research Foundation within the Priority Program SPP-1803 "EarthShape:  
807 Earth Surface Shaping by Biota" (grant TI 338/14-1&2 and BA 3843/6-1). PB was supported by grant project VEGA of the Ministry of  
808 Education of the Slovak Republic and the Slovak Academy of Sciences No. 2/0132/18. Forest Research received funding from the Forestry  
809 Commission (climate change research programme). JCB acknowledges the support of Universidad Javeriana. JLBA received funding from  
810 the Dirección General de Cambio Climático del Gobierno de Aragón; JLBA acknowledges fieldwork assistance by Ana Acín, the Ordesa y  
811 Monte Perdido National Park, and the Servicio de Medio Ambiente de Soria de la Junta de Castilla y León. RGB and MPB received funding  
812 from BECC - Biodiversity and Ecosystem services in a Changing Climate. MPB received funding from The European Union's Horizon 2020  
813 research and innovation program under the Marie Skłodowska-Curie Grant Agreement No. 657627 and The Swedish Research Council  
814 FORMAS – future research leaders No. 2016-01187. JB received funding from the Czech Academy of Sciences (grant nr. RVO 67985939).  
815 NB received funding from the SNF (grant numbers 40FA40\_154245, 20FI21\_148992, 20FI20\_173691, 407340\_172433) and from the EU  
816 (contract no. 774124). ICOS EU research infrastructure. EU FP7 NitroEurope. EU FP7 ECLAIRE. The authors from Biological Dynamics of  
817 Forest Fragments Project, PDBFF, Instituto Nacional de Pesquisas da Amazônia, Brazil were supported by the MCTI/CNPq/FNDCT – Ação  
818 Transversal n°68/2013 – Programa de Grande Escala da Biosfera-Atmosfera na Amazônia – LBA; Project "Como as florestas da Amazônia  
819 Central respondem às variações climáticas? Efeitos sobre dinâmica florestal e sinergia com a fragmentação florestal." to The EUCFLUX  
820 Cooperative Research Program and Forest Science and Research Institute-IPEF. NC acknowledges funding by Stelvio National Park. JC was  
821 funded by the Spanish government grant CGL2016-78093-R. ANID-FONDECYT 1181745 AND INSTITUTO ANTARTICO CHILENO (INACH FR-  
822 0418). SC received funding from the German Research Foundation (grant no. DFG– FZT 118, 202548816). The National Science Foundation,  
823 Poland (grant no. UMO-2017/27/B/ST10/02228), within the framework of the "Carbon dioxide uptake potential of sphagnum peatlands in  
824 the context of atmospheric optical parameters and climate changes"(KUSCO2) project. SLC received funding from the South African  
825 National Research Foundation and the Australian Research Council. FM, MČ, KU and MU received funding from Slovak Research and  
826 Development Agency (no. APVV-19-0319). Instituto Antartico Chileno (INACH\_RT-48\_16), Iniciativa Científica Milenio Núcleo Milenio de  
827 Salmónidos Invasores INVASAL, Institute of Ecology and Biodiversity (IEB), CONICYT PIA APOYO CCTE AFB170008. PC is supported by NERC  
828 core funding to the BAS 'Biodiversity, Evolution and Adaptation Team. EJC received funding from the Norwegian Research Council (grant n  
829 umber 230970). GND was supported by NERC E3 doctoral training partnership grant (NE/L002558/1) at the University of Edinburgh and  
830 the Carnegie Trust for the Universities of Scotland. Monitoring stations on Livingston Island, Antarctica were funded by different research  
831 projects of the Govern of Spain (PERMAPLANET CTM2009-10165-E; ANTARPERMA CTM2011-15565-E; PERMASNOW CTM2014-52021-R),  
832 and the PERMATHERMAL arrangement between the University of Alcalá and the Spanish Polar Committee. GN received funding from the  
833 Autonomous Province of Bolzano (ITA). The infrastructure, part of the UK Environmental Change Network, was funded historically in part  
834 by ScotNature.and and NERC National Capability LTS-S: UK-SCAPE; NE/R016429/1). JD was supported by the Czech Science Foundation  
835 (GA17-19376S) and MSMT (LTAUSA18007). ED received funding from the Kempe Foundation (JCK-1112 and JCK-1822). The infrastructure  
836 was supported by the Ministry of Education, Youth and Sports of the Czech Republic within the National Sustainability Programme I (NPU  
837 I), grant number LO1415 and by the project for national infrastructure support CzeCOS/ICOS Reg.No. LM2015061. NE received funding  
838 from the German Research Foundation (DFG– FZT 118, 202548816). BE received funding from the GLORIA-EU project no EVK2-CT2000-  
839 00056, the Autonomous Province of Bolzano (ITA), from the Tiroler Wissenschaftsfonds and from the University of Innsbruck. RME was  
840 supported by funding to the SAFE Project from the Sime Darby Foundation. OF received funding from the German Research Foundation  
841 (DFG– FZT 118, 202548816). EFP was supported by the Jardín Botánico Atlántico (SV-20-GIJON-JBA). MF was funded by the German  
842 Federal Ministry of Education and Research (BMBF) in the context of The Future Okavango (Grant No. 01LL0912) and SASSCAL  
843 (01LG1201M; 01LG1201N) projects. RAG received funding from Fondecyt 11170516 and CONICYT PIA AFB170008. MBG received funding  
844 from National Parks (DYNBIO, #1656/2015) and The Spanish Research Agency (VULBIMON, #CGL2017-90040-R). MG received funding from  
845 the Swiss National Science Foundation (ICOS-CH Phase 2 20FI20\_173691). FG received funding from the German Research Foundation  
846 (DFG– FZT 118, 202548816). KG and TS received funding from the UK Biotechnology and Biological Research Council (grant = 206/D16053).  
847 SG was supported by the Research Foundation Flanders (FWO) (project G0H1517N). KJ and PH received funding from the EU Horizon2020  
848 INFRAIA project eLTER-PLUS (871128), the project LTER-CWN (FFG, F&E Infrastrukturförderung, project number 858024) and the Austrian  
849 Climate Research Program (ACRP7 – CentForCSink – KR14AC7K11960). SH and ARB received funding through iDiv funded by the German  
850 Research Foundation (DFG– FZT 118, 202548816). LH received funding from the Czech Science Foundation (grant nr. 20-28119S) and the  
851 Czech Academy of Sciences (grant nr. RVO 67985939). MH received funding from the Baden-Württemberg Ministry of Science, Research  
852 and Arts via the project DRleR (Drought impacts, processes and resilience: making the in-visible visible). LH received funding from  
853 International Polar Year, Weston Foundation, and ArcticNet. DH received funding from Natural Sciences and Engineering Council (Canada)  
854 (RGPIN-06691). TTH received funding from Independent Research Fund Denmark (grant no. 8021-00423B) and Villum Foundation (grant  
855 no. 17523). Ministry of Education, Youth and Sports of the Czech Republic (projects LM2015078, VAN2020/01 and  
856 CZ.02.1.01/0.0/0.0/16\_013/0001708). KH and CG received funding from Bolin Centre for Climate Research, Stockholm University and from  
857 the Swedish research council Formas [grant n:o 2014-00530 to KH]. JJ received funding from the Funding Org. Swedish Forest Society  
858 Foundation (grant nr. 2018-485-Steg 2 2017) and Swedish Research Council FORMAS (grant nr. 2018-00792). Project LAS III 77/2017/B  
859 entitled: "Estimation of net carbon dioxide fluxes exchanged between the forest ecosystem on post-agricultural land and between the  
860 tornado-damaged forest area and the atmosphere using spectroscopic and numerical methods", source of funding: General Directorate  
861 of State Forests, Warsaw, Poland. AJ received funding from the German Federal Ministry of Education and Research BMBF (Grant Nr. FKZ  
862 031B0516C SUSALPS) and the Oberfrankenstiftung (Grant Nr. OFS FP00237). ISJ received funding from the Energy Research Fund (NÝR-11 -  
863 2019, NÝR-18 - 2020). TJ was supported by a UK NERC Independent Research Fellowship (grant number: NE/S01537X/1). RJ received  
864 funding from National Science Centre of Poland (grant number: 2016/21/B/ST10/02271) and Polish National Centre for Research and  
865 Development (grant number: Pol-Nor/203258/31/2013). VK received funding from the Czech Academy of Sciences (grant nr. RVO  
866 67985939). AAK received funding from MoEFCC, Govt of India (AICOPTAX project F. No. 22018/12/2015/RE/Tax). NK received funding



867 from FORMAS, VR, support from the research infrastructure ICOS. BK received funding from the National Research, Development and  
868 Innovation Fund of Hungary (grant nr. K128441). Ministry of Education, Youth and Sports of the Czech Republic (projects LM2015078 and  
869 CZ.02.1.01/0.0/0.0/16\_013/0001708). Project B1-RNM-163-UGR-18-Programa Operativo FEDER 2018, partially funded data collection.  
870 Norwegian Research Council (NORKLIMA grants #184912 and #244525) awarded to Vigdis Vandvik. MM received funding from the Czech  
871 Science Foundation (grant nr. 20-28119S) and the Czech Academy of Sciences (grant nr. RVO 67985939). Project CONICYT-PAI 79170119  
872 awarded to Roy Mackenzie. This work was partly funded by project MIUR PON Cluster OT4CLIMA. RM received funding from the SNF  
873 project number 407340\_172433. FM received funding from the Stelvio National Park. PM received funding from AIAS-COFUND fellowship  
874 programme supported by the Marie Skłodowska-Curie actions under the European Union's Seventh Framework Programme for  
875 Research, Technological development and Demonstration (grant agreement no 609033) and the Aarhus University Research Foundation,  
876 Denmark. RM received funding from the Ministry of Education, Youth and Sports of the Czech Republic (project LTT17033). SM and VM  
877 received funding from EU FP6 NitroEurope (grant nr. 17841), EU FP7 ÉCLAIRE (grant nr. 282910), the Ministry of Education and Science of  
878 Ukraine (projects nr. 505, 550, 574, 602), GEF-UNEP funded "Toward INMS" project (grant nr. NEC05348) and ENI CBC BSB PONTOS (grant  
879 nr. BSB 889). STM received funding from New Frontiers in Research Fund-Exploration (grant nr. NFRF-2018-02043) and NSERC Discovery.  
880 MMR received funding from the Australian Research Council Discovery Early Career Research Award (grant nr. DE180100570). JAM  
881 received funding from the National Science Foundation (DEB 1557094), International Center for Advanced Renewable Energy and  
882 Sustainability (I-CARES) at Washington University in St. Louis, ForestGEO, and Tyson Research Center. IM-S was funded by the UK Natural  
883 Environment Research Council through the ShrubTundra Project (NE/M016323/1). MBN received funding from FORMAS, VR, Kempe  
884 Foundations support from the research infrastructures ICOS and SITES. MDN received funding from CONICET (grant nr. PIP 112-201501-  
885 00609). Spanish Ministry of Science grant PID2019-110521GB-I00 and Catalan government grant 2017-1005. French National Research  
886 Agency (ANR) in the frame of the Cluster of Excellence COTE (project HydroBeech, ANR-10-LABX-45). VLIR-OUS, under the Institutional  
887 University Cooperation programme (IUC) with Mountains of the Moon University. Max Planck Society (Germany), RFBR, Krasnoyarsk  
888 Territory and Krasnoyarsk Regional Fund of Science, project number 20-45-242908. Estonian Research Council (PRG609), and the  
889 European Regional Development Fund (Centre of Excellence EcolChange). Canada-Denmark Arctic Research Station Early Career Scientist  
890 Exchange Program, from Polar Knowledge Canada (POLAR) and the Danish Agency for Science and Higher Education. Fondecyt 1180205  
891 and CONICYT PIA AFB170008. MP received funding from the Funding Org. Knut and Alice Wallenberg Foundation (grant nr. 2015.0047),  
892 and acknowledges funding from the Swedish Research Council (VR) with contributing research institutes to both the SITES and ICOS  
893 Sweden infrastructures. Spanish Ministry of Science grant PID2019-110521GB-I00, fundación Ramón Areces ELEMENTAL-CLIMATE project,  
894 and Catalan government grant 2017-1005. MPB received funding from the Svalbard Environmental Protection Fund (grant project number  
895 15/128) and the Research Council of Norway (Arctic Field Grant, project number 269957). RP received funding from the Ministry of  
896 Education, Youth and Sports of the Czech Republic (grant INTER-TRANSFER nr. LTT20017). LTSER Zone Atelier Alpes; Fédération FREE-  
897 Alpes. RP received funding from a Humboldt Fellowship for Experienced Researchers. RPU received funding from the Polish National  
898 Science Centre (grant project number 2017/27/B/NZ8/00316). ODYSSEE project (ANR-13-ISV7-0004, PN-II-ID-JRP-RO-FR-2012). KR was  
899 supported through an Australian Government Research Training Program Scholarship. Fieldwork was supported by the Global Challenges  
900 program at the University of Wollongong, the ARC the Australian Antarctic Division and INACH. Project SUBANTECO IPEV 136 (French Polar  
901 Institute Paul-Emile Victor), Zone Atelier CNRS Antarctique et Terres Australes, SAD Région Bretagne (Project INFLICT), BiodivERsa 2019-  
902 2020 BioDivClim call 'ASICS' (ANR-20-EBIS-0004). SAR received funding from the Australian Research Council. NSF grant #1556772 to the  
903 University of Notre Dame. Pavia University (Italy). OR received funding from EU-LEAP-Agri (RAMSES II), EU-DESIRA (CASSECS), EU-H2020  
904 (SustainSahel), AGROPOLIS and TOTAL Foundations (DSCATT), CGIAR (GLDC). AR was supported by the Russian Science Foundation (Grant  
905 18-74-10048). Parc national des Ecrins. JS received funding from Vetenskapsrådet grant nr (No: 2014-04270), ALTER-net multi site grant,  
906 River LIFE project (LIFE08 NAT/S/000266), Flexpeil. Helmholtz Association long-term research program TERENO (Terrestrial Environmental  
907 Observatories). PS received funding from the Polish Ministry of Science and Higher Education (grant nr. N N305 304840). AS received  
908 funding from the ETH Research grant (grant number ETH-27 19-1). LSC received funding from NSERC Canada Graduate Scholarship  
909 (Doctoral) Program; LSC was also supported by ArcticNet-NCE. Conselho Nacional de Desenvolvimento Científico e Tecnológico  
910 (141513/2017-9); Fundação Carlos Chagas Filho de Amparo à Pesquisa do Estado do Rio de Janeiro (E26/200.84/2019). ZS received funding  
911 from the SRDA (nr. APVV-16-0325) and from the ERDF (grant nr. ITMS 3130115735, CE LignoSilva). JS, MB, and CA received funding from  
912 core budget of ETH Zurich. State excellence Program M-V \ "WETSCAPES". AfricanBioServices project funded by the EU Horizon 2020 grant  
913 number 641918. The authors from KIT/IMK-IFU acknowledge the funding received within the German Terrestrial Environmental  
914 Observatories (TERENO) research program of the Helmholtz Association and from the Bavarian Ministry of the Environment and Public  
915 Health (UGV06080204000). Deutsche Forschungsgemeinschaft (DFG, German Research Foundation), project number 192626868, in the  
916 framework of the collaborative German-Indonesian research project CRC 990 (SFB): "EFForTS, Ecological and Socioeconomic Functions of  
917 Tropical Lowland Rainforest Transformation Systems (Sumatra, Indonesia)". MS received funding from the Ministry of Education, Youth  
918 and Sports of the Czech Republic (grant nr. INTER-TRANSFER LTT19018). TT received funding from the Swedish National Space Board (SNSB  
919 Dnr 95/16) and the CASSECS project supported by the European Union. HJDT received funding from the UK Natural Environment Research  
920 Council (NERC doctoral training partnership grant NE/L002558/1). German Science Foundation (DFG) GraKo 2010 \ "Response". PDT  
921 received funding from the MEMOIRE project (PN-III-P1-1.1-PD2016-0925). Arctic Challenge for Sustainability II (ArCS II;  
922 JPMXD1420318865). JU received funding from Czech Science Foundation (grant nr. 21-11487S). TU received funding from the Romanian  
923 Ministry of Education and Research (CCCDI - UEFISCDI -project PN-III-P2-2.1-PED-2019-4924 and PN2019-2022/19270201-Ctr. 25N  
924 BIODIVERS 3-BIOSERV). LvdB, KT, MYB and RC acknowledge funding from the German Research Foundation within the Priority Program  
925 SPP-1803 "EarthShape: Earth Surface Shaping by Biota" (grant TI 338/14-1&2 and BA 3843/6-1). AV acknowledge funding from RSF,  
926 project 21-14-00209. GFV received funding from the Dutch Research Council NWO (Veni grant, no. 863.14.013). Australian Research  
927 Council Discovery Early Career Research Award DE140101611. FGAV received funding from the Portuguese Science Foundation (FCT)  
928 under CECEIND/02509/2018, CESAM (UIDP/50017/2020+UIDB/50017/2020), FCT/MCTES through national funds, and the co-funding by  
929 the FEDER, within the PT2020 Partnership Agreement and Compete 2020. Ordesa y Monte Perdido National Park. MVI received funding  
930 from the Spanish Ministry of Science and Innovation through a doctoral grant (FPU17/05869). JW received funding from the Czech Science  
931 Foundation (grant nr. 20-28119S) and the Czech Academy of Sciences (grant nr. RVO 67985939). CR and SW received funding from the  
932 Swiss Federal Office for the Environment (FOEN) and the de Giacomo foundation. YY received funding from the National Natural Science

933 Foundation of China (Grant no. 41861134039 and 41941015). ZY received funding from the National Natural Science Foundation of China  
934 (grant nr. 41877458). FZ received funding from the Swiss National Science Foundation (grant nr. 172198 and 193645). PZ received funding  
935 from the Funding Org. Knut and Alice Wallenberg Foundation (grant no. 2015.0047). JL received funding from: (i) the Agence Nationale de  
936 la Recherche (ANR), under the framework of the young investigators (JCJC) funding instrument (ANR JCJC Grant project N°ANR-19-CE32-  
937 0005-01: IMPRINT); (ii) the Centre National de la Recherche Scientifique (CNRS) (Défi INFINITI 2018: MORFO); and the Structure Fédérative  
938 de Recherche (SFR) Condorcet (FR CNRS 3417: CREUSE).

939 Fieldwork in the Arctic got facilitated by funding from the EU INTERACT program. SN, UAT, JJA, and JvO would like to thank the field team  
940 of the Vegetation Dynamics group for their efforts and hard work. We acknowledge Dominique Tristan for letting access to the field. for  
941 the logistic support the crew of INACH and Gabriel de Castilla Station team on Deception Island. We thank the Inuvialuit and Kluane First  
942 Nations for the opportunity to work on their land. MAdP acknowledges fieldwork assistance and logistics support to Unidad de Tecnología  
943 Marina CSIC, and the crew of Juan Carlos I and Gabriel de Castilla Spanish Antarctic Stations, as well as to the different colleagues from  
944 UAH that helped on the instruments maintenance. ERF acknowledges fieldwork assistance by Martin Heggli. MBG acknowledges fieldwork  
945 and technical assistance by P Abadía, C Benedé, P Bravo, J Gómez, M Grasa, R Jimenez, H Miranda, B Ponz, J Revilla and P Tejero, and the  
946 Ordesa and Monte Perdido National Park staff. LH acknowledges field assistance by John Jacobs, Andrew Trant, Robert Way, Darroch  
947 Whitaker; I acknowledge the Inuit of Nunatsiavut, and the Cooperative Management Board of Torngat Mountains National Park for their  
948 support of this project and acknowledge that the field research was conducted on their traditional lands. We thank our many bear guides,  
949 especially Boonie, Eli, Herman, John, and Maria Merkuratsuk. AAK acknowledges field support of Akhtar Malik, Rameez Ahmad. Part of  
950 microclimatic records from Saxony was funded by the Saxon Switzerland National Park Administration. Tyson Research Center. JP  
951 acknowledges field support of Emmanuel Malet (Edytem) and Rangers of Reserves Naturelles de Haute-Savoie (ASTERS). practical help:  
952 Roel H. Janssen, N. Huig, E. Bakker, Schools in the tepåseförsöket, Forskar fredag, Erik Herberg. The support by the Bavarian Forest  
953 National Park administration is highly appreciated. Liesbeth acknowledges CONAF and onsite support from the park rangers from PN Pan  
954 de Azucar, PN La Campana, PN Nahuelbuta and from comunidad agricola Quebrada de Talca. JL and FS acknowledge Manuel Nicolas and  
955 all forest officers from the Office National des Forêts (ONF) who are in charge of the RENECOFOR network and who provided help and  
956 local support for the installation and maintenance of temperature loggers in the field.

## 957 **Author contributions**

958 JJJ and JL conceptualized the project, JJJ, JvdH, MBA, PDF, MK, ML, IMDM, TWC, IN and JL designed  
959 the paper, the SoilTemp consortium acquired the data, JJJ, JVDH, JK, and PN analysed the data, JJJ,  
960 JvdH, JA, MBA, PDF, JK, MK, ML, IMDM, TWC, JJB, SH, DHK, PN, BRS and KVM interpreted the  
961 analyses. All authors significantly revised the manuscript and approved it for submission.

## 962 **The authors declare no competing interests.**

## 963 **Affiliations**

964 1) Research Group PLECO (Plants and Ecosystems), University of Antwerp, 2610 Wilrijk, Belgium, 2) Department of Environmental Systems  
965 Science, Institute of Integrative Biology, ETH Zürich, Zürich, Switzerland, 3) Finnish Meteorological Inst., P.O. Box 503, FI-00101 Helsinki,  
966 Finland, 4) Dept of Geosciences and Geography, Gustaf Hällströmin katu 2a, FIN-00014 Univ. of Helsinki, Finland, 5) Centre for Sustainable  
967 Ecosystem Solutions, School of Biological Sciences, University of Wollongong, Wollongong, Australia, 6) Australian Museum, Sydney,  
968 Australia, 7) Forest & Nature Lab, Department of Environment, Ghent University, Geraardsbergsesteenweg 267, 9090 Melle-Gontrode,  
969 Belgium, 8) Geography Research Unit, University of Oulu, Oulu, Finland, 9) Institute of Botany of the Czech Academy of Sciences, Zámek 1,  
970 CZ-25243, Průhonice, Czech Republic, 10) Faculty of Forestry and Wood Sciences, Czech University of Life Sciences Prague, Kamýcká 129,  
971 CZ-165 21, Prague 6 - Suchbát, Czech Republic, 11) Environment and Sustainability Institute, University of Exeter, Penryn Campus, Penryn,  
972 UK, TR10 9FE, 12) Department of Geography, York St John University, Lord Mayor's Walk, York, YO31 7EX, United Kingdom, 13)  
973 Department of Earth and Environmental Sciences, KU Leuven, Celestijnenlaan 200E, 3001 Leuven, Belgium, 14) School of Natural  
974 Resources and Environment, University of Florida, Gainesville, FL 32611, USA, 15) Smithsonian Environmental Research Center, Edgewater  
975 MD 21037 USA, 16) Department of Wildlife Ecology and Conservation, University of Florida, Gainesville, FL 32611, USA, 17) Department of  
976 Natural Sciences and Environmental Health, University of South-Eastern Norway, Gullbringvegen 36, NO-3800, Bø, Norway, 18) Alpine  
977 Ecosystems Research Program, Institute of Ecology, Ilia State University, Tbilisi, Georgia, 19) Department of Range Management, Faculty of  
978 Natural Resources and Marine Sciences, Tarbiat Modares University, Noor, Mazandaran Province, I. R. Iran, 20) Department of Ecological  
979 Science, Vrije Universiteit Amsterdam, The Netherlands., 21) Royal Botanic Garden Edinburgh, 20A Inverleith Row, EH3 5LR, Edinburgh,  
980 UK, 22) Environmental Science Center, Qatar University, Doha, Qatar, 23) Department of Environmental Systems Science, Institute of  
981 Integrative Biology, ETH Zurich, Universitätsstrasse 16, CH-8092 Zürich, Switzerland, 24) Research group ECOBE, University of Antwerp,  
982 2610 Wilrijk, Belgium, 25) Department of Agroecology and Environment, Agroscopie Research Institute, Reckenholzstrasse 191, 8046  
983 Zürich, Switzerland, 26) Department of Environmental Systems Science, ETH Zurich, Universitaetstrasse 2, 8092 Zurich, Switzerland, 27) UK  
984 Centre for Ecology & Hydrology, Bush Estate, Penicuik, Midlothian, EH26 0QB, United Kingdom, 28) Department of Physical Geography and  
985 Ecosystem Science, Lund University, Sölvegatan 12, 223 62 Lund, Sweden, 29) European Commission, Joint Research Centre (JRC), Ispra,  
986 Italy, 30) Siberian Federal University, 660041 Krasnoyarsk, Russia, 31) Instituto Argentino de Nivología, Glaciología y Ciencias Ambientales  
987 (IANIGLA), CONICET, CCT-Mendoza; Facultad de Ciencias Exactas y Naturales, Universidad Nacional de Cuyo, 32) Instituto Argentino de  
988 Nivología, Glaciología y Ciencias Ambientales (IANIGLA), CONICET, CCT-Mendoza, 33) Natural History Museum, University of Oslo, 0318,  
989 Oslo, Norway, 34) Section for Ecoinformatics & Biodiversity, Department of Biology, Aarhus University, Aarhus C, Denmark, 35) Center for  
990 Biodiversity Dynamics in a Changing World, Department of Biology, Aarhus University, Aarhus C, Denmark, 36) Ecological Plant Geography,

991 Faculty of Geography, University of Marburg, Deutschhausstrasse 10, 35032, Marburg, Germany, 37) Institute of Landscape Ecology Slovak  
992 Academy of Sciences, Štefánikova 3, 81499 Bratislava, Slovakia, 38) Faculty of Environmental and Forest Sciences, Agricultural University of  
993 Iceland, Árleyni 22, 112 Reykjavík, Iceland, 39) Instituto Argentino de Nivología, Glaciología y Ciencias Ambientales (IANIGLA), CONICET,  
994 CCT-Mendoza, 40) Isotope Bioscience Laboratory - ISOFYS, Ghent University, Coupure Links 653, 9000 Gent, Belgium, 41) Université de  
995 Rennes, CNRS, EcoBio (Ecosystèmes, biodiversité, évolution) - UMR 6553, F-35000 Rennes, France, 42) Department of Sustainable Agro-  
996 ecosystems and Bioresources, Research and Innovation Centre, Fondazione Edmund Mach, Via E. Mach 1, 38010 San Michele all'Adige,  
997 Italy, 43) Forest Research, Alice Holt Lodge, Wrecclesham, Farnham, UK, 44) Department of Ecology, Pontificia Universidad Javeriana,  
998 Bogota, Colombia, 45) Jolube Consultor Botánico. C/Mariano R de Ledesma, 4. E-22700 Jaca, Huesca, SPAIN, 46) Institute of Landscape and  
999 Plant Ecology, Department of Plant Ecology, University of Hohenheim, Otilie-Zeller\_weg 2, 70599 Stuttgart, Germany, 47) Disturbance  
1000 Ecology, BayCEER, University of Bayreuth, Universitätsstr. 30, 95447 Bayreuth, Germany, 48) Norwegian Institute for Nature Research,  
1001 FRAM - High North Research Centre for Climate and the Environment, P.O. Box 6606 Langnes, N-9296 Tromsø, Norway, 49) Department of  
1002 Earth Sciences, University of Gothenburg, P.O. Box 460, SE-40530 Gothenburg, Sweden, 50) Gothenburg Global Biodiversity Centre, P.O.  
1003 Box 461, SE-405 30 Gothenburg, Sweden, 51) Department of Biological and Environmental Sciences, University of Gothenburg, P.O. Box  
1004 461, 43 Gothenburg SE-405 30, Sweden, 52) Department of Environmental Science, Policy, and Management, University of California,  
1005 Berkeley, CA 94720 USA, 53) Alfred Wegener Institute Helmholtz Center for Polar and Marine Research, Telegrafenberg A45, 14473  
1006 Potsdam, Germany, 54) Geography Department, Humboldt-Universität zu Berlin, Germany, 55) Pós-Graduação em Ciências de Florestas  
1007 Tropicais, Instituto Nacional de Pesquisas da Amazônia, Manaus, Brasil, CEP: 69060-001, 56) UMR ECOSYS INRAE, AgroParisTech,  
1008 Université Paris Saclay, France, 57) Biological Dynamics of Forest Fragments Project, BDFFP, Instituto Nacional de Pesquisas da Amazônia,  
1009 Av. André Araujo, 2936 - Petrópolis, Manaus, Amazonas, 69067-375, Brazil, 58) Department of Forest Sciences, Federal University of  
1010 Lavras, 37.200-900, Lavras, MG, Brazil, 59) Faculty of Arts and Sciences, Department of Molecular Biology and Genetics, Ordu University,  
1011 52200, Ordu, Turkey, 60) Ecological Plant Geography, Faculty of Geography, University of Marburg, Deutschhausstrasse 10, 35032,  
1012 Marburg, Germany., 61) Plant Ecology Group, Department of Evolution and Ecology, University of Tübingen, Auf der Morgenstelle 5, 72076  
1013 Tübingen, Germany, 62) Department of Science and High Technology, Insubria University, Via Valleggio 11, 22100 Como, Italy, 63)  
1014 Department of Chemistry, Life Sciences and Environmental Sustainability, University of Parma, Parco Area delle Scienze 11/A, 43124  
1015 Parma, Italy, 64) Department of Evolutionary Biology, Ecology and Environmental Sciences, Biodiversity Research Institute (IRBio),  
1016 University of Barcelona, 08028 Barcelona, Catalonia, Spain, 65) CREAF, E08193 Bellaterra (Cerdanyola del Vallès), Catalonia, Spain, 66)  
1017 Laboratorio de Ecofisiología vegetal y Cambio Climático and Núcleo de Estudios Ambientales (NEA), Universidad Católica de Temuco,  
1018 Campus Luis Rivas del Canto, Rudecindo Ortega 02950, Temuco, Chile., 67) German Centre for Integrative Biodiversity Research (iDiv)  
1019 Halle-Jena-Leipzig, Leipzig, Germany, 68) Institute of Biology, Leipzig University, Leipzig, Germany, 69) Laboratory of Bioclimatology,  
1020 Department of Ecology and Environmental Protection, Poznan University of Life Sciences, ul. Piatkowska 94, 60-649, Poznan, Poland, 70)  
1021 Univ. Grenoble Alpes, Univ. Savoie Mont Blanc, CNRS, LECA, F-38000 Grenoble, France, 71) Univ. Grenoble Alpes, Univ. Savoie Mont Blanc,  
1022 CNRS, LTSER Zone Atelier Alpes, F-38000 Grenoble, France, 72) Securing Antarctica's Environmental Future, School of Biological Sciences,  
1023 Monash University, Victoria 3800, Australia, 73) Forest Ecology and Conservation Group, Department of Plant Sciences, University of  
1024 Cambridge, Cambridge CB23EA, UK, 74) Faculty of Ecology and Environmental Sciences, Technical University in Zvolen, T. G. Masaryka 24,  
1025 960 01 Zvolen, Slovakia, 75) Sub-Antarctic Biocultural Conservation Program, Universidad de Magallanes, Pdte. Manuel Bulnes 01855,  
1026 Punta Arenas, Magallanes y la Antártica Chilena, 76) Núcleo Milenio de Salmónidos Invasores, INVASAL, Concepción, Chile, 77) British  
1027 Antarctic Survey, NERC, High Cross, Madingley Road, Cambridge CB3 0ET, United Kingdom, 78) Department of Arctic and Marine Biology,  
1028 Faculty of Biosciences Fisheries and Economics, UiT-The Arctic University of Norway, N-9037 Tromsø, Norway, 79) Climate Change Unit,  
1029 Environmental Protection Agency of Aosta Valley, Italy, 80) Department of Biological Sciences, University of Notre Dame, Notre Dame, IN  
1030 46556, USA, 81) Department of Science, University of Roma Tre, 00146 Rome, Italy, 82) Department of Ecology, Environment and Plant  
1031 Sciences and Bolin Centre for Climate Research, Stockholm University, 106 91 Stockholm, Sweden, 83) the County Administrative Board of  
1032 Västra Götaland, SE-403 40 Gothenburg, Sweden, 84) School of GeoSciences, University of Edinburgh, King's Buildings, Edinburgh, EH9 3FF,  
1033 United Kingdom, 85) Department of Geology, Geography and Environment. University of Alcalá. 28805 Alcalá de Henares, Madrid, Spain.,  
1034 86) Chair of Geoinformatics, Technische Universität Dresden, Dresden Germany, 87) Vegetation Ecology, Institute of Natural Resource  
1035 Sciences, ZHAW Zurich University of Applied Sciences, Grüental, 8820 Wädenswil, Switzerland, 88) Plant Ecology, Bayreuth Center of  
1036 Ecology and Environmental Research (BayCEER), University of Bayreuth, Universitätsstr. 30, 95447 Bayreuth, Germany, 89) VITO-TAP,  
1037 Boeretang 200, 2400-Mol, Belgium, 90) Swiss Federal Research Institute WSL, 8903 Birmensdorf, Switzerland, 91) Majella Seed Bank,  
1038 Majella National Park, Colle Madonna, 66010 Lama dei Peligni, Italy, 92) Department of Life, Health and Environmental Sciences,  
1039 University of L'Aquila, Piazzale Salvatore Tommasi 1, 67100 L'Aquila, Italy, 93) Grupo de Ecología de Poblaciones de Insectos, IFAB (INTA -  
1040 CONICET), Modesta Victoria 4450, Bariloche, Argentina, 94) Department of Biology and Biochemistry, University of Houston, Houston,  
1041 Texas, 77204 USA, 95) Faculty of Science, Department of Botany, University of South Bohemia, Na Zlaté Stoce 1, 37005 České Budějovice,  
1042 Czech Republic, 96) Climate Impacts Research Centre, Department of Ecology and Environmental Sciences, Umeå University, Abisko,  
1043 Sweden, 97) Global Change Research Institute, Academy of Sciences of the Czech Republic, 98) Department of Ecology & Evolutionary  
1044 Biology, University of Arizona, USA, 99) School of Biological Sciences, The University of Western Australia, Crawley, WA 6009, Australia,  
1045 100) Kings Park Science, Department of Biodiversity, Conservation & Attractions, Kings Park, 6005 WA, Australia, 101) Department of  
1046 Botany, Faculty of Biology, University of Innsbruck, Sternwartestraße 15, 6020 Innsbruck, Austria, 102) Imperial College London, Silwood  
1047 Park Campus, Ascot SL5 7PY, UK, 103) Operation Wallacea, Wallace House, Old Bolingbroke, Lincolnshire, PE23 4EX, UK, 104) INRAE,  
1048 Bordeaux Sciences Agro, UMR 1391 ISPA, F-33140 Villenave d'Ornon, France, 105) Department of Life and Environmental Sciences,  
1049 University of Cagliari, Viale Sant'Ignazio da Laconi 13, 09123, Cagliari, Italy., 106) Department of Botany, University of Granada, 18071,  
1050 Granada, Spain, 107) IMIB – Biodiversity Research Institute, University of Oviedo, Mieres, Spain, 108) Institute for Plant Science and  
1051 Microbiology, University of Hamburg, Ohnhorststr. 18, 22609 Hamburg, Germany, 109) Dartmouth College, Hanover, NH, USA, 110)  
1052 Ecosystems and Global Change Group, Department of Plant Sciences, University of Cambridge, Cambridge, CB2 3EA, United Kingdom, 111)  
1053 WSL Institute for Snow and Avalanche Research SLF, 7260 Davos, Switzerland, 112) Swiss Federal Research Institute for Forest, Snow and  
1054 Landscape Research WSL, 8903 Birmensdorf, Switzerland, 113) Laboratorio de Invasiones Biológicas (LIB), Facultad de Ciencias Forestales,  
1055 Universidad de Concepción, Concepción, Chile, 114) School of Education and Social Sciences, Adventist University of Chile, Chile, 115)  
1056 Instituto de Ecología y Biodiversidad (IEB), Santiago, Chile, 116) Pyrenean Institute of Ecology (CSIC), Av. Montañana 1005, 50059

1057 Zaragoza, Spain, 117) Biodiversity and Landscape, TERRA research centre, Gembloux Agro-Bio Tech, University of Liège, Gembloux, 5032,  
 1058 Belgium ; Research Group PLECO (Plants and Ecosystems), University of Antwerp, 2610 Wilrijk, Belgium, 118) Department of Geo-  
 1059 information in Environmental Management, Mediterranean Agronomic Institute of Chania, PO Box 85, 73100 Chania, Greece, 119)  
 1060 Georgian Institute of Public Affairs, department of Environmental management ad policy, Tbilisi, Georgia, 120) Flemish Institute for  
 1061 Technological Research, 2400 Mol, Belgium, 121) Department of Earth and Environmental Science, Faculty of BioScience Engineering,  
 1062 KULeuven, Belgium, 122) Max Planck Institute for Biogeochemistry, Department of Biogeochemical Signals, Jena, Germany, 123)  
 1063 Sustainable Agricultural Sciences Department, Rothamsted Research, Harpenden, AL5 2JQ, UK, 124) Department of Biology, Norwegian  
 1064 University of Science and Technology, 7491 Trondheim, Norway, 125) Biodiversity, Wildlife and Ecosystem Health, Biomedical Sciences,  
 1065 University of Edinburgh, Edinburgh, EH8 9JZ, UK, 126) Department of Ecology, Swedish University of Agricultural Sciences, Box 7042, S-750  
 1066 07 Uppsala, 127) School of Biological Sciences, The University of Hong Kong, Pok Fu Lam Road, Hong Kong SAR, China, 128) Department of  
 1067 Theoretical and Applied Sciences, Insubria University, Via Dunant 3, 21100 Varese, Italy, 129) CIRAD, UMR Eco&Sols, 34060 Montpellier,  
 1068 France, 130) Eco&Sols, Univ Montpellier, CIRAD, INRAE, IRD, Montpellier SupAgro, 34060 Montpellier, France, 131) Senckenberg Research  
 1069 Institute and Natural History Museum Frankfurt, 63571 Gelnhausen, Germany, 132) Faculty of Biology, University of Duisburg-Essen,  
 1070 45141 Essen, Germany, 133) Institute of Biology / Geobotany and Botanical Garden, Martin Luther University Halle-Wittenberg, Halle  
 1071 (Saale), Germany, 134) Department of Biological Sciences and Bjerknes Centre for Climate Research, University of Bergen, N-5020 Bergen,  
 1072 Norway, 135) Centre for Biodiversity & Taxonomy, Department of Botany, University of Kashmir, Srinagar - 190006, J&K, India, 136)  
 1073 Department of Ecology, University of Innsbruck, 6020 Innsbruck, Austria, 137) INRAE, Univ. Bordeaux, BIOGECO, F-33610 Cestas, France,  
 1074 138) Museumsenteret i Hordaland, Lyngheisenteret, Alver, Norway, 139) TERRA Teaching and Research Center, Faculty of Gembloux Agro-  
 1075 Bio Tech, University of Liege, Passage des déportés, 2, 5030 Gembloux, Belgium, 140) UK Centre for Ecology & Hydrology, Penicuik, EH26  
 1076 0QB, Scotland, UK., 141) Institute for Botany, University of Natural Resources and Life Sciences Vienna (BOKU), Gregor-Mendel-Straße  
 1077 33/I, 1180 Vienna, Austria, 142) Centre for Agrometeorological Research (ZAMF), German Meteorological Service (DWD), Bundesallee 33,  
 1078 38116 Braunschweig, Germany, 143) Dept of Biology, Memorial University, St. John's, NL, A1B 3X9. Canada, 144) Department of Biological  
 1079 Sciences, Simon Fraser University, Burnaby, BC, V5A 1S6, Canada, 145) Department of Geography, University of Zaragoza, Pedro Cerbuna  
 1080 12, 50009 Zaragoza, Spain, 146) Plant Ecology, Albrecht-von-Haller-Institute for Plant Sciences, Georg-August University of Goettingen,  
 1081 Untere Karspuele 2, 37073 Goettingen, Germany, 147) Department of Bioscience and Arctic Research Centre, Aarhus University, Grenåvej  
 1082 14, 8410 Rønnde, Denmark, 148) Department of Geography, Masaryk University, Faculty of Science, Kotlarska 2, 611 37, Brno, Czech  
 1083 Republic, 149) Department of Environmental Science, Shinshu University, Matsumoto, Japan, 150) Department of Bioscience and Arctic  
 1084 Research Centre, Aarhus University, Frederiksborgvej 399, 4000 Roskilde, Denmark, 151) INRAE, University of Bordeaux, BIOGECO, F-  
 1085 33610 Cestas, France, 152) Department of Forest Ecology and Management, Swedish University of Agricultural Sciences, 90183 Umeå,  
 1086 Sweden, 153) Laboratory of Meteorology, Department of Construction and Geoengineering, Faculty of Environmental Engineering and  
 1087 Mechanical Engineering, Poznan University of Life Sciences, ul. Piatkowska 94, 60-649, Poznan, Poland, 154) Forest Research Institute,  
 1088 Department of Silviculture and Forest Tree Genetics, Braci Lesnej Street, No 3, Sekocin Stary, 05-090 Raszyn, Poland, 155) Bayreuth Center  
 1089 of Ecology and Environmental Research, 156) ARAID/IPE-CSIC, Pyrenean Institute of Ecology, Avda. Llano de la Victoria, 16, Jaca 22700,  
 1090 Spain, 157) Life and Environmental Sciences, University of Iceland, Sturlugata 7, 102 Reykjavík, Iceland, 158) Soil Science Department,  
 1091 Federal University of Viçosa, Prof. Peter Henry Rolfs Ave., 36570-900, Viçosa-MG, Brazil, 159) School of Biological Sciences, University of  
 1092 Bristol, Bristol, United Kingdom, 160) Biological and Environmental Sciences, Faculty of Natural Sciences, University of Stirling, Scotland,  
 1093 FK9 4LA, 161) Faculty of Environmental Sciences, Czech University of Life Sciences Prague, Kamýcká 129, 165 21 Prague 6 - Suchdol, Czech  
 1094 Republic, 162) Centre for Environmental and Climate Science, Lund University, Sölvegatan 37, 223 62, Lund, Sweden, 163) University of  
 1095 Goettingen, Bioclimatology, Büsgenweg 2, 37077 Göttingen, Germany., 164) Environment Agency Austria, Spittelauer Lände 5, 1090  
 1096 Vienna, Austria, 165) Max Planck Institute for Biogeochemistry, Jena, Thuringia, Germany, 166) Centre for Ecological Research, Institute of  
 1097 Ecology and Botany, H-2163 Vácrátót, Alkotmány út 2-4., Hungary, 167) Experimental Plant Ecology, Institute of Botany and Landscape  
 1098 Ecology, University of Greifswald, D-17487 Greifswald, Germany, 168) GLORIA Coordination, Institute for Interdisciplinary Mountain  
 1099 Research, Austrian Academy of Sciences (ÖAW) & Department of Integrative Biology and Biodiversity Research, University of Natural  
 1100 Resources and Life Sciences, Vienna (BOKU), Silbergasse 30/3, 1190 Vienna, Austria, 169) Department of Arctic Biology, The University  
 1101 Centre in Svalbard (UNIS), 9171 Longyearbyen, Svalbard, Norway, 170) Department of Land Resources and Environmental Sciences,  
 1102 Montana State University, Bozeman MT, USA, 59717, 171) Climate Impacts Research Centre, Department of Ecology and Environmental  
 1103 Sciences, Umeå University, Vetenskapens väg 38, 98107 Abisko, Sweden, 172) Centre for Polar Ecology, Faculty of Science, University of  
 1104 South Bohemia, Na Zlaté Stoce 3, CZ-370 05, České Budějovice, Czech Republic, 173) School of Biological Sciences, Monash University,  
 1105 Victoria 3800, Australia, 174) Terrestrial Ecology Unit, Dept. of Biology, Ghent University, B-9000 Gent, Belgium, 175) Finnish  
 1106 Meteorological Institute, Climate System Research, PoB503, 00101 Helsinki, Finland, 176) INAR Institute for Atmospheric and Earth System  
 1107 Research/Physics, Faculty of Science, POBox 68 FI-00014 University of Helsinki, Finland, 177) Interuniversity Institute for Earth System  
 1108 Research, University of Granada, Granada 18006 Spain, 178) CNR Institute for Agricultural and Forestry Systems in the Mediterranean, P.le  
 1109 Enrico Fermi 1 - Loc. del Granatello, 80055, Portici (Napoli) Italy, 179) Faculty of Forestry, Technical University in Zvolen, T.G.Masaryka 24,  
 1110 960 01 Zvolen, Slovakia, 180) CNR Institute for Agricultural and Forestry Systems in the Mediterranean, P.le Enrico Fermi 1 - Loc. del  
 1111 Granatello, 80055, Portici (Napoli) Italy, 181) School of Pure & Applied Sciences, Environmental Conservation & Management Programme  
 1112 Open University of Cyprus, PO Box 12794, 2252 Latsia, Nicosia, 182) Department of Biology - Aquatic Biology, Aarhus University, Ole  
 1113 Worms Allé 1, 8000 Aarhus C, Denmark, 183) Aarhus Institute of Advanced Studies, AIAS Høegh-Guldbergs Gade 6B, 8000 Aarhus,  
 1114 Denmark, 184) CNR Institute of BioEconomy, Via Gobetti 101, 40129 Bologna, Italy, 185) Department of Forest Botany, Dendrology and  
 1115 Geobiocoenology, Faculty of Forestry and Wood Technology, Mendel University in Brno, Zemedelska 1, 613 00 Brno, Czech Republic, 186)  
 1116 Regional Centre for Integrated Environmental Monitoring, Odesa National I.I. Mechnikov University, 7 Mayakovskogo lane, 65082 Odesa,  
 1117 Ukraine, 187) Department of Agroecology, Aarhus University, 20 Blichers Allé, 8830 Tjele, Denmark, 188) NGO New Energy, 11 Bakulina  
 1118 str., 61166 Kharkiv, Ukraine, 189) Biological Dynamics of Forest Fragments Project, Coordenação de Dinâmica Ambiental, Instituto  
 1119 Nacional de Pesquisas da Amazônia, Manaus, AM CEP 69067-375, Brazil., 190) Swiss Federal Institute for Forest, Snow and Landscape  
 1120 Research (WSL), CH-8903 Birmensdorf, Switzerland., 191) Department of Biology, University of Antwerp, Universiteitsplein 1, 2610 Wilrijk,  
 1121 Belgium, 192) Department of Botany and Biodiversity Research Centre, University of British Columbia, Vancouver, BC, Canada, 193)  
 1122 Province of Antwerp, Koningin Elisabethlei 22, 2018 Antwerpen, Belgium, 194) Institute of Plant and Animal Ecology of Ural Division of

1123 Russian Academy of Science, 8 Marta st., 202, Ekaterinburg, Russia, 195) Department of Earth and Environmental Sciences, University of  
 1124 Pavia, Via S. Epifanio 14, Pavia, Italy, 196) Faculty of Science and Technology, Free University of Bolzano, Piazza Università 5, 39100  
 1125 Bolzano, Italy, 197) Climate Change Unit, Environmental Protection Agency of Aosta Valley, Loc. La Maladière, 48, 11020 Saint-Christophe,  
 1126 Italy, 198) University of Freiburg, Chair of Geobotany, Schänzlestrasse 1, 79104 Freiburg, Germany, 199) Environment and Sustainability  
 1127 Institute, University of Exeter, Penryn Campus, Cornwall TR10 9FE, United Kingdom, 200) Centre for Ecosystem Science, School of  
 1128 Biological, Earth and Environmental Sciences, UNSW Sydney, NSW 2052, Sydney, Australia, 201) Department of Biology, Washington  
 1129 University in St. Louis, St. Louis, MO 63130, USA., 202) Department of Animal Biology, Institute of Biology, University of Campinas,  
 1130 Campinas, SP, CEP 13083-862, Brazil, 203) National Wildlife Research Centre, Environment and Climate Change Canada, Carleton  
 1131 University, 1125 Colonel by Drive, Ottawa, ON K1A 0H3, Canada, 204) School of Life and Environmental Sciences, Deakin University,  
 1132 Burwood, Victoria, Australia, 3125, 205) Institute for Alpine Environment, Eurac Research, Viale Druso 1, 39100 Bozen/Bolzano, Italy, 206)  
 1133 Institute of Biology, Dept. of Molecular Botany, University of Hohenheim, 70599 Stuttgart, Germany, 207) Instituto de Matemática  
 1134 Aplicada San Luis, IMASL, CONICET and Universidad Nacional de San Luis, Ejército de los Andes 950, D5700HHW San Luis, Argentina, 208)  
 1135 Cátedra de Climatología Agrícola (FCA-UNER), Ruta 11, km 10, Oro Verde, Entre Ríos, Argentina, 209) Grupo de Ecología de Invasiones,  
 1136 INIBIOMA, CONICET/ Universidad Nacional del Comahue, Av. de los Pioneros 2350, Bariloche 8400, Argentina, 210) CSIC, Global Ecology  
 1137 Unit CREAM- CSIC-UAB, Bellaterra, 08193, Catalonia, Spain., 211) CREAM, E08193, Cerdanyola del Vallès, Catalonia, Spain, 212) Mountains  
 1138 of the Moon University, P.O Box 837, Fort Portal, Uganda, 213) National Agricultural Research Organisation, Mbarara Zonal Agricultural  
 1139 Research and Development Institute, P.O Box 389, Mbarara , Uganda, 214) Department of Agroecology, Aarhus University, Blichers Allé  
 1140 20, 8830 Tjele, Denmark, 215) Department of Biology, Lund University, SE-223 62 Lund, Sweden, 216) Department of Earth and  
 1141 Environmental Sciences, University of Pavia, Via S. Epifanio 14, 27100 Pavia, Italy, 217) Institute of Botany and Landscape Ecology,  
 1142 University Greifswald, D-17487 Greifswald, Germany, 218) V.N. Sukachev Institute of Forest SB RAS, Krasnoyarsk, Russia, 219) Institute of  
 1143 Ecology and Earth Sciences, University of Tartu, Lai 40, Tartu 51005, Estonia, 220) Department of Biology , Aarhus University, Ole Worms  
 1144 Allé 1, 8000 Aarhus C, Denmark, 221) Department of Biology and Ecology Center, Utah State University, 5305 Old Main Hill, Logan, UT  
 1145 84322, USA, 222) Department of Life Sciences, Imperial College, Silwood Park Campus, Ascot, Berkshire SL5 7PY, UK, 223) Landscape  
 1146 Ecology, Institute of Terrestrial Ecosystems, Department of Environmental Systems Science, ETH Zürich, 8092 Zürich, Switzerland, 224)  
 1147 Unit of Land Change Science, Swiss Federal Research Institute WSL, 8903 Birmensdorf, Switzerland, 225) Department of Biology,  
 1148 Washington University in St. Louis, Campus Box 1137, 1 Brookings Drive, St. Louis, MO 63130 USA, 226) School of Ecology and  
 1149 Environment Studies, Nalanda University, Rajgir, India, 227) Department of Animal and Plant Sciences, University of Sheffield, Western  
 1150 Bank, Sheffield, S10 2TN, U.K., 228) CESAM & Department of Environment, University of Aveiro, 3810-193 Aveiro, Portugal, 229)  
 1151 Department of Agronomy, Food, Natural resources, Animals and Environment - University of Padua, 35020 Legnaro, Italy, 230) Univ.  
 1152 Savoie Mont Blanc, CNRS, Univ. Grenoble Alpes, EDYTEM, F-73000 Chambéry, France, 231) Universitat Autònoma de Barcelona, E08193  
 1153 Bellaterra (Cerdanyola del Vallès), Catalonia, Spain, 232) Department of Ecology and Biogeography, Faculty of Biological and Veterinary  
 1154 Sciences, Nicolaus Copernicus University, Toruń, Poland, 233) Centre for Climate Change Research, Nicolaus Copernicus University, Toruń,  
 1155 Poland, 234) A. Borza Botanic Garden, Babeş-Bolyai University, Cluj-Napoca, Romania, 235) Faculty of Biology and Geology, Department of  
 1156 Taxonomy and Ecology, Babeş-Bolyai University, Cluj-Napoca, Romania, 236) E. G. Racoviță Institute, Babeş-Bolyai University, Cluj-Napoca,  
 1157 Romania, 237) Centre for Sustainable Ecosystem Solutions, School of Earth, Atmospheric and Life Sciences, University of Wollongong,  
 1158 Wollongong, New South Wales, 2522, Australia, 238) University of Applied Sciences Trier, Environmental Campus Birkenfeld, 55761  
 1159 Birkenfeld, Germany, 239) Institut Universitaire de France, 1 Rue Descartes, 75231 Paris cedex 05, France, 240) Swiss Federal Institute for  
 1160 Forest, Snow and Landscape Research WSL, Zuercherstrasse 111, 8903 Birmensdorf, Switzerland, 241) Securing Antarctica's Environmental  
 1161 Future, School of Earth, Atmospheric and Life Sciences, University of Wollongong, 2522 Australia, 242) Aquatic Ecology & Environmental  
 1162 Biology, Institute for Water and Wetland Research, Faculty of Science, Radboud University Nijmegen, AJ 6525 Nijmegen, The Netherlands.,  
 1163 243) University of Notre Dame, Department of Biological Sciences and the Environmental Change Initiative, 244) Swiss National Park,  
 1164 Chastè Planta-Wildenberg, 7530 Zerne, Switzerland, 245) Remote Sensing Laboratories, Dept. of Geography, University of Zurich,  
 1165 Winterthurerstrasse 190, 8057 Zurich, Switzerland, 246) CIRAD, UMR Eco&Sols, BP1386, CP18524, Dakar, Senegal, 247) Eco&Sols, Univ  
 1166 Montpellier, CIRAD, INRAE, IRD, Institut Agro, Montpellier, France, 248) LMI IESOL, Centre IRD-ISRA de Bel Air, BP1386, CP18524, Dakar,  
 1167 Senegal, 249) Parc national des Ecrins - Domaine de Charance - 05000 GAP - France, 250) Universidad Nacional de San Antonio Abad del  
 1168 Cusco, Cusco, Perú, 251) Centro de Investigación de la Biodiversidad Wilhelm L. Johannsen, Cusco, Perú, 252) Biological Dynamics of Forest  
 1169 Fragments Project, PDBFF, Instituto Nacional de Pesquisas da Amazônia, Av. André Araujo, 2936 - Petrópolis, Manaus, Amazonas, 69067-  
 1170 375, Brazil, 253) Department of Ecology and Environmental Science, Umeå University, 901 87 Umeå, Sweden, 254) Institute of Bio- and  
 1171 Geosciences (IBG-3): Agrosphere, Forschungszentrum Jülich GmbH, Jülich, Germany, 255) Chair of Soil Science and Geomorphology,  
 1172 Department of Geosciences, University of Tuebingen, 72070 Tuebingen, Germany, 256) Department of Geography, The University of  
 1173 British Columbia, Vancouver, BC V6T 1Z2, 257) Department of Ecology, University of Innsbruck, Technikerstrasse 25, 6020 Innsbruck,  
 1174 Austria, 258) Department of Botany and Biodiversity Research, Rennweg 14, 1030 Vienna, 259) Princeton School of Public and  
 1175 International Affairs, Princeton University, Princeton, NJ 08540, USA, 260) Université de Lorraine, AgroParisTech, INRAE, Silva, 54000  
 1176 Nancy, France., 261) Department of Soil Science and Landscape Management, Faculty of Earth Sciences and Spatial Management, Nicolaus  
 1177 Copernicus University, Toruń, Poland, 262) Terra Nova National Park, Parks Canada Agency, Glovertown NL, A0G3Y0, 263) Universidade  
 1178 Estadual do Norte Fluminense Darcy Ribeiro, Campos dos Goytacazes, Rio de Janeiro, Brazil, 264) National Forest Centre, Forest Research  
 1179 Institute Zvolen, T. G. Masaryka 22, 96001 Zvolen, Slovakia, 265) Asian School of Environment, Nanyang Technological University, 42  
 1180 Nanyang Ave, Singapore 639815, Singapore, 266) Department of Geography, University of British Columbia, 1984 West Mall, Vancouver,  
 1181 BC V6T 1Z2, 267) Department of Earth and Environmental Sciences, Celestijnenlaan 200E, 3001 Leuven, Belgium, 268) Universidade  
 1182 Federal da Paraíba, Departamento de Geociências. Cidade Universitária, João Pessoa - PB, CEP 58051-900, Brasil, 269) Goethe-Universität  
 1183 Frankfurt, Department of Physical Geography, Altenhöferallee 1, 60438 Frankfurt am Main, Germany, 270) Department of Evolution,  
 1184 Ecology, and Organismal Biology, University of California Riverside, Riverside, CA, 92521, USA, 271) Department of Natural History, NTNU  
 1185 University Museum, Norwegian University of Science and Technology, NO-7491 Trondheim Norway, 272) UR 'Ecologie et Dynamique des  
 1186 Systèmes Anthropisés' (EDYSAN, UMR 7058 CNRS-UPJV), Univ. de Picardie Jules Verne, Amiens, France, 273) EnvixLab, Dipartimento di  
 1187 Bioscienze e Territorio, Università degli Studi del Molise, Via Duca degli Abruzzi s.n.c., 86039 Termoli, Italy, 274) Institute of Meteorology  
 1188 and Climate Research (IMK), Department of Atmospheric Environmental Reserach (IFU), Karlsruhe Institute of Technology (KIT),

1189 Kreuzebahn Straße 19, 82467 Garmisch-Partenkirchen, Germany, 275) Swedish University of Agricultural Sciences, SLU Swedish Species  
1190 Information Centre, Almas allé 8 E, 75651 Uppsala, Sweden, 276) University Duisburg-Essen, Faculty for Biology, Universitätsstr. 5, 45141  
1191 Essen, Germany, 277) Department of Geosciences and Natural Resource Management, University of Copenhagen, Øster Voldgade 10, DK-  
1192 1350 Copenhagen, Denmark, 278) Experimental Plant Ecology, Institute of Botany and Landscape Ecology, University of Greifswald,  
1193 partner in the Greifswald Mire Centre, D-17487 Greifswald, Germany, 279) Fondation J.-M. Aubert, 1938 Champex-Lac, Switzerland, 280)  
1194 Département de Botanique et Biologie végétale, Université de Genève, Case postale 71, CH-1292 Chambésy, Switzerland, 281)  
1195 Department of Geography and Earth Sciences, Aberystwyth University, Wales, UK, 282) Center for Systematic Biology, Biodiversity and  
1196 Bioresources - 3B, Babeş-Bolyai University, Cluj-Napoca, Romania, 283) Northern Environmental Geoscience Laboratory, Department of  
1197 Geography and Planning, Queen's University, 284) Graduate School of Life and Environmental Sciences, Osaka Prefecture University, 599-  
1198 8531, Japan, 285) Nature Research Centre, Akademijos 2, 08412 Vilnius, Lithuania, 286) Institute of Biological Research Cluj-Napoca,  
1199 National Institute of Research and Development for Biological Sciences, Bucharest, Romania, 287) CNR Institute for BioEconomy, Via  
1200 Giovanni Caproni, 50144 Firenze, Italy, 288) The Ecosystem Management Research Group (ECOBE), University of Antwerp, 2610 Wilrijk  
1201 (Antwerpen), Belgium, 289) Plant Conservation and Population Biology, Department of Biology, KU Leuven, Kasteelpark Arenberg 31, 3001  
1202 Heverlee, Belgium, 290) A.N. Severtsov Institute of Ecology and Evolution, Russian Academy of Sciences, 119071, Leninsky pr.33, Moscow,  
1203 Russia, 291) Netherlands Institute of Ecology, Droevendaalsesteeg 10, 6708 PB, Wageningen, 292) Plant Ecology & Nature Conservation  
1204 Group Wageningen University, Droevendaalse Steeg 3a 6708 PB Wageningen, 293) Centre for Integrative Ecology, School of Life and  
1205 Environmental Sciences, Deakin University, Burwood, Victoria, Australia, 3125, 294) CAVELab - Computational and Applied Vegetation  
1206 Ecology, Department of Environment, Ghent University, Coupure Links 653, 9000 Gent, Belgium, 295) Earth Surface Processes Team,  
1207 Centre for Environmental and Marine Studies (CESAM), Dept. Environment and Planning, University of Aveiro, 3810-193, Aveiro, Portugal,  
1208 296) Instituto Pirenaico de Ecología, IPE-CSIC. Av. Llano de la Victoria, 16. 22700 Jaca (Huesca) Spain, 297) CNR - Institute for Agricultural  
1209 and Forestry Systems in the Mediterranean, P.le Enrico Fermi 1- Loc. del Granatello, 80055, Portici, (Napoli), Italy, 298) Institute of Earth  
1210 Surface Dynamics, Faculty of Geosciences and Environment, University of Lausanne, Géopolis, 1015 Lausanne, Switzerland, 299) Forest  
1211 Research, Northern Research Station, Roslin, EH25 9SY, UK, 300) Institute of Mountain Hazards and Environment, Chinese Academy of  
1212 Sciences, Chengdu, P.R. China, 301) Department of Earth and Environmental Sciences, Lehigh University, Bethlehem, PA 18015, United  
1213 States, 302) Institute for Peat and Mire Research, School of Geographical Sciences, Northeast Normal University, Changchun, Jilin 130024,  
1214 China, 303) High Meadows Environmental Institute, Princeton University, NJ 08544, USA, 304) Zhejiang Tiantong Forest Ecosystem  
1215 National Observation and Research Station, School of Ecological and Environmental Sciences, East China Normal University, Shanghai  
1216 200241, China, 305) J.J.L. received funding from the National Natural Science Foundation of China (grant nr. 32071538), 306) University of  
1217 Bayreuth, Ecological-Botanical Gardens, Universitaetsstr. 30, Bayreuth, Germany, 307) Key Laboratory of Geographical Processes and  
1218 Ecological Security in Changbai Mountains, Ministry of Education, School of Geographical Sciences, Northeast Normal University,  
1219 Changchun 130024, China

1220

## 1221 References

- 1222 Abatzoglou JT, Dobrowski SZ, Parks SA, Hegewisch KC (2018) TerraClimate, a high-resolution global  
1223 dataset of monthly climate and climatic water balance from 1958–2015. *Scientific data*, **5**,  
1224 170191.
- 1225 Amatulli G, Domisch S, Tuanmu M-N, Parmentier B, Ranipeta A, Malczyk J, Jetz W (2018) A suite of  
1226 global, cross-scale topographic variables for environmental and biodiversity modeling.  
1227 *Scientific data*, **5**, 180040.
- 1228 Antão LH, Bates AE, Blowes SA, Waldock C, Supp SR, Magurran AE, Dornelas M, Schipper AM (2020)  
1229 Temperature-related biodiversity change across temperate marine and terrestrial systems.  
1230 *Nature ecology & evolution*, **4**, 927-933.
- 1231 Ashcroft MB, Cavanagh M, Eldridge MDB, Gollan JR (2014) Testing the ability of topoclimatic grids of  
1232 extreme temperatures to explain the distribution of the endangered brush-tailed rock-  
1233 wallaby (*Petrogale penicillata*). *Journal of biogeography*, **41**, 1402-1413.
- 1234 Ashcroft MB, Chisholm LA, French KO (2008) The effect of exposure on landscape scale soil surface  
1235 temperatures and species distribution models. *Landscape Ecology*, **23**, 211-225.
- 1236 Ashcroft MB, Gollan JR (2012) Fine-resolution (25 m) topoclimatic grids of near-surface (5 cm)  
1237 extreme temperatures and humidities across various habitats in a large (200 x 300 km) and  
1238 diverse region. *International Journal of Climatology*, **32**, 2134-2148.
- 1239 Barnes R, Sahr K, Evenden G, Johnson A, Warmerdam F (2017) dggridR: discrete global grids for R. R  
1240 package version 0.1.12.
- 1241 Bergstrom DM, Wienecke BC, Van Den Hoff J, Hughes L, Lindenmayer DB, Ainsworth TD, Baker CM,  
1242 Bland L, Bowman DM, Brooks ST (2021) Combating ecosystem collapse from the tropics to  
1243 the Antarctic. *Global change biology*, **27**, 1692-1703.
- 1244 Berner LT, Massey R, Jantz P, Forbes BC, Macias-Fauria M, Myers-Smith I, Kumpula T, Gauthier G,  
1245 Andreu-Hayles L, Gaglioti BV (2020) Summer warming explains widespread but not uniform  
1246 greening in the Arctic tundra biome. *Nature Communications*, **11**, 1-12.
- 1247 Bond-Lamberty B, Thomson A (2018) A Global Database of Soil Respiration Data, Version 4.0. ORNL  
1248 DAAC.
- 1249 Booth TH, Nix HA, Busby JR, Hutchinson MF (2014) BIOCLIM: the first species distribution modelling  
1250 package, its early applications and relevance to most current MAXENT studies. *Diversity and*  
1251 *Distributions*, **20**, 1-9.
- 1252 Bramer I, Anderson B, Bennie J, Bladon A, De Frenne P, Hemming D, Hill RA, Kearney MR, Körner C,  
1253 Korstjens AH, Lenoir J, Maclean IMD, Marsh CD, Morecroft MD, Ohlemüller R, Slater HD,  
1254 Suggitt AJ, Zellweger F, Gillingham PK (2018) Advances in monitoring and modelling climate  
1255 at ecologically relevant scales. *Advances in Ecological Research*, **58**, 101-161.
- 1256 Bruelheide H, Dengler J, Purschke O, Lenoir J, Jiménez-Alfaro B, Hennekens SM, Botta-Dukát Z,  
1257 Chytrý M, Field R, Jansen F (2018) Global trait–environment relationships of plant  
1258 communities. *Nature ecology & evolution*, **2**, 1906.
- 1259 Bütikofer L, Anderson K, Bebbler DP, Bennie JJ, Early RI, Maclean IM (2020) The problem of scale in  
1260 predicting biological responses to climate. *Global change biology*, **26**, 6657-6666.
- 1261 Chen L, Aalto J, Luoto M (2021) Significant shallow–depth soil warming over Russia during the past  
1262 40 years. *Global and Planetary Change*, **197**, 103394.
- 1263 Cooper EJ (2014) Warmer shorter winters disrupt Arctic terrestrial ecosystems. *Annual Review of*  
1264 *Ecology, Evolution, and Systematics*, **45**, 271-295.
- 1265 Copernicus Climate Change Service (C3s) (2019) C3S ERA5-Land reanalysis. (ed Copernicus Climate  
1266 Change Service).
- 1267 Coûteaux M-M, Bottner P, Berg B (1995) Litter decomposition, climate and litter quality. *Trends in*  
1268 *ecology & evolution*, **10**, 63-66.
- 1269 Crowther TW, Todd-Brown KE, Rowe CW, Wieder WR, Carey JC, Machmuller MB, Snoek B, Fang S,  
1270 Zhou G, Allison SD (2016) Quantifying global soil carbon losses in response to warming.  
1271 *Nature*, **540**, 104-108.

1272 Daly C (2006) Guidelines for assessing the suitability of spatial climate data sets. *International*  
1273 *Journal of Climatology*, **26**, 707-721.

1274 Davis E, Trant A, Hermanutz L, Way RG, Lewkowicz AG, Collier LS, Cuerrier A, Whitaker D (2020)  
1275 *Plant–Environment Interactions in the Low Arctic Torngat Mountains of Labrador.*  
1276 *Ecosystems*, 1-21.

1277 De Frenne P, Lenoir J, Luoto M, Scheffers BR, Zellweger F, Aalto J, Ashcroft M, Christiansen D,  
1278 Decocq G, De Pauw K, Govaert S, Greiser C, Gril E, Hampe A, Jucker T, Klings D, Koelemeijer  
1279 I, Lembrechts J, Marrec R, Meeussen C, Ogee J, Tyystjarvi V, Vangansbeke P, Hylander K  
1280 (2021) Forest microclimates and climate change: importance, drivers and future research  
1281 agenda. *Global change biology*, **In press**.

1282 De Frenne P, Rodríguez-Sánchez F, Coomes DA, Baeten L, Verstraeten G, Vellend M, Bernhardt-  
1283 Römermann M, Brown CD, Brunet J, Cornelis J (2013) Microclimate moderates plant  
1284 responses to macroclimate warming. *Proceedings of the National Academy of Sciences*, **110**,  
1285 18561-18565.

1286 De Frenne P, Zellweger F, Rodríguez-Sánchez F, Scheffers BR, Hylander K, Luoto M, Vellend M,  
1287 Verheyen K, Lenoir J (2019) Global buffering of temperatures under forest canopies. *Nature*  
1288 *ecology & evolution*, **3**, 744-749.

1289 Dinerstein E, Olson D, Joshi A, Vynne C, Burgess ND, Wikramanayake E, Hahn N, Palminteri S, Hedao  
1290 P, Noss R (2017) An ecoregion-based approach to protecting half the terrestrial realm.  
1291 *BioScience*, **67**, 534-545.

1292 Du E, Terror C, Pellegrini AF, Ahlström A, Van Lissa CJ, Zhao X, Xia N, Wu X, Jackson RB (2020) Global  
1293 patterns of terrestrial nitrogen and phosphorus limitation. *Nature Geoscience*, **13**, 221-226.

1294 Fick SE, Hijmans RJ (2017) WorldClim 2: new 1-km spatial resolution climate surfaces for global land  
1295 areas. *International Journal of Climatology*, **37**, 4302-4315.

1296 Geiger R (1950) *The climate near the ground*, Cambridge, Massachusetts, USA, Harvard University  
1297 Press.

1298 Gistemp Team (2021) GISS Surface Temperature Analysis (GISTEMP), version 4. NASA Goddard  
1299 Institute for Space Studies.

1300 Gorelick N, Hancher M, Dixon M, Ilyushchenko S, Thau D, Moore R (2017) Google Earth Engine:  
1301 Planetary-scale geospatial analysis for everyone. *Remote Sensing of Environment*, **202**, 18-  
1302 27.

1303 Gottschall F, Davids S, Newiger-Dous TE, Auge H, Cesarz S, Eisenhauer N (2019) Tree species identity  
1304 determines wood decomposition via microclimatic effects. *Ecology and evolution*, **9**, 12113-  
1305 12127.

1306 Graae BJ, Vandvik V, Armbruster WS, Eiserhardt WL, Svenning J-C, Hylander K, Ehrlén J, Speed JD,  
1307 Klanderud K, Bråthen KA, Milbau A, Opedal OH, Alsos IG, Ejrnaes R, Bruun HH, Birks HJB,  
1308 Westergaard KB, Birks HH, Lenoir J (2018) Stay or go—how topographic complexity influences  
1309 alpine plant population and community responses to climate change. *Perspectives in plant*  
1310 *ecology, evolution and systematics*, **30**, 41-50.

1311 Greiser C, Meineri E, Luoto M, Ehrlén J, Hylander K (2018) Monthly microclimate models in a  
1312 managed boreal forest landscape. *Agricultural and Forest Meteorology*, **250**, 147-158.

1313 Grünberg I, Wilcox EJ, Zwieback S, Marsh P, Boike J (2020) Linking tundra vegetation, snow, soil  
1314 temperature, and permafrost. *Biogeosciences*, **17**, 4261-4279.

1315 Grundstein A, Todhunter P, Mote T (2005) Snowpack control over the thermal offset of air and soil  
1316 temperatures in eastern North Dakota. *Geophysical Research Letters*, **32**.

1317 Hall DK, Riggs GA, Salomonson VV, Digirolamo NE, Bayr KJ (2002) MODIS snow-cover products.  
1318 *Remote Sensing of Environment*, **83**, 181-194.

1319 Hengl T, De Jesus JM, Heuvelink GB, Gonzalez MR, Kilibarda M, Blagotić A, Shangguan W, Wright  
1320 MN, Geng X, Bauer-Marschallinger B (2017) SoilGrids250m: Global gridded soil information  
1321 based on machine learning. *Plos One*, **12**, e0169748.



1322 Hennon PE, D'amore DV, Witter DT, Lamb MB (2010) Influence of forest canopy and snow on  
1323 microclimate in a declining yellow-cedar forest of Southeast Alaska. *Northwest Science*, **84**,  
1324 73-87.

1325 Hursh A, Ballantyne A, Cooper L, Maneta M, Kimball J, Watts J (2017) The sensitivity of soil  
1326 respiration to soil temperature, moisture, and carbon supply at the global scale. *Global  
1327 change biology*, **23**, 2090-2103.

1328 Johnston AS, Meade A, Ardö J, Arriga N, Black A, Blanken PD, Bonal D, Brümmer C, Cescatti A, Dušek  
1329 J (2021) Temperature thresholds of ecosystem respiration at a global scale. *Nature ecology  
1330 & evolution*, **5**, 487-494.

1331 Karger DN, Conrad O, Böhner J, Kawohl T, Kreft H, Soria-Auza RW, Zimmermann NE, Linder HP,  
1332 Kessler M (2017a) Climatologies at high resolution for the earth's land surface areas.  
1333 *Scientific data*, **4**, 170122.

1334 Karger DN, Conrad O, Böhner J, Kawohl T, Kreft H, Soria-Auza RW, Zimmermann NE, Linder HP,  
1335 Kessler M (2017b) Data from: Climatologies at high resolution for the earth's land surface  
1336 areas. In: *Dryad Digital Repository*.

1337 Kattge J, Bönisch G, Diaz S, Lavorel S, Prentice IC, Leadley P, Tautenhahn S, Werner G, Günther A  
1338 (2019) TRY plant trait database-enhanced coverage and open access. *Global change biology*,  
1339 **26**, 119-188.

1340 Kearney M, Shine R, Porter WP (2009) The potential for behavioral thermoregulation to buffer “cold-  
1341 blooded” animals against climate warming. *Proceedings of the National Academy of  
1342 Sciences*, **106**, 3835-3840.

1343 Kearney MR, Gillingham PK, Bramer I, Duffy JP, Maclean IM (2019) A method for computing hourly,  
1344 historical, terrain-corrected microclimate anywhere on Earth. *Methods in Ecology and  
1345 Evolution*, **11**, 38-43.

1346 Kissling WD, Walls R, Bowser A, Jones MO, Kattge J, Agosti D, Amengual J, Basset A, Van Bodegom  
1347 PM, Cornelissen JH (2018) Towards global data products of Essential Biodiversity Variables  
1348 on species traits. *Nature ecology & evolution*, **2**, 1531-1540.

1349 Körner C, Hiltbrunner E (2018) The 90 ways to describe plant temperature. *Perspectives in plant  
1350 ecology, evolution and systematics*, **30**, 16-21.

1351 Körner C, Paulsen J (2004) A world-wide study of high altitude treeline temperatures. *Journal of  
1352 biogeography*, **31**, 713-732.

1353 Lembrechts J, Aalto J, Ashcroft M, De Frenne P, Kopecký M, Lenoir J, Luoto M, Maclean IM,  
1354 Consortium S, Nijs I (2020) SoilTemp: call for data for a global database of near-surface  
1355 temperature. *Global change biology*, **26**, 6616-6629.

1356 Lembrechts J, Lenoir J, Scheffers BR, De Frenne P (2021) Time for countrywide microclimate  
1357 networks. *Global Ecology and Biogeography*.

1358 Lembrechts JJ, Lenoir J (2019) Microclimatic conditions anywhere at any time! *Global change  
1359 biology*.

1360 Lembrechts JJ, Lenoir J, Roth N, Hattab T, Milbau A, Haider S, Pellissier L, Pauchard A, Ratier Backes  
1361 A, Dimarco RD (2019) Comparing temperature data sources for use in species distribution  
1362 models: From in-situ logging to remote sensing. *Global Ecology and Biogeography*, **28**, 1578-  
1363 1596.

1364 Lembrechts JJ, Nijs I (2020) Microclimate shifts in a dynamic world. *Science*, **368**, 711-712.

1365 Lenoir J, Bertrand R, Comte L, Bourgeaud L, Hattab T, Murielle J, Grenouillet G (2020) Species  
1366 better track climate warming in the oceans than on land. *Nature ecology & evolution*, **4**,  
1367 1044-1059.

1368 Luojus K, Pulliainen J, Takala M, Derksen C, Rott H, Nagler T, Solberg R, Wiesmann A, Metsamaki S,  
1369 Malnes E (2010) Investigating the feasibility of the GlobSnow snow water equivalent data for  
1370 climate research purposes. In: *2010 IEEE International Geoscience and Remote Sensing  
1371 Symposium*. IEEE.

1372 Maclean IM, Duffy JP, Haesen S, Govaert S, De Frenne P, Vanneste T, Lenoir J, Lembrechts JJ, Rhodes  
1373 MW, Van Meerbeek K (2021) On the measurement of microclimate. *Methods in Ecology and*  
1374 *Evolution*.

1375 Maclean IM, Klings DH (2021) Microclimc: A mechanistic model of above, below and within-canopy  
1376 microclimate. *Ecological Modelling*, **451**, 109567.

1377 Maclean IM, Mosedale JR, Bennie JJ (2019) Microclima: An r package for modelling meso-and  
1378 microclimate. *Methods in Ecology and Evolution*, **10**, 280-290.

1379 Myers-Smith IH, Kerby JT, Phoenix GK, Bjerke JW, Epstein HE, Assmann JJ, John C, Andreu-Hayles L,  
1380 Angers-Blondin S, Beck PS (2020) Complexity revealed in the greening of the Arctic. *Nature*  
1381 *Climate Change*, **10**, 106-117.

1382 Niittynen P, Heikkinen RK, Aalto J, Guisan A, Kemppinen J, Luoto M (2020) Fine-scale tundra  
1383 vegetation patterns are strongly related to winter thermal conditions. *Nature Climate*  
1384 *Change*, **10**, 1143-1148.

1385 Niittynen P, Luoto M (2018) The importance of snow in species distribution models of arctic  
1386 vegetation. *Ecography*, **41**, 1024-1037.

1387 O'donnell MS, Ignizio DA (2012) Bioclimatic predictors for supporting ecological applications in the  
1388 conterminous United States. *US Geological Survey Data Series*, **691**, 4-9.

1389 Obu J, Westermann S, Bartsch A, Berdnikov N, Christiansen HH, Dashtseren A, Delaloye R, Elberling  
1390 B, Etzelmüller B, Kholodov A (2019) Northern Hemisphere permafrost map based on TTOP  
1391 modelling for 2000–2016 at 1 km<sup>2</sup> scale. *Earth-Science Reviews*, **193**, 299-316.

1392 Olden JD, Lawler JJ, Poff NL (2008) Machine learning methods without tears: a primer for ecologists.  
1393 *The Quarterly review of biology*, **83**, 171-193.

1394 Opedal OH, Armbruster WS, Graae BJ (2015) Linking small-scale topography with microclimate, plant  
1395 species diversity and intra-specific trait variation in an alpine landscape. *Plant Ecology &*  
1396 *Diversity*, **8**, 305-315.

1397 Overland JE, Wang M, Walsh JE, Stroeve JC (2014) Future Arctic climate changes: Adaptation and  
1398 mitigation time scales. *Earth's Future*, **2**, 68-74.

1399 Pastorello G, Papale D, Chu H, Trotta C, Agarwal D, Canfora E, Baldocchi D, Torn M (2017) A new data  
1400 set to keep a sharper eye on land-air exchanges. *Eos, Transactions American Geophysical*  
1401 *Union (Online)*, **98**.

1402 Perera-Castro AV, Waterman MJ, Turnbull JD, Ashcroft MB, Mckinley E, Watling JR, Bramley-Alves J,  
1403 Casanova-Katny A, Zuniga G, Flexas J (2020) It is hot in the sun: Antarctic mosses have high  
1404 temperature optima for photosynthesis despite cold climate. *Frontiers in Plant Science*, **11**,  
1405 1178.

1406 Pleim JE, Gilliam R (2009) An indirect data assimilation scheme for deep soil temperature in the  
1407 Pleim–Xiu land surface model. *Journal of Applied Meteorology and Climatology*, **48**, 1362-  
1408 1376.

1409 Portillo-Estrada M, Pihlatie M, Korhonen JFJ, Levula J, Frumau AKF, Ibrom A, Lembrechts JJ, Morillas  
1410 L, Horvath L, Jones SK, Niinemets U (2016) Climatic controls on leaf litter decomposition  
1411 across European forests and grasslands revealed by reciprocal litter transplantation  
1412 experiments. *Biogeosciences*, **13**, 1621-1633.

1413 Potter KA, Woods HA, Pincebourde S (2013) Microclimatic challenges in global change biology.  
1414 *Global change biology*, **19**, 2932-2939.

1415 R Core Team (2020) R: a language and environment for statistical computing, R Foundation for  
1416 Statistical Computing.

1417 Richardson LF (1922) *Weather prediction by numerical process*, Cambridge university press.

1418 Rosenberg NJ, Kimball B, Martin P, Cooper C (1990) From climate and CO<sub>2</sub> enrichment to  
1419 evapotranspiration. *Climate change and US water resources.*, 151-175.

1420 Santoro M (2018) GlobBiomass—Global datasets of forest biomass. *PANGAEA10*, **1594**.

1421 Scherrer D, Schmid S, Körner C (2011) Elevational species shifts in a warmer climate are  
1422 overestimated when based on weather station data. *International journal of*  
1423 *Biometeorology*, **55**, 645-654.

1424 Schimel DS, Braswell B, Mckeown R, Ojima DS, Parton W, Pulliam W (1996) Climate and nitrogen  
1425 controls on the geography and timescales of terrestrial biogeochemical cycling. *Global*  
1426 *Biogeochemical Cycles*, **10**, 677-692.

1427 Schimel JP, Bilbrough C, Welker JM (2004) Increased snow depth affects microbial activity and  
1428 nitrogen mineralization in two Arctic tundra communities. *Soil Biology and Biochemistry*, **36**,  
1429 217-227.

1430 Senior RA, Hill JK, Edwards DP (2019) Global loss of climate connectivity in tropical forests. *Nature*  
1431 *Climate Change*, **9**, 623-626.

1432 Smith M, Riseborough D (1996) Permafrost monitoring and detection of climate change. *Permafrost*  
1433 *and Periglacial Processes*, **7**, 301-309.

1434 Smith M, Riseborough D (2002) Climate and the limits of permafrost: a zonal analysis. *Permafrost*  
1435 *and Periglacial Processes*, **13**, 1-15.

1436 Soudzilovskaia NA, Douma JC, Akhmetzhanova AA, Van Bodegom PM, Cornwell WK, Moens EJ,  
1437 Treseder KK, Tibbett M, Wang YP, Cornelissen JH (2015) Global patterns of plant root  
1438 colonization intensity by mycorrhizal fungi explained by climate and soil chemistry. *Global*  
1439 *Ecology and Biogeography*, **24**, 371-382.

1440 Stefan V, Levin S (2018) Plotbiomes: Plot Whittaker biomes with ggplot2. R package version 0.0.  
1441 0.9001.

1442 Steidinger BS, Crowther TW, Liang J, Van Nuland ME, Werner GD, Reich PB, Nabuurs G-J, De-Miguel  
1443 S, Zhou M, Picard N (2019) Climatic controls of decomposition drive the global biogeography  
1444 of forest-tree symbioses. *Nature*, **569**, 404-408.

1445 Van Den Hoogen J, Geisen S, Routh D, Ferris H, Traunspurger W, Wardle DA, De Goede RG, Adams  
1446 BJ, Ahmad W, Andriuzzi WS (2019) Soil nematode abundance and functional group  
1447 composition at a global scale. *Nature*, **572**, 194-198.

1448 Van Den Hoogen J, Robmann N, Routh D, Lauber T, Van Tiel N, Danylo O, Crowther TW (2021) A  
1449 geospatial mapping pipeline for ecologists. *bioRxiv*.

1450 Wang K, Dickinson RE (2012) A review of global terrestrial evapotranspiration: Observation,  
1451 modeling, climatology, and climatic variability. *Reviews of Geophysics*, **50**.

1452 Way RG, Lewkowicz AG (2018) Environmental controls on ground temperature and permafrost in  
1453 Labrador, northeast Canada. *Permafrost and Periglacial Processes*, **29**, 73-85.

1454 White HJ, León-Sánchez L, Burton VJ, Cameron EK, Caruso T, Cunha L, Dirilgen T, Jurburg SD, Kelly R,  
1455 Kumaresan D (2020) Methods and approaches to advance soil macroecology. *Global Ecology*  
1456 *and Biogeography*, **29**, 1674-1690.

1457 Whiteman CD (1982) Breakup of temperature inversions in deep mountain valleys: Part I.  
1458 Observations. *Journal of Applied Meteorology*, **21**, 270-289.

1459 Wild J, Kopecký M, Macek M, Šanda M, Jankovec J, Haase T (2019) Climate at ecologically relevant  
1460 scales: A new temperature and soil moisture logger for long-term microclimate  
1461 measurement. *Agricultural and Forest Meteorology*, **268**, 40-47.

1462 Wood S (2012) mgcv: Mixed GAM Computation Vehicle with GCV/AIC/REML smoothness estimation.

1463 World Meteorological Organization (2008) *Guide to Meteorological Instruments and Methods of*  
1464 *Observation*, Geneva, WMO-No. 8.

1465 Xu T, Hutchinson M (2011) ANUCLIM version 6.1 user guide. The Australian National University,  
1466 Fenner School of Environment and Society, Canberra.

1467 Xu Y, Ramanathan V, Victor DG (2018) Global warming will happen faster than we think. *Nature*.

1468 Zellweger F, De Frenne P, Lenoir J, Vangansbeke P, Verheyen K, Bernhardt-Römermann M, Baeten L,  
1469 Hédli R, Berki I, Brunet J, Van Calster H, Chudomelová M, Decocq G, Dirnböck T, Durak T,  
1470 Heinken T, Jaroszewicz B, Kopecký M, Malis F, Macek M, Marek M, Naaf T, Nagel TA,  
1471 Ortmann-Ajkai A, Petrik P, Pielech R, Reczynska K, Schmidt W, Standovár T, Swierkosz K,

1472 Teleki B, Vild O, Wulf M, Coomes D (2020) Forest microclimate dynamics drive plant  
1473 responses to warming. *Science*, **368**, 772-775.

1474 Zhang Y, Sherstiukov AB, Qian B, Kokelj SV, Lantz TC (2018) Impacts of snow on soil temperature  
1475 observed across the circumpolar north. *Environmental Research Letters*, **13**, 044012.

1476 Zhang Y, Wang S, Barr AG, Black T (2008) Impact of snow cover on soil temperature and its  
1477 simulation in a boreal aspen forest. *Cold Regions Science and Technology*, **52**, 355-370.

1478 Zhou S, Williams AP, Lintner BR, Berg AM, Zhang Y, Keenan TF, Cook BI, Hagemann S, Seneviratne SI,  
1479 Gentile P (2021) Soil moisture–atmosphere feedbacks mitigate declining water availability  
1480 in drylands. *Nature Climate Change*, 1-7.

1481 Zomer RJ, Trabucco A, Bossio DA, Verchot LV (2008) Climate change mitigation: A spatial analysis of  
1482 global land suitability for clean development mechanism afforestation and reforestation.  
1483 *Agriculture, ecosystems & environment*, **126**, 67-80.

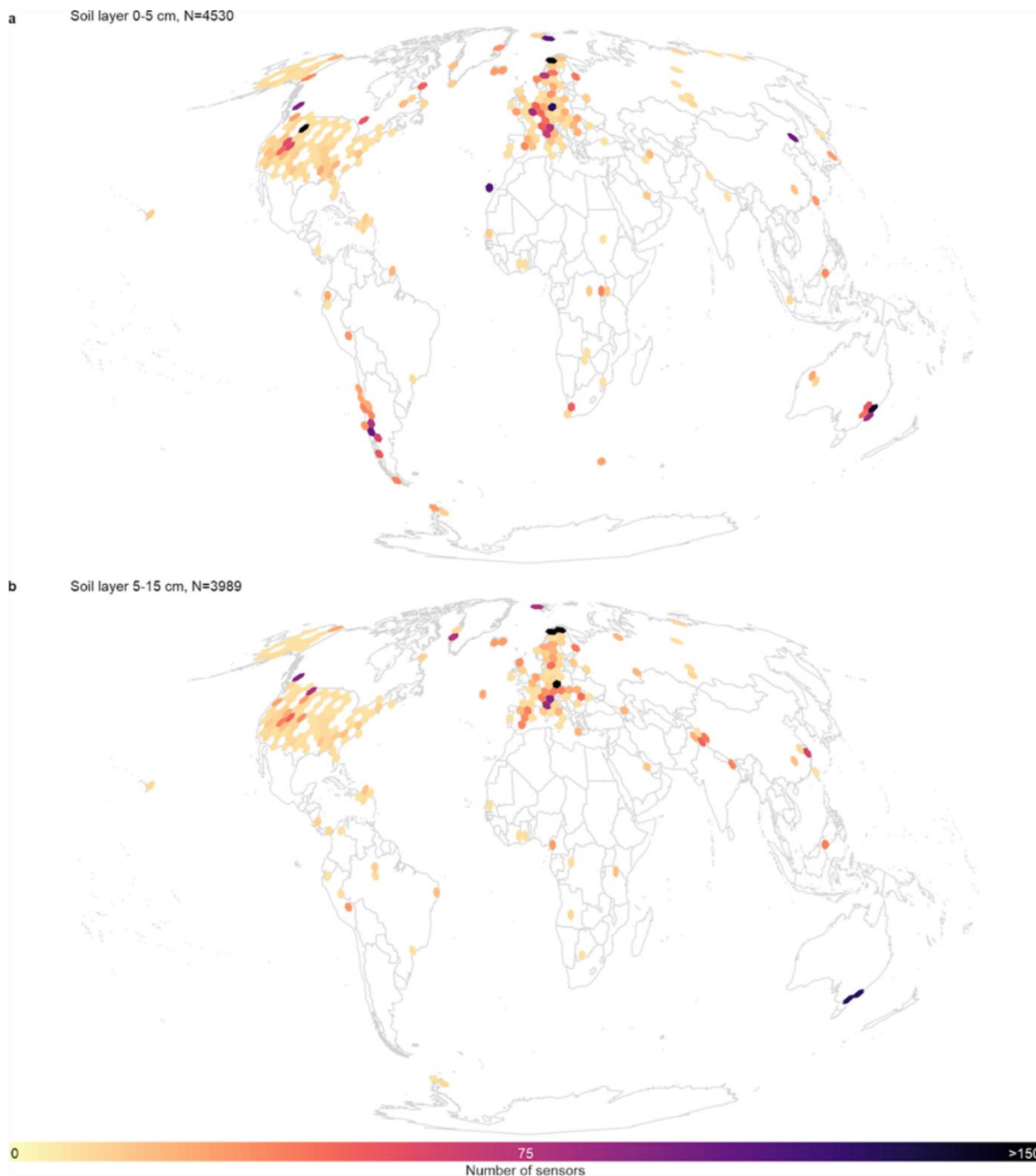
1484

1485

1486

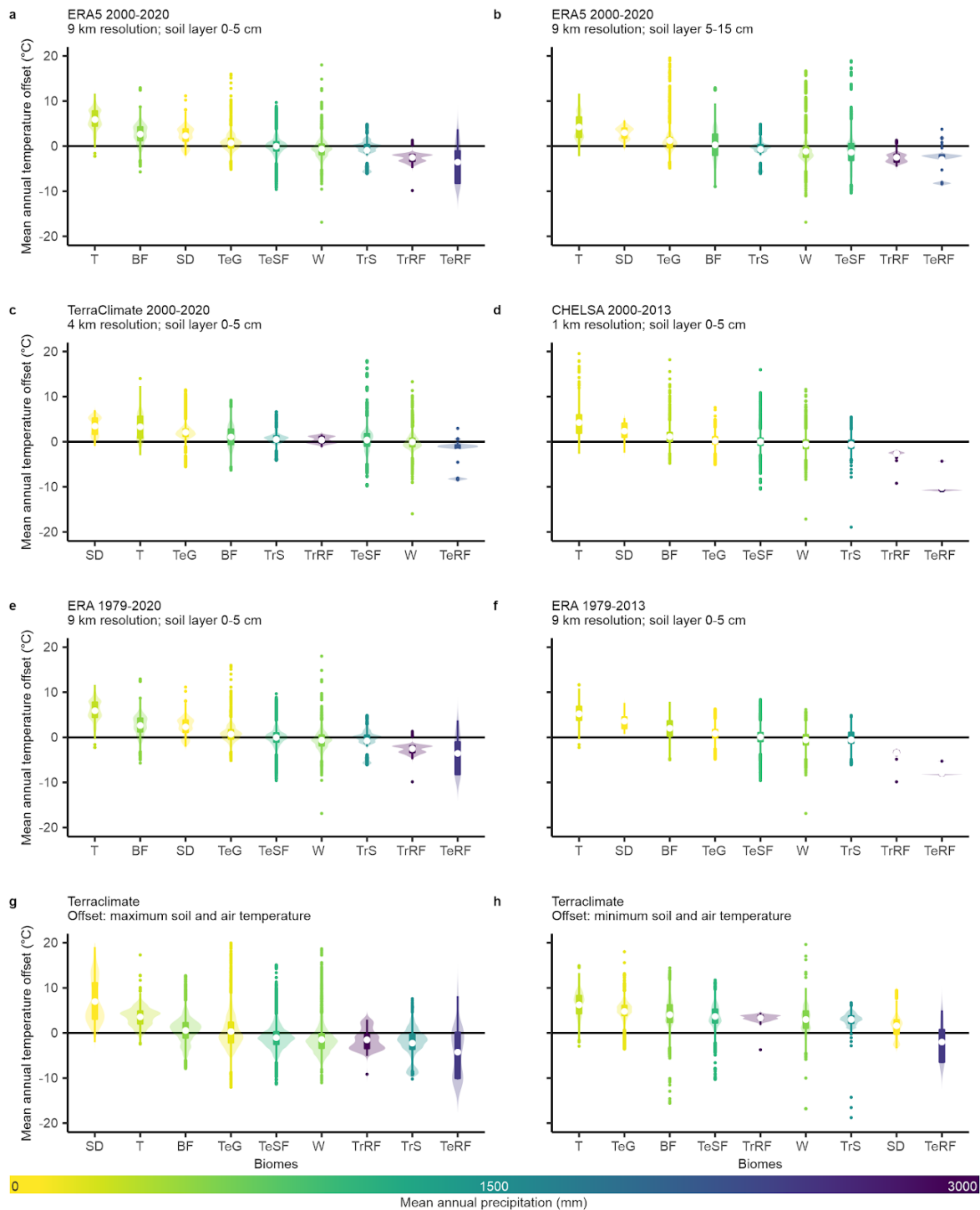
### Supplementary figures and tables

1487



1488

1489 **Fig. S1: Global distribution of the in-situ measurements.** Distribution of all sensors in the topsoil (0–  
1490 5 cm depth, (a), N = 4,530) and the second layer (5–15 cm depth, (b), N = 3,989). Background world  
1491 map in Mollweide projection, hexagons with a resolution of approximately 70,000 km<sup>2</sup>. Note that  
1492 sensors appearing here and not in Fig. 1a or Fig. S3 covered time series of less than one year, and thus  
1493 were only used in the monthly models (see methods for details).

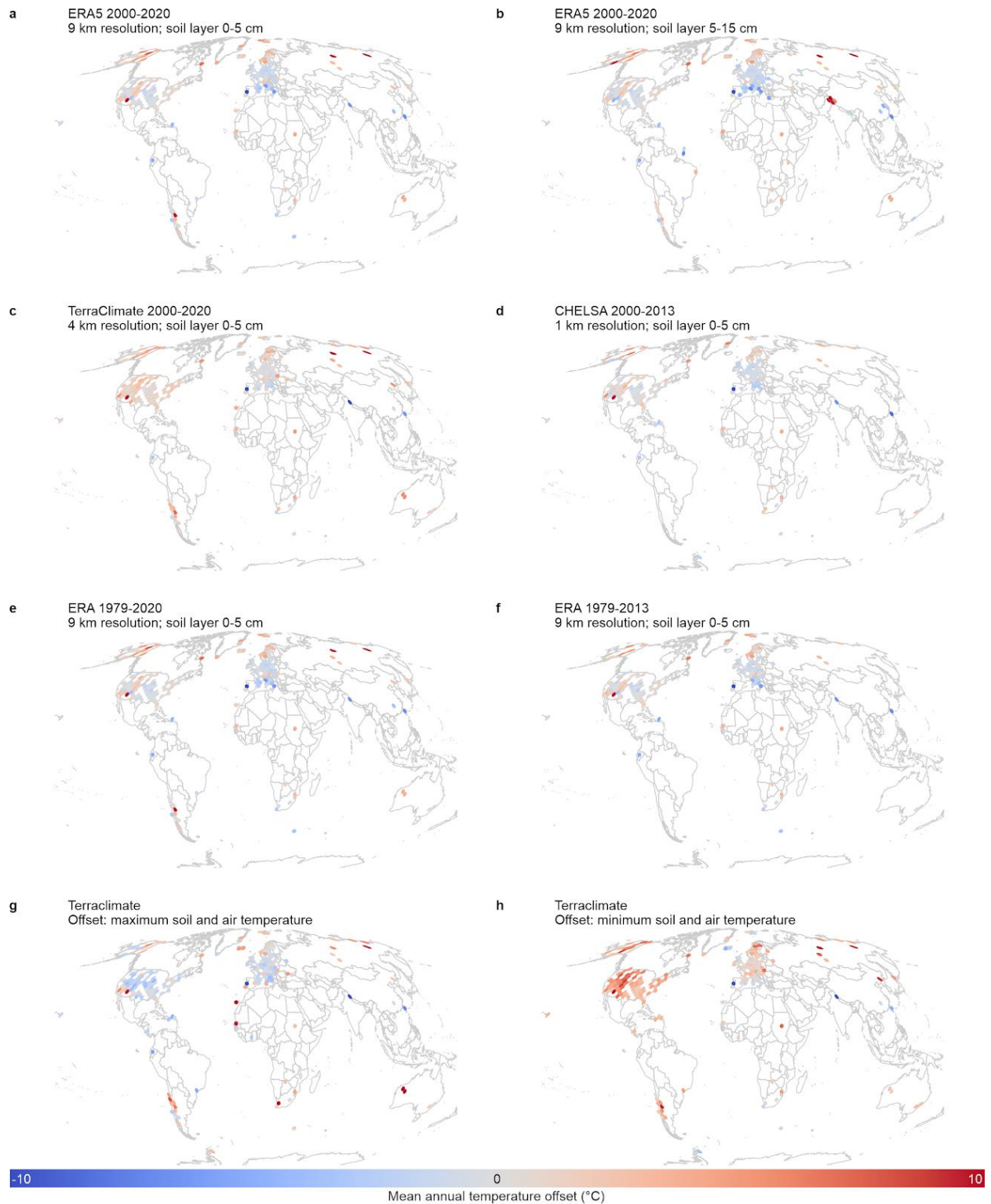


1494  
 1495  
 1496  
 1497  
 1498  
 1499  
 1500  
 1501  
 1502  
 1503  
 1504

**Fig. S2: Annual temperature offsets per biome** (as in Fig. 1b), for the first (0–5 cm depth) and second soil layer (5–15 cm depth) and for different air temperature data sources and time periods. Box- and violin plots of the mean annual temperature offsets per Whittaker biome, ordered and coloured by mean annual precipitation. As a standard, we used ERA5L (2000–2020, 9 km resolution) and the topsoil (0–5 cm, (a), see also Fig. 1b). We compare now with the second soil layer (5–15 cm depth, b), with TerraClimate (2000–2020, 4 km resolution, c) and CHELSA (2000–2013, 1 km resolution, d), with ERA5L for the full period (1979–2020, e) and the period matching the bioclimatic variables (1979–2013, f). We also calculate offsets between maximum (95<sup>th</sup> percentile, g) soil and air temperature, and minimum (5<sup>th</sup> percentile, h) soil and air temperature, with maximum and minimum air temperature based on TerraClimate. Panels (c) to (h) all use the topsoil data (0–5 cm depth). All panels show relatively

1505 consistent results (i.e. strongly positive offsets in tundra, boreal forests, subtropical deserts and  
1506 temperate grasslands, and weakly negative offsets in tropical savannas and temperate and tropical  
1507 rainforests). Only annual soil temperature minima were on average higher than corresponding air  
1508 temperature minima in all but one biomes.

1509

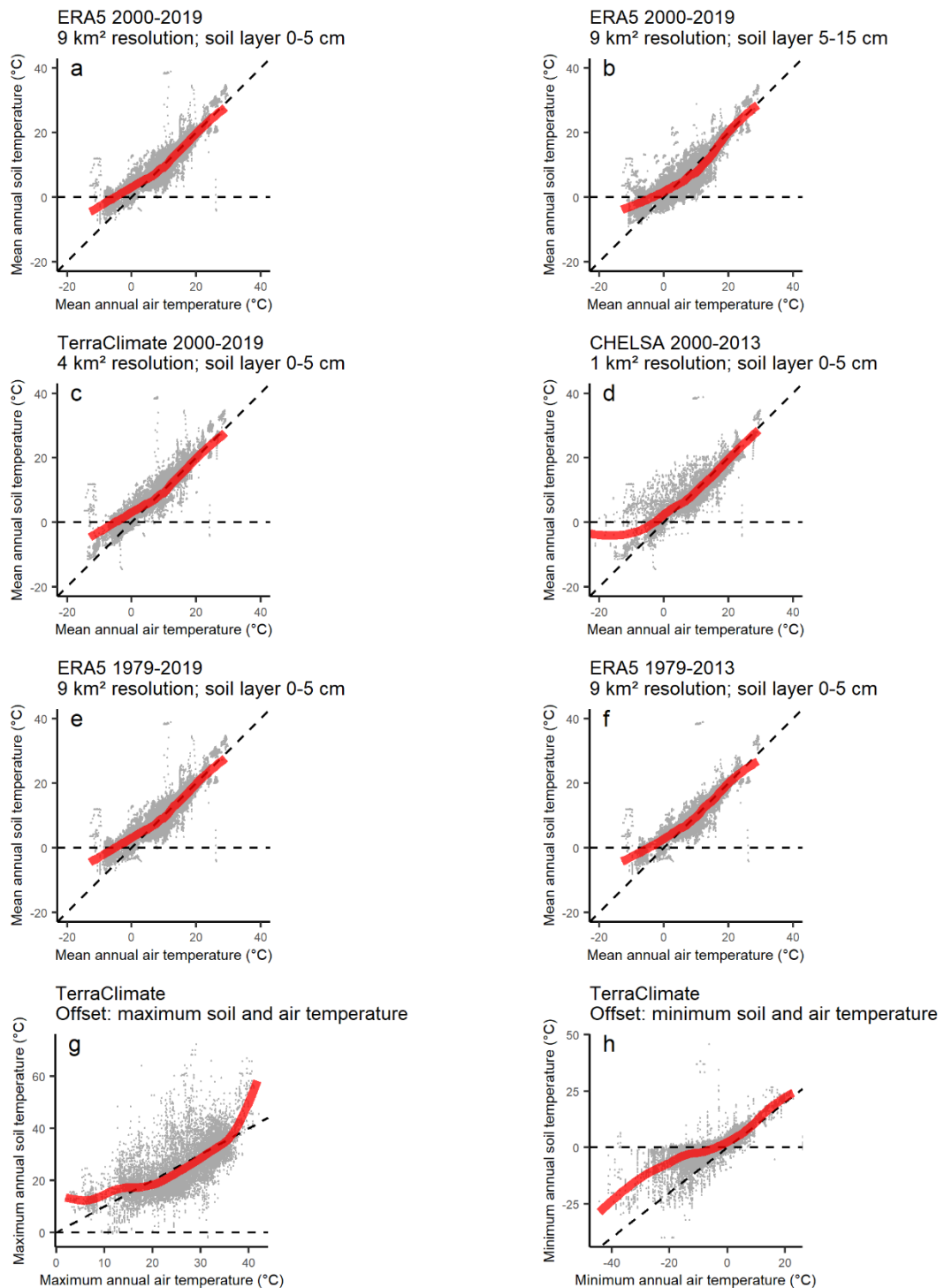


1510

1511 **Fig. S3: Annual temperature offset maps** (as in Fig. 1a), for the first (0–5 cm depth) and second soil  
 1512 layer (5–15 cm depth), for different air temperature data sources and time periods, and for  
 1513 maximum and minimum temperature. Distribution of sensors across the globe, coloured by the  
 1514 annual offset (in °C) between in-situ measured soil temperature and modelled air temperature. As a  
 1515 standard in Fig. 1a, we used ERA5L (2000–2020, 9 km<sup>2</sup> resolution) and the topsoil (0–5 cm, also here  
 1516 in a). We compare now with the second soil layer (5–15 cm depth, b), with TerraClimate (2000–2020,  
 1517 4 km<sup>2</sup> resolution, c) and CHELSA (2000–2013, 1 km<sup>2</sup> resolution, d) for the topsoil layer, and with  
 1518 ERA5L for the full period (1979–2020,e) and the period matching the bioclimatic variables (1979–



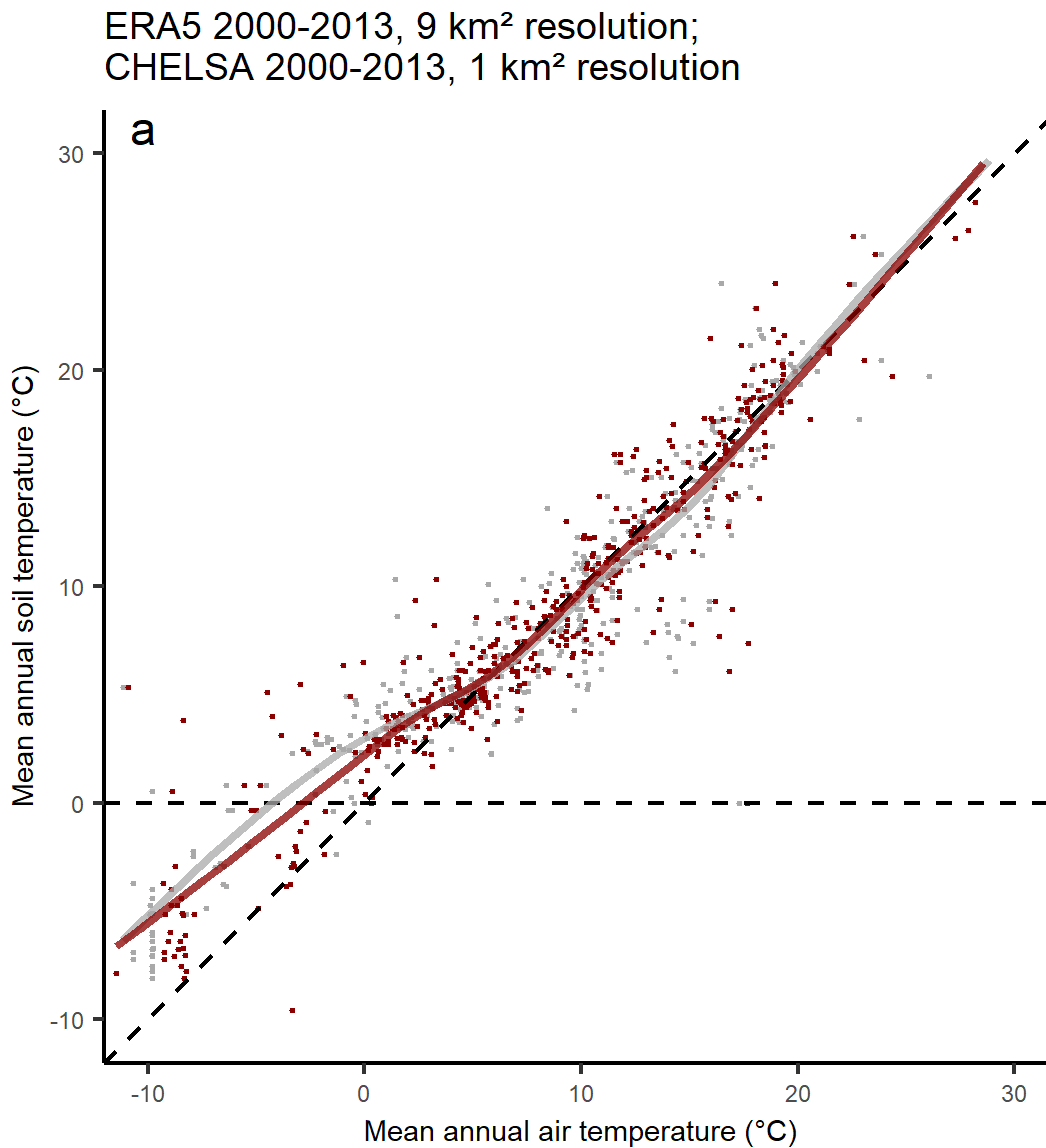
1519 2013, f). We also calculate offsets between maximum (95<sup>th</sup> percentile, g) soil and air temperature,  
1520 and minimum (5<sup>th</sup> percentile, h) soil and air temperature, with maximum and minimum air  
1521 temperature based on TerraClimate. Background world map in MollWeide projection, offsets  
1522 averaged per hexagon with a resolution of approximately 70,000 km<sup>2</sup>, made using the dggridR-  
1523 package in R. Conclusions about consistency between methods similar as in Fig. S2.



1524

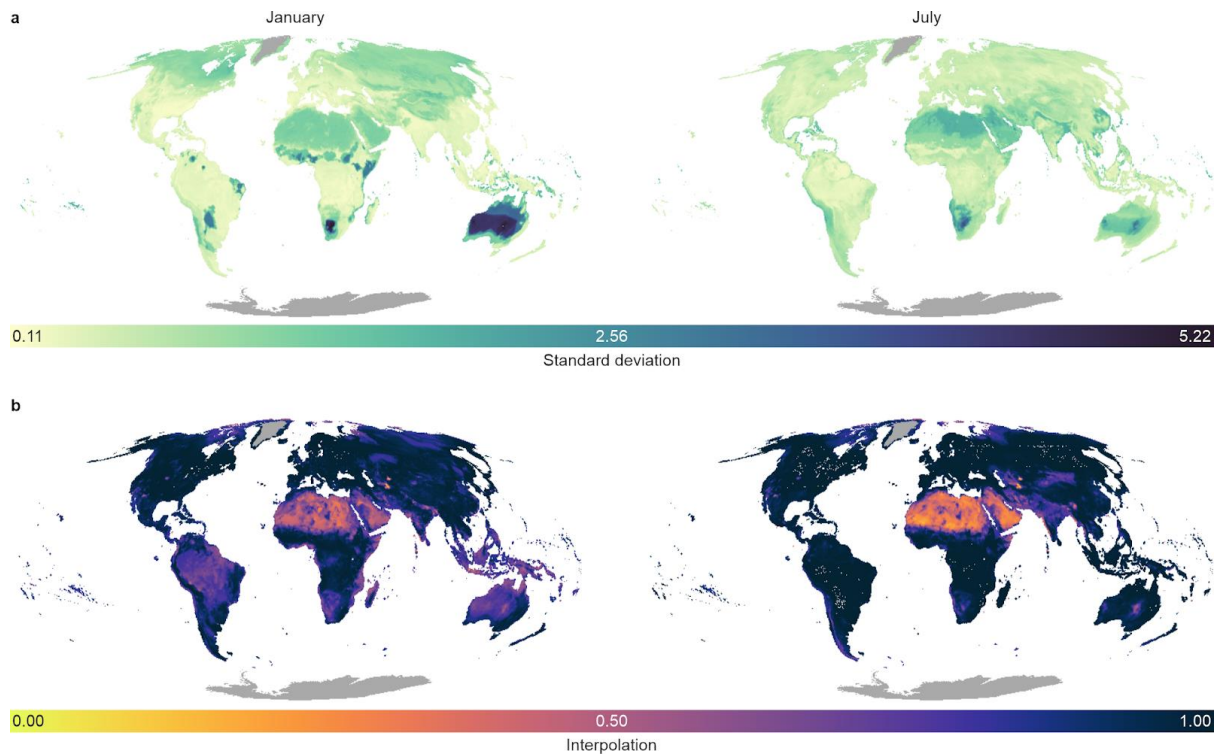
1525 **Fig. S4: Relationship between mean annual soil and air temperature at a 1 × 1 km resolution.** Point  
 1526 cloud of in-situ mean annual soil temperature (°C) as a function of gridded mean annual air  
 1527 temperature for all in-situ measurements averaged at a 1 × 1 km resolution. As a standard, we used  
 1528 ERA5L (2000-2020, 9 km<sup>2</sup> resolution) and the topsoil (0–5 cm depth, a). We compare this first with the  
 1529 second soil layer (5–15 cm depth, b). We also compare with analyses for the top soil layer using  
 1530 TerraClimate (2000-2020, 4 km<sup>2</sup> resolution, c) and CHELSA (2000-2013, 1 km<sup>2</sup> resolution, d), and with  
 1531 ERA5L for the full period (1979-2020, e) and the period matching the bioclimatic variables (1979-2013,  
 1532 f). We also plot offsets between maximum (95<sup>th</sup> percentile, g) soil and air temperature, and minimum  
 1533 (5<sup>th</sup> percentile, h) soil and air temperature, with maximum and minimum air temperature based on

1534 TerraClimate. Straight dashed line indicate a thermal offset of 0°C, and the 1:1-relationship between  
1535 soil and air temperature, thick red lines the relationship based on generalized additive models,  
1536 indicating in all cases warmer soil than air temperatures in cold extremes, yet slightly cooler soils at  
1537 intermediate temperatures (except for h).



1539

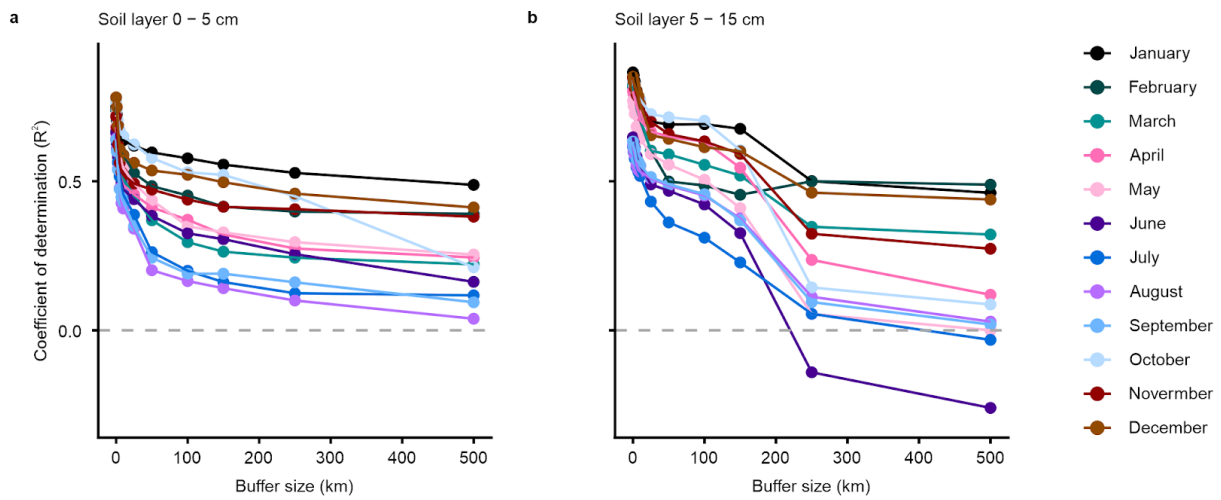
1540 **Fig. S5: Relationship between mean annual soil and air temperature for ERA5L (grey) versus CHELSA**  
 1541 **(red).** Point cloud of in-situ mean annual soil temperature (°C) as a function of gridded mean annual  
 1542 air temperature for all in-situ measurements averaged at 1 km<sup>2</sup>, between 2000 and 2013, for ERA5L  
 1543 (grey, 9-km<sup>2</sup> resolution) and CHELSA (dark red, 1 × 1 km resolution). Straight dashed line indicate a  
 1544 thermal offset of 0°C, and the 1:1-relationship between soil and air temperature, grey and red lines  
 1545 the relationship based on generalized additive models. As in Fig. S4, yet highlighting the strong overlap  
 1546 in pattern when using CHELSA vs ERA5L.



1547

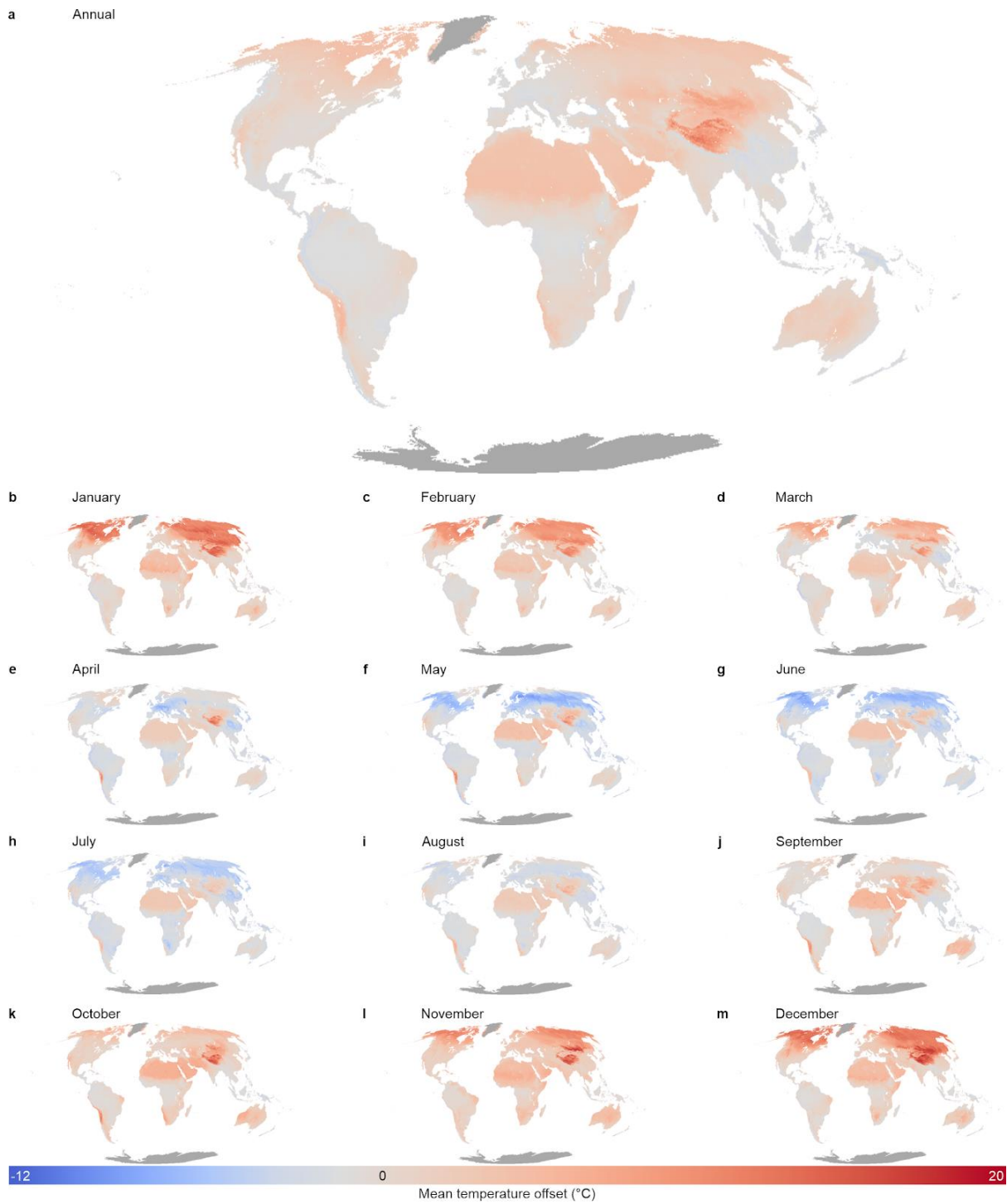
1548 **Fig. S6: Predictive performance of the temperature offset models in the second soil layer (5–15 cm**  
 1549 **depth).** Analyses for the temperature offset between in-situ second soil layer (5–15 cm depth)  
 1550 temperature and free-air temperature. (a) Predicted standard deviation from a cross-validation  
 1551 analysis that iteratively varied the set of covariates (explanatory data layers) and model  
 1552 hyperparameters (i.e., number of variables per split; minimum leaf population) across 100 models  
 1553 and evaluated model strength using 10-fold cross-validation, for January (left) and July (right), as  
 1554 examples of the two most contrasting months. (b) The fraction of axes in the multidimensional  
 1555 environmental space for which the pixel lies inside the range of data covered by the sensors in the  
 1556 database. Pixels with low values indicate that the model has to extrapolate for many of the  
 1557 environmental layers for that specific pixel.

1558



1559

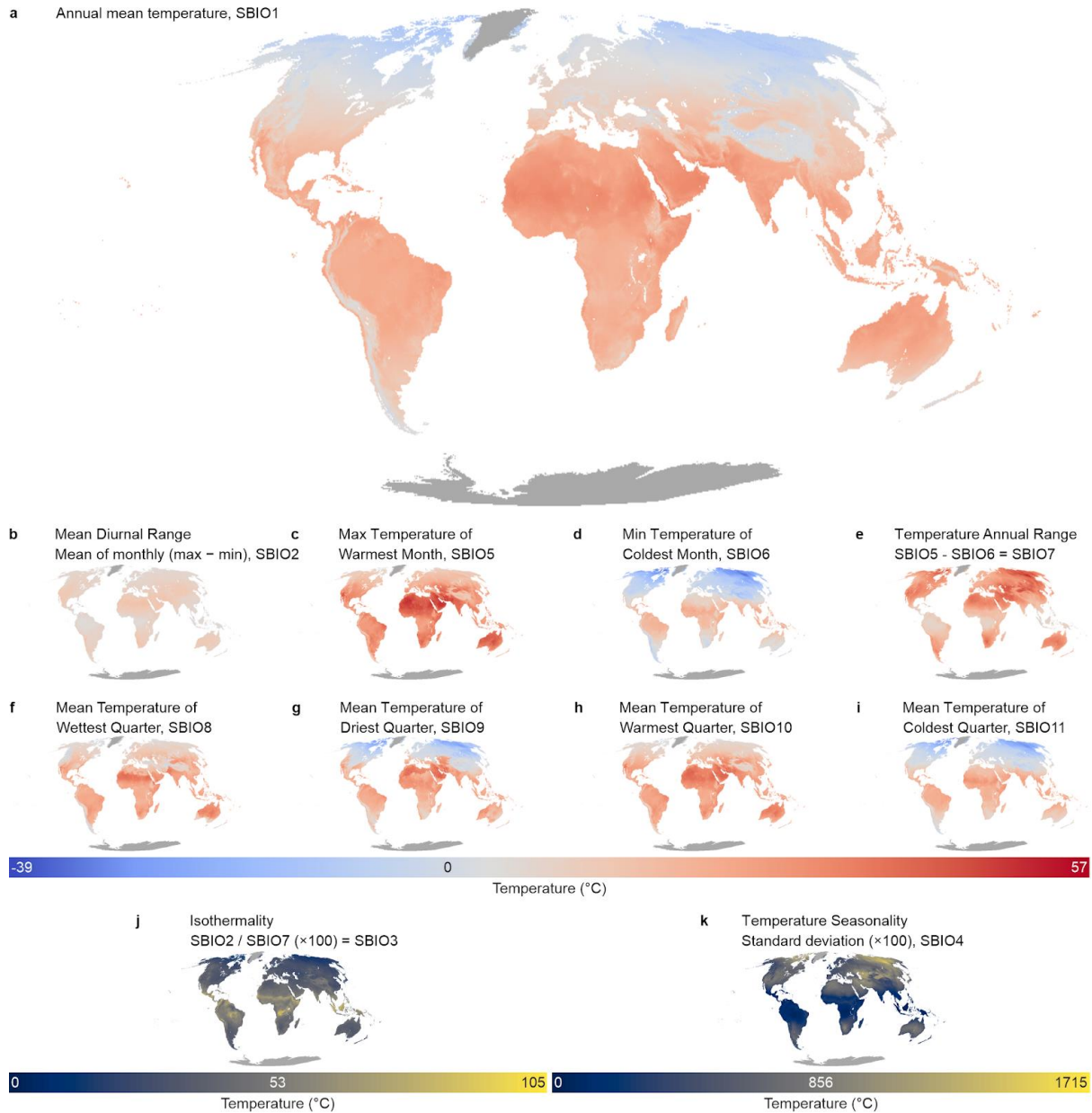
1560 **Fig. S7: spatial leave-one-out cross-validation.**  $R^2$  of all monthly models at the two soil depths using  
1561 a spatial leave-one-out cross validation approach. This approach trains a model for each sample in  
1562 the dataset on all remaining samples, with an increasingly large buffer around that focal sample.  
1563 Note that a decrease in  $R^2$  should be expected with increasing buffer size due to the removal of parts  
1564 of the environmental gradient from the training dataset. Nevertheless, results show that spatial  
1565 autocorrelation differs across the months, with uneven global data coverage likely causing lowest  
1566 confidence for May to September at 5–15 cm depth, where use of data outside of the environmental  
1567 gradient as covered by the data is thus particularly discouraged (see Fig 5b and Fig. S6b).



1568

1569  
1570  
1571  
1572

**Fig. S8: Modelled mean temperature offset in the second soil layer (5–15 cm depth).** Modelled annual (a) and monthly (b-m) temperature offset (in °C) between in-situ measured soil temperature (second soil layer, 5–15 cm depth) and modelled air temperature, in addition to the first soil layer (0–5 cm depth) used in Fig. 2.



1573

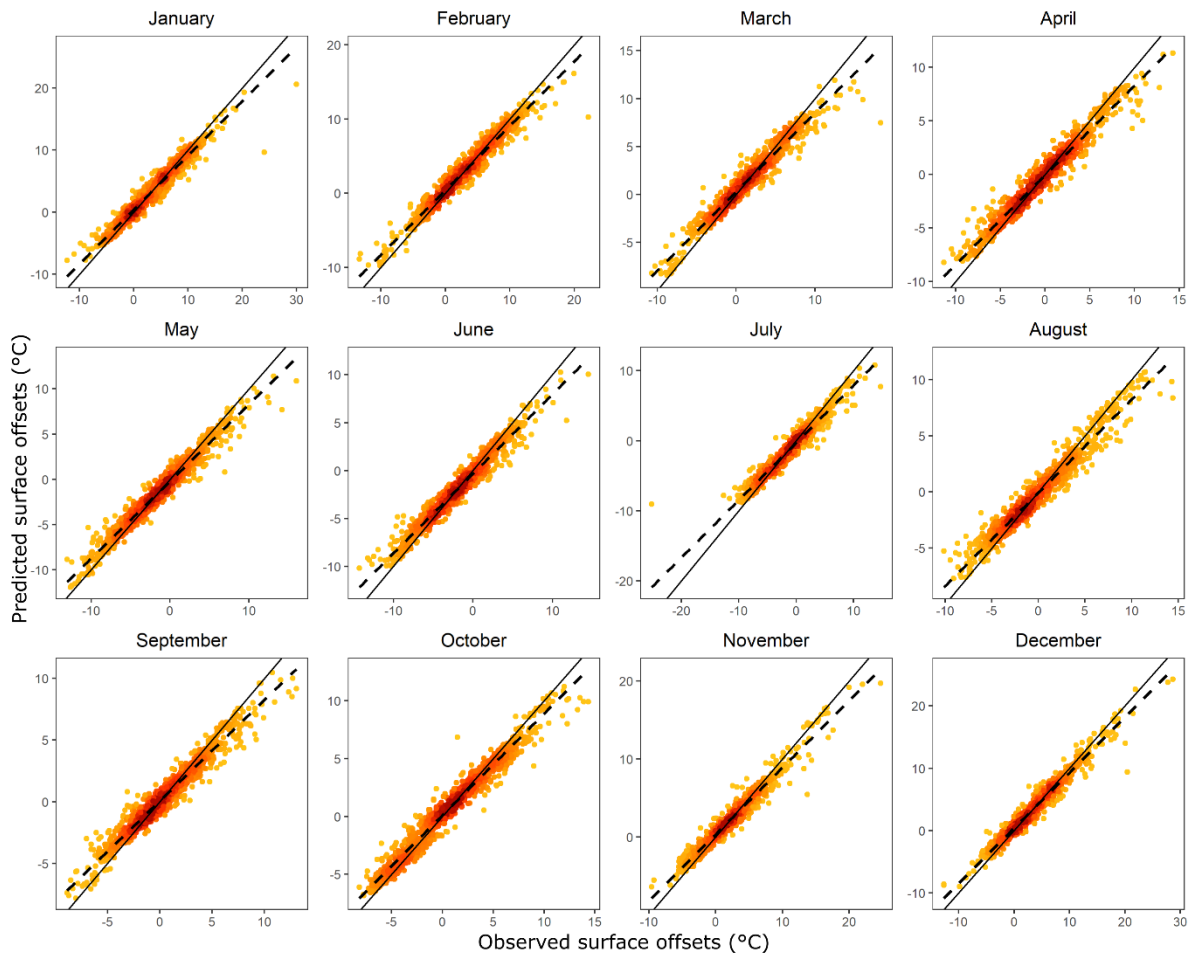
1574

1575

1576

**Fig. S9: Bioclimatic variables for the second soil layer.** Global maps of bioclimatic variables for the second soil layer (5–15 cm depth) climate, calculated using the maps of monthly temperature offsets (see Fig. 2, Fig. S8) and the bioclimatic variables for air temperature from CHELSA (4).

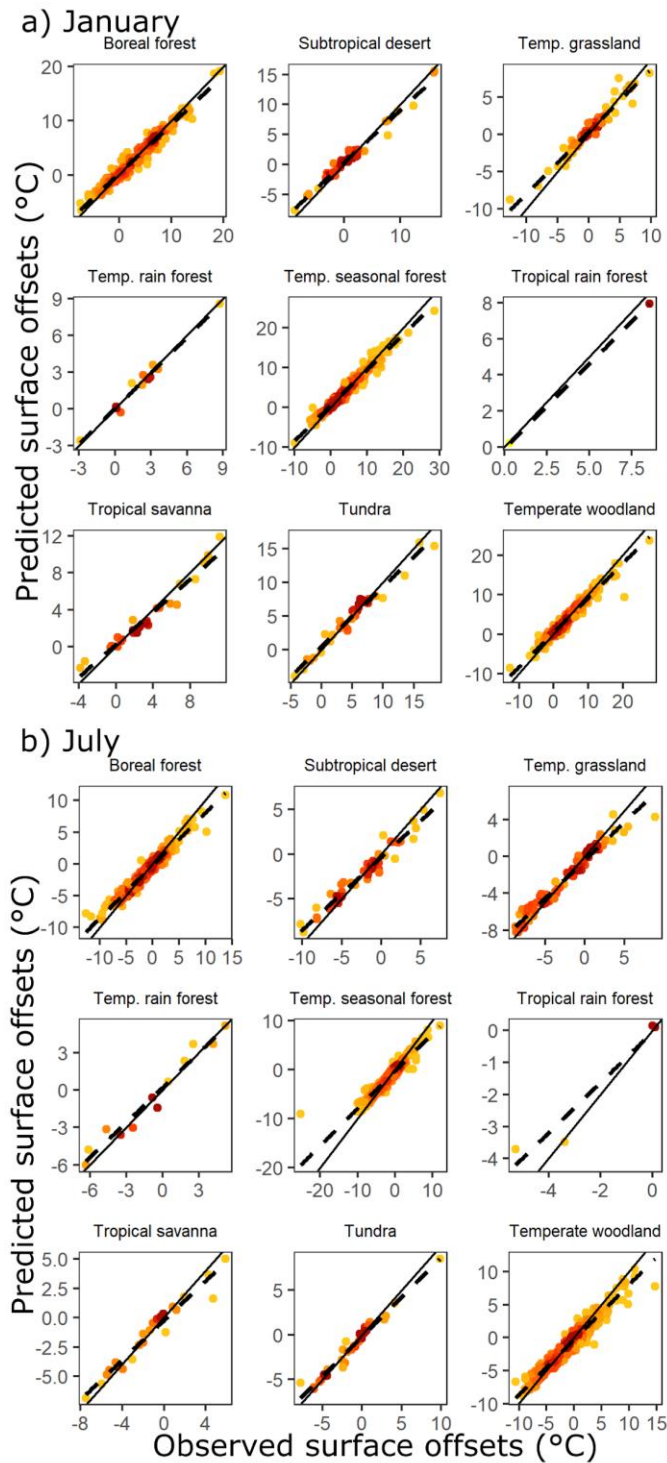




1577

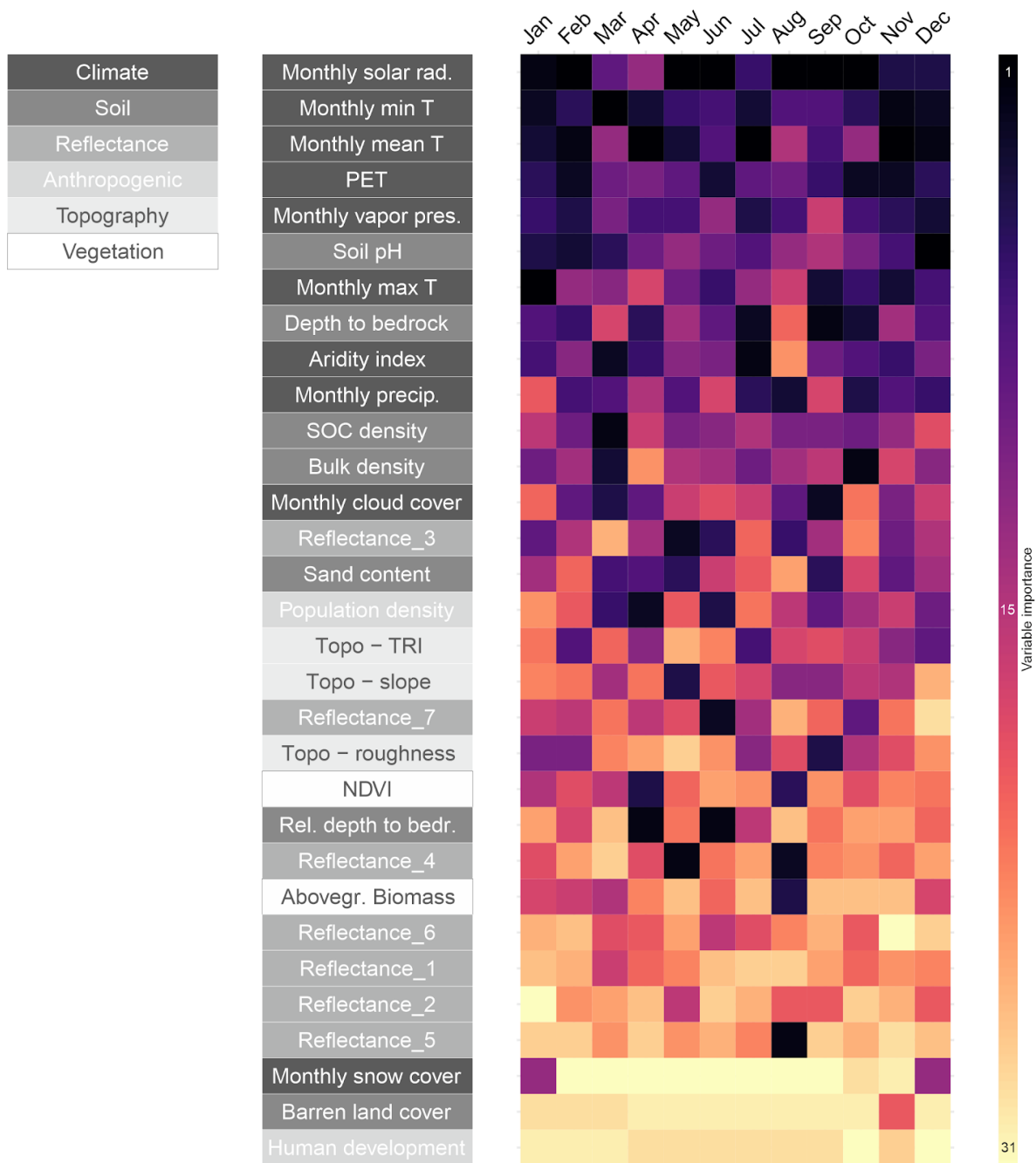
1578 **Fig. S10: Observed versus predicted temperature offsets.** Correlative plots showing temperature  
 1579 offsets – averaged at a  $1 \times 1$  km resolution – as observed in the field, versus those as predicted by the  
 1580 models, separately for each month. Colours show density of points (darker = higher point density).  
 1581 Dashed lines from linear regressions; solid lines refer to the 1:1-line of perfect correlation between  
 1582 predicted and observed offsets.

1583



1584

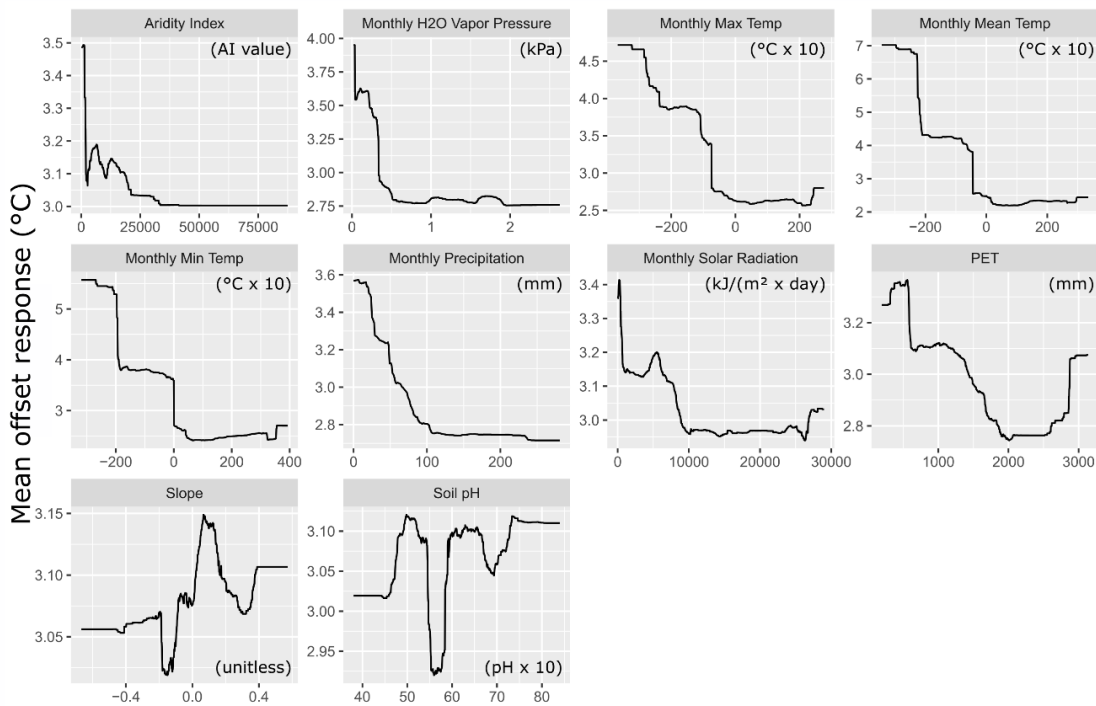
1585 **Fig. S11: Observed versus predicted temperature offsets per biome.** Correlative plots showing  
 1586 temperature offsets – averaged at a  $1 \times 1$  km resolution – as observed in the field, versus those as  
 1587 predicted by the models, separately for each biome, for January (a) and July (b). Colours show density  
 1588 of points (darker = high point density). Dashed lines from linear regressions; solid lines refer to the  
 1589 1:1-line of perfect correlation between predicted and observed offsets.



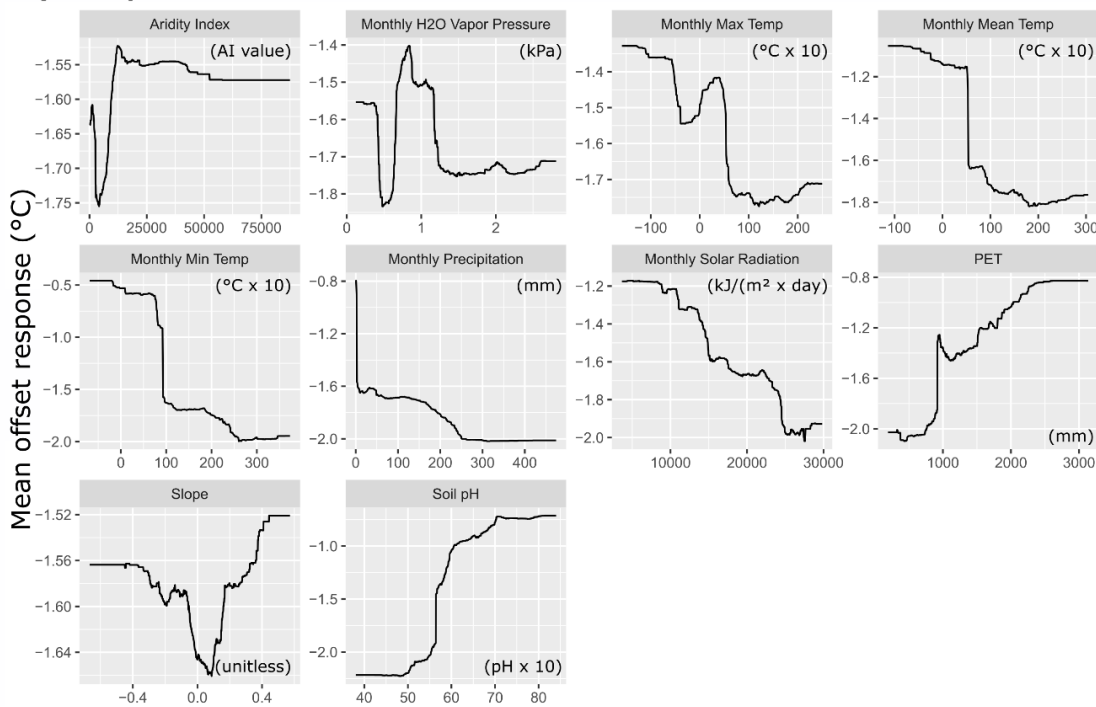
1590

1591 **Fig. S12: Relative importance of explanatory variables.** Explanatory variables in all twelve monthly  
 1592 analyses sorted by mean Variable Importance (computed based on the summed decrease of impurity  
 1593 over all trees in the forest that results from the variable used at a node; higher for variables with a  
 1594 higher importance) across all models of the first soil layer (0–5 cm depth) (first variable = ranked on  
 1595 average most importantly across all twelve monthly models). Colours represent relative variable  
 1596 importance (ranked from 1 to 31, with 1 the highest importance) within each monthly model for the  
 1597 topsoil (0–5 cm depth). T = temperature, PET = potential evapotranspiration, SOC = soil organic  
 1598 carbon, TRI = topographic roughness index, NDVI = normalized difference vegetation index. For full  
 1599 details on all explanatory variable layers, see Data S1.

## a) January



## b) July



1600

1601 **Fig. S13: Partial dependency plots of main effects.** Partial dependency plots of the 10 most important  
 1602 variables (selection based on the mean Feature Importance from Fig. S12) for January (a; top) and July  
 1603 (b; bottom), as examples of the two most contrasting months. Results for the first soil layer (0–5 cm  
 1604 depth).

1605 **Supplementary Tables**

1606

1607 **Table S1:** Number of sensors from the most common logger brands in the top soil (left, 0–5 cm  
 1608 depth) and the second soil layer (right, 5–15 cm depth). Other sensors include among others  
 1609 Decagon devices, GeoPrecision data loggers, thermocouples and TinyTags.

Logger brand	Number of sensors	
	0–5 cm	5–15 cm
iButton	1840	1685
TOMST	512	1090
HOBO	689	491
Lascar	247	0
Others	1025	587

1610

1611

1612 **Table S2:** Number of sensors in each soil layer

Depth of soil layer (cm)	Number of sensors
0–5	4530
5–15	3989
15–30	484
30–60	294
60–100	54
100–200	11

1613

1614

1615 **Table S3:** Number of data points (in brackets the number of unique pixels after averaging at 1 × 1 km  
 1616 pixel resolution) for each month as used in the models.

Month	N° of data points (0–5 cm)	N° of data points (5–15 cm)
January	6674 (1212)	10130 (977)
February	6649 (1223)	10214 (986)
March	6527 (1184)	10345 (979)
April	6439 (1093)	10266 (989)
May	6611 (1150)	10510 (1003)

June	6537 (1154)	10546 (1011)
July	6874 (1352)	10515 (1141)
August	6960 (1383)	10950 (1098)
September	6690 (1317)	10484 (1019)
October	6991 (1299)	10429 (1018)
November	6995 (1215)	10683 (996)
December	6846 (1193)	10607 (988)

---

1617

1618

1619

1620 **Table S4:** Number of unique pixels after averaging the annual data at 1 × 1 km pixel resolution for  
 1621 each biome, as used in Fig. 1. The number of individual annual averages on which this number is  
 1622 based is shown between brackets.

<b>Biome</b>	<b>N° of pixels (0–5 cm)</b>
Boreal forest	240 (10168)
Sub-tropical desert	37 (802)
Temperate grassland	66 (9558)
Temperate rainforest	10 (27)
Temperate seasonal forest	245 (21566)
Tropical rainforest	2 (299)
Tropical savanna	13 (2062)
Tundra	29 (1584)
Temperate woodland	224 (16952)

1623

1624

1625

1626 **Table S5:** Number of unique pixels after averaging the monthly data at a 1 × 1 km pixel resolution for  
 1627 each biome as used in the models, averaged across all months.

1628

<b>Biome</b>	<b>N° of pixels (0–5 cm)</b>	<b>N° of pixels (5–15 cm)</b>
Boreal forest	284	323
Sub-tropical desert	46	4
Temperate grassland	82	63
Temperate rainforest	12	2
Temperate seasonal forest	349	304
Tropical rainforest	5	9
Tropical savannah	26	31
Tundra	35	34
Temperate woodland	466	353

1629

1630

1631

1632

1633 **Table S6:** Biome-specific quantile distribution of the estimated aboveground biomass at the 1 x 1 km  
 1634 pixel level (unit: tons/ha i.e., Mg/ha, for the year 2010, Santoro, 2018) for each sensor identified as  
 1635 either measuring in forests (top) or open vegetation (bottom), for all sensors for which the latter  
 1636 information was available (numbers between brackets). Numbers in green indicate sensors under  
 1637 aboveground biomass of 1.00 tons/ha or higher, here identified as forested.

1638

Biome	1%	5%	25%	50%	75%	95%	99%
<b>Forests</b>							
Boreal forest (18)	53.70	60.50	77.50	84.50	106.00	114.15	114.83
Subtropical desert (3)	2.00	2.00	2.00	2.00	38.00	66.80	72.56
Temperate grassland (12)	3.00	3.00	16.00	45.00	86.00	98.00	98.00
Temperate rain forest (7)	53.12	53.60	63.50	76.00	220.00	296.60	322.52
Temperate seasonal for. (227)	17.00	32.50	63.00	101.00	177.00	291.00	431.00
Tropical rain forest (6)	149.50	167.50	245.50	277.50	284.00	313.75	321.15
Tropical savanna (17)	186.00	186.00	186.00	186.00	207.00	224.00	224.00
Tundra (3)	8.04	8.20	9.00	10.00	12.00	13.60	13.92
Temperate woodland (145)	0.00	0.20	8.00	24.00	120.00	218.00	242.36
<b>Open vegetation</b>							
Boreal forest (463)	0.00	0.00	0.00	0.00	53.00	53.00	105.00
Subtropical desert (13)	0.00	0.00	0.00	0.00	0.00	0.00	0.00
Temperate grassland (44)	0.00	0.00	0.00	0.00	0.00	32.00	107.00
Temperate rain forest (0)	-	-	-	-	-	-	-
Temperate seasonal for. (89)	0.00	0.00	0.00	0.00	32.00	223.00	248.08
Tropical rain forest (0)	-	-	-	-	-	-	-
Tropical savanna (0)	-	-	-	-	-	-	-
Tundra (75)	0.00	0.00	0.00	0.00	0.00	6.00	10.00
Temperate woodland (93)	0.00	0.00	1.00	19.00	66.00	171.00	172.00

1639

1640

1641 **Table S7:** Difference in temperature offset between forested and unforested habitats. Mean and  
 1642 standard deviation of offsets per Whittaker biome for all sensors, and for sensors in forested and  
 1643 non-forested habitats separately. All values averaged at a 1 x 1 km resolution (number between  
 1644 brackets = number of unique 1 x 1 km pixels), only biomes with sufficient number of loggers in  
 1645 forested habitats are shown. Habitat assessment at the location of the sensor based on observations  
 1646 by the contributors, whenever available (60% of sensors).



1647

<b>Biome</b>	<b>All</b>	<b>Forested</b>	<b>Non-forested</b>
Boreal forest	2.47 ± 2.01 (240)	3.40 ± 1.64 (41)	3.12 ± 1.77 (105)
Temperate grasslands	0.92 ± 2.13 (66)	1.39 ± 2.79 (4)	1.30 ± 2.79 (27)
Temperate seasonal forests	0.46 ± 2.79 (245)	-0.82 ± 2.21 (53)	1.00 ± 3.95 (20)
Temperate woodland	-0.12 ± 3.38 (224)	-0.71 ± 3.11 (31)	1.22 ± 4.31 (35)

1648

1649

1650

1651 **Data S1. (separate file)**

1652 Final selection of global covariate layers used for geospatial modelling. A total of 31 global covariate  
1653 layers was used in our modelling approach.

1654